QUALIFYING SILICON-GERMANIUM ELECTRONICS FOR HARSH RADIATION ENVIRONMENTS

A Dissertation
Presented to
The Academic Faculty

by

Zachary E. Fleetwood

In Partial Fulfillment
of the Requirements for the Degree
Doctor of Philosophy in the
School of Electrical and Computer Engineering

Georgia Institute of Technology
May 2018

QUALIFYING SILICON-GERMANIUM ELECTRONICS FOR HARSH RADIATION ENVIRONMENTS

Approved by:

Professor John D. Cressler, Advisor
School of Electrical and Computer Engineering
Georgia Institute of Technology

Professor Britney E. Schmidt
Earth and Atmospheric Sciences
Georgia Institute of Technology

Professor P. Douglas Yoder
School of Electrical and Computer Engineering
Georgia Institute of Technology

Professor Muhannad S. Bakir
School of Electrical and Computer Engineering
Georgia Institute of Technology

Professor Eric M. Vogel
Materials Science and Engineering
Georgia Institute of Technology

Date Approved: 22 February 2018

ACKNOWLEDGEMENTS

First and foremost I would like to thank my advisor Dr. John Cressler for his sage advice over the years. His influence has impacted not only my professional life but also my personal life. His guidance has helped me to be become a self-sufficient researcher and to prioritize the important things in life.

I would like to thank my reading committee members Dr. Yoder and Dr. Vogel who both also served as members of my proposal committee. Their technical feedback and direction has proved extremely beneficial to my thesis work. Our discussions served as a useful reminder to delve deeper into my simulations and models and ensure that the physics made sense. An additional thank you to Dr. Yoder for serving on my Master's Thesis committee and for never being bothered by my unannounced visits to his office.

I would like to thank my defense committee members Dr. Bakir and Dr. Schmidt for not only agreeing to serve on my committee but also for being excellent teachers during my time at tech. Our classes together not only helped develop my technical skills but also provided direction for the career that I wanted to pursue after graduate school.

I would also like to thank the staff members at Georgia Tech, especially Lisa, Scott, Carolyn, and Daniela – who were all willing to take time out of their days to help me handle travel and university concerns.

A big shout out to all the members of the Silicon-Germanium Devices and Circuits group at Georgia tech. It was our interactions together that drove my intellectual curiosity and excited me about my research. An additional thank you to all the members who participated on radiation effects testing trips with me. Adrian, Nelson,

George, Delli, Keisuke, Anup, Ickhyun, Uppili, Mason, Moon-Kyu, Adilson, Troy, and Stan. Without you guys, I would not have had any successful test campaigns and would not have really known what direction my work should take on.

I would like to extend my thanks to my collaborators in the radiation effects field. A huge thank you to Dale McMorrow, Stephen Buchner, Ani Khachatrian, Nicolas Roche, Jeffrey Warner, and Joel Hales at the Naval Research Laboratory for their invaluable help in making our pulsed-laser experiments a success and guiding the direction of our work there. I would say that we spent countless hours testing at the facility, but that would not be true – we spent over 400 hours of testing time together. And I think all that time spent is well-reflected by the quality of work we have produced over the last five years. A big thank you as well to Pauline Paki at DTRA and Enxia Zhang at Vanderbilt University for contributing to the success of our pulsed-laser experiments and total ionizing dose experiments respectively.

I would finally like to thank my family and loved ones. Mom, Dad, Aaron, Nathan, Ellen, Luke, and Ansley – you all mean the world to me. Your support and encouragement to follow my own career path and to do what is important to me means so much.

TABLE OF CONTENTS

LIST OF TABLES

LIST OF FIGURES

SUMMARY

The objective of this thesis is to investigate the robustness of Silicon-Germanium Heterojunction Bipolar Transistors (SiGe HBTs) to radiation-induced damage. The work described in this document delves into both total ionizing dose (TID) and single-event effect (SEE) mechanisms. Background information is provided for the general operation of SiGe HBTs and basic radiation effects (generic and specifically for SiGe HBTs). Four unique investigations are covered in this work: the first two focus on TID effects for high dose environments and to investigate enhanced-low-dose-rate-sensitivity, and the latter two studies investigate advances in hardening SiGe HBT profiles and methods to conduct SEE experiments using pulsed-lasers in place of highly energetic ionized particles. These four studies have been published across 5 separate IEEE publications (enumerated below). Per IEEE copyright law, 4 of these publications have been reprinted within this work with permission and without alteration. In the case of investigation #4, additional (unpublished) simulations and analysis are included. It is of utmost importance to mention that the research conducted for these studies was not an individual effort and contributing persons are listed with the associated publication below. The following is a summary of the knowledge gained for each investigation:

1. Investigation One [1]

   Advanced SiGe BiCMOS Technology for Multi-Mrad Electronic Systems – This work investigates Jazz Semiconductor's SBC-18-HXL BiCMOS technology platform for TID tolerance up to doses expected for NASA's Europa mission (6 Mrad(SiO_2) at Jupiter's moon). Results show from this work that

both the SiGe HBTs and CMOS (nfet + pfet) are highly tolerant to TID. The high dose tolerance of the CMOS is unexpected and unique for this technology.

2. Investigation Two [2]

   Evaluation of Enhanced Low Dose Rate Sensitivity in Fourth-Generation SiGe HBTs – This work investigates state-of-the-art SiGe HBTs fabricated by GlobalFoundries (formerly IBM) for dose rate effects. Both the device and circuit level are considered in addition to older technology generations. No presence of ELDRS is identified in this work, further advocating the use of SiGe HBTs for high dose environments. Simply stated, the rate of dose does not impact the TID degradation mechanism – only the accumulated dose matters.

3. Investigation Three [3, 4]

   SiGe HBT Profiles With Enhanced Inverse-Mode Operation and Their Impact on Single-Event Transients – This work investigates doping profile changes that can be implemented to improve inverse-mode (IM) device operation. The impact of these changes on the radiation tolerance of the resulting profiles shows IM operational improvement comes with a degraded TID response. The SET response worsens for an equivalent strike condition in IM, although the sensitive area is still reduced compared to the forward active bias.

4. Investigation Four [5]

   Using TCAD Modeling to Compare Heavy-Ion and Laser Induced Single Event Transients in SiGe HBTs – This work investigates the differences between heavy-ion and two-photon absorption (TPA) pulsed-laser induced single event transients (SETs) in SiGe HBTs. This investigation shows how to extract and analyze heavy-ion broadbeam transients with uncertain

strike locations. In addition, basic laser strike simulations are implemented in technology computer aided design (TCAD) to provide insight into future design practices for using simulation software to describe TPA pulsed-lasers in terms of an equivalent or an effective linear energy transfer (LET).

Copyright Statement

G. N. Tzintzarov, B. R. Wier, U. S. Raghunathan, M.-K. Cho, I. Song, M. T. Wachter, D. Nergui, A. Khachatrian, J. H. Warner, P. McMarr, H. Hughes, E. X. Zhang, D. McMorrow, P. Paki, A. J. Joseph, V. Jain, and J. D. Cressler, *SiGe HBT Profiles with Enhanced Inverse-Mode Operation and their Impact on Single-Event Transients*, IEEE Transactions on Nuclear Science, Jan. 2018. This publication built off of an initial conference publication: ©2015 IEEE [3]. From Z. E. Fleetwood, B. R. Wier, U. S. Raghunathan, N. E. Lourenco, M. A. Oakley, A. J. Joseph, and J. D. Cressler, *Optimizing the Vertical Profile of SiGe HBTs to Mitigate Radiation-Induced Upsets*, 2015 IEEE Bipolar/BiCMOS Circuits and Technology Meeting - BCTM, Oct. 2015.

©2016 IEEE [5]. Reprinted, with permission, from Z. E. Fleetwood, N. E. Lourenco, A. Ildefonso, J. H. Warner, M. T. Wachter, J. M. Hales, G. N. Tzintzarov, N J.-H. Roche, A. Khachatrian, S. P. Buchner, D. McMorrow, P. Paki, J. D. Cressler, *Using TCAD Modeling to Compare Heavy-Ion and Laser-Induced Single Event Transients in SiGe HBTs*, IEEE Transactions on Nuclear Science, Dec. 2016

CHAPTER 1

INTRODUCTION

1.1 Thesis Background

Radiation hardening of microelectronics is vital to the progression of science. Space-based missions (satellites, exploration, and rovers) must carefully consider physical mechanisms that occur as high-energy particles and electromagnetic waves (radiation) pass through and interact with matter. At the simplest level, these interactions result in the ionization of the material where electrons are abruptly stripped from their native lattice sites, become mobile, and are capable of causing damage in the material. For humans, this may result in damage to extremely sensitive tissues and interfere with the body's ability to both create healthy cells and to fight off infections. For microelectronics, radiation may result in an unintended output just as the incident radiation imparts energy into the material, may result in an accumulation of defects which cause key system parameters to drift, and may lead to raised current levels causing the system to effectively 'bleed out' more power than it is able to provide, equivalent to death in the world of electronics.

Engineers must be able to not only identify plausible failure mechanisms for electronic hardware that is considered for radiation-intense environments, but also be able to establish strategies for mitigating or even eliminating the negative effects associated with radiation. It is not sufficient to merely deal with radiation at any cost necessary – methods must be proposed that provide high-performance solutions which maximize the attainable information desired from the mission. This dissertation work discusses radiation concerns for a high-performance microelectronic technology, the silicon-germanium heterojunction bipolar transistor (SiGe HBT).

1.2 Thesis Layout

This thesis is segmented into eleven primary sections: 1) Introduction, 2) Summary, 3) Silicon-Germanium Technology, 4) Basic Radiation Mechanisms, 5) TID in a BiCMOS Technology, 6) ELDRS in SiGe HBTs, 7) Vertical SiGe HBT Profile Changes, 8) Two Photon Absorption to Heavy-Ion Correlation, 9) Correlation 3D Model Development and Improvement, 10) Conclusion, and 11) Future Work. The 'Summary' section gives an overview of the research topics and objectives covered in this work. The 'Silicon-Germanium Technology' section provides a background of SiGe HBTs and how they differ from the more common silicon bipolar junction transistor. The 'Basic Radiation Mechanisms' section provides a background of different types of radiation-induced damage followed by mitigation strategies and a more thorough description of how radiation effects are exhibited in SiGe HBTs. The 'TID in a BiCMOS Technology' section covers an investigation of a BiCMOS technology with a robust TID response (SiGe HBT and more importantly CMOS). The 'ELDRS in SiGe HBTs' section covers dose rate effects in SiGe HBTs including a state-of-the-art technology. The 'Vertical SiGe HBT Profile Changes' section analyzes (in simulation) what profile changes to inverse-mode operated SiGe HBTs will boost performance. These profile changes are then implemented in process controlled TCAD (technology computer aided design) decks, fabricated, and then tested for the TID and SEE response. The 'Two Photon Absorption to Heavy-Ion Correlation' section investigates how to go about comparing heavy-ion SEE results to pulsed-laser SEE results. The 'Correlation 3D Model Development and Improvement' section then expands upon the correlation investigation by adding more advanced 3D TCAD simulations. And finally, the 'Conclusion' and 'Future Work' sections serve to both summarize the findings of this work and recommend logical next steps to continue and improve upon these research endeavors.

CHAPTER 2

OVERVIEW

2.1 Investigations in Total Ionizing Dose

2.1.1 TID in a BiCMOS Technology

One of the challenges in leveraging the TID hardness of SiGe HBTs is that the on-board CMOS device components in BiCMOS (bipolar and CMOS) technologies normally limit the allowable mission dose. Although SiGe HBTs may be able to tolerate multi-Mrad of dose, the CMOS components normally start to fail on the order of 100s of krad [7]. There are two ways to get around this TID sensitivity: 1) implement *npn* SiGe HBT only circuit designs or 2) improve the capability of the CMOS to handle TID. As having on-board digital components can be very beneficial for circuit designers – the second approach is much more advantageous.

As part of this research investigation, a TowerJazz SiGe BiCMOS technology (SBC-18-HXL) was targeted with such a goal in mind. The MOSFET transistors in this technology are designed using a 'triple-well' process. Essentially an additional implant is added to the body of the transistor to allow for better control of the threshold voltage of the device. This additional implant will contain higher densities of dopants, which according to theory, will help to prevent parasitic TID-induced leakage paths from forming up to higher levels of dose when compared to a lowly doped body region as is traditionally used (i.e. more resistant to inversion at the Si-SiO_2 interface). To test this hypothesis, a number of NMOS and PMOS transistors were experimented on in addition to *npn* SiGe HBTs. These parts were tested at Vanderbilt University using a 10 keV X-ray source with a dose rate of 525 rad(SiO_2)/s and at UC Davis using a 63 MeV proton source at a dose rate of approximately

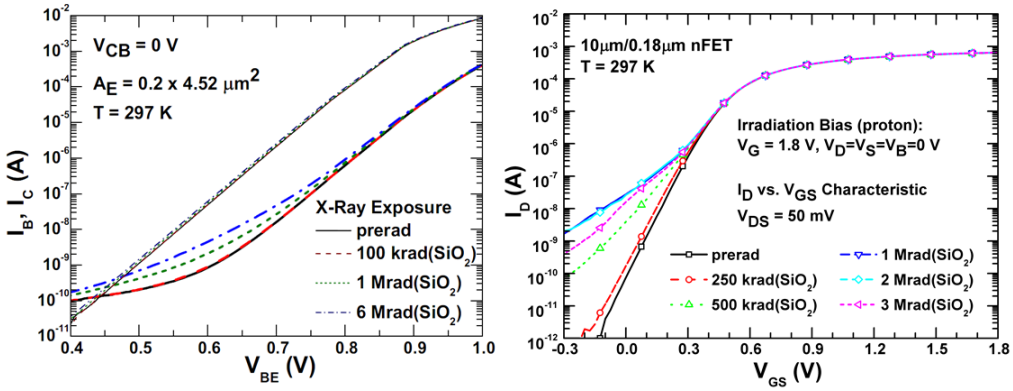

Figure 2.1: Left image shows *npn* SiGe HBT leakage as a result of X-ray damage, and the right image shows nFET drain leakage as a result of proton damage.

1 krad(SiO_2)/s (described in [8]).

Results from this investigation show that both the NMOS and PMOS transistors are much more resistant to TID when compared to similar transistors in an equivalent, non triple-well, technology [7]. TID results for a large nFET and a SiGe HBT are shown in Fig. 2.1. There is still pronounced shallow trench isolation (STI) leakage in the platform; however, there is negligible charge trapping in the gate oxides. This is verified by comparing different geometry nFETs. Longer devices (10 μm vs. 0.6 μm) show very little threshold voltage shift when compared to smaller structures [9]. In addition, the PMOS transistors are more robust to TID when compared to the NMOS transistors. This is due to the buildup of oxide traps (positive) and interface traps (negative) accommodating one another [10]. As expected, the SiGe HBTs in this technology still retain their multi-Mrad TID hardness. Such a study shows the feasibility of a BiCMOS technology for use in a high dose environment such as seen at the moons of Jupiter [11].

2.1.2 Enhanced Low Dose Rate Sensitivity in SiGe HBTs

There is a vast difference between dose rates seen in space and in the testing environment [12]. For most space missions it takes on the order of months or years in order

to attain an equivalent dose that may be created in the lab on an order of minutes or hours. This difference in dose rate may give rise to a number of serious hardness assurance issues that must be addressed. Some of these issues are time dependent and may be accounted for easily with room temperature annealing to an equivalent operation time [13] (i.e. continue testing the high dose rate test to an equivalent time need to achieve the low dose rate time). However, some of these issues are "true dose rate effects" where the parts tested receive more degradation in the low dose rate condition even when accounting for time dependent effects (TDE). This is a serious concern for space electronics as these parts, known as being sensitive to Enhanced Low Dose Rate Sensitivity (ELDRS), may be drastically more sensitive to total ionizing dose radiation than expected through standard experimentation [14].

ELDRS is normally associated with bipolar devices and as SiGe HBTs are bipolar and no such study had investigated the effects of low dose rate irradiation. This inspired a study that involved investigating this in a number of SiGe HBT device generations. For this study, both low and high dose experiments were conducted at NASA Goddard Spaceflight Center (GSFC) Radiation Effects Facility (REF). The exposures were made using a gamma source at a dose rate of 50 rad(SiO_2)/s (for the high dose rate) and 10 mrad(SiO_2)/s (for the low dose rate). This study looked into individual devices (1^{st}, 3^{rd}, and 4^{th}-generation) and also a bandgap reference circuit fabricated in the 4^{th}-generation technology.

The results from this study show that SiGe HBTs are not sensitive to ELDRS. This is due primarily to the fact that the fabrication environment for these structures must be kept extraordinarily clean to fabricate them properly. Having high quality oxides, combined with a heavily doped base region and vertical device typology explain the robustness to ELDRS.

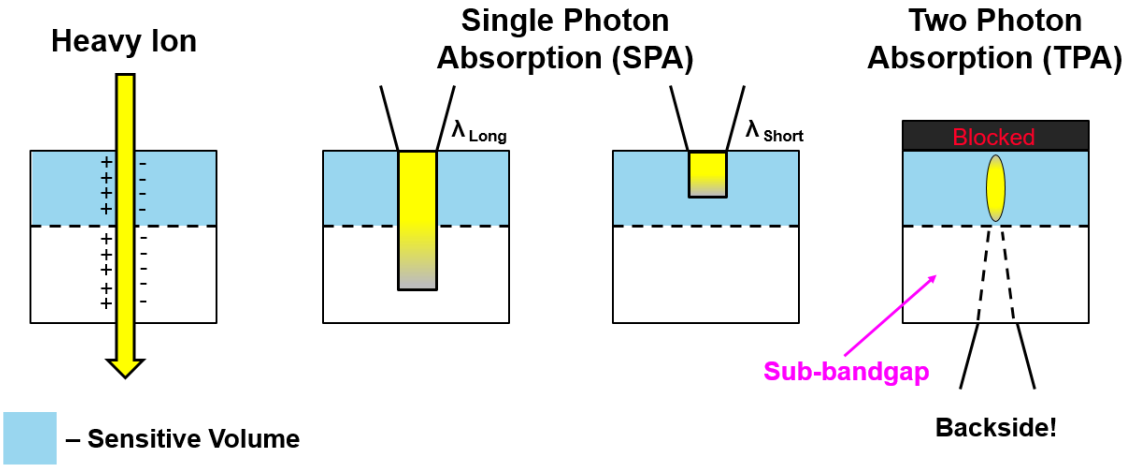

Figure 2.2: Differences between heavy-ion and laser sources at different wavelengths of light. The goal is to get the TPA device response to match that of the heavy-ion case.

2.2 Investigations in Single-Event Transients

2.2.1 TPA (Laser) Correlation

One of the challenging issues with radiation effects testing is trying to accurately recreate a radiation environment at a test facility [15]. Heavy-ion broad beam testing facilities allow for specific energies with a given particle species; however, the strike location of any given particle is obfuscated (example beam profile can be described by a 5 cm diameter circle with strikes occurring randomly about the circle). Based off of voltage/current transients, one may sometimes have an indication of what is being hit, but in very large circuits or systems this can sometimes be impossible. This is where focused-laser testing is of great use. Two-photon absorption laser-injection systems allow for charge to be imparted in a known area and can mimic heavy-ion charge deposition (refer to Fig. 2.2). When a specific wavelength of light is chosen (i.e., $\lambda = 1260$ nm) that is sub-bandgap to the material of interest (Si) – one may, in fact, inject charge through a material and rely on only dense packets of photons to generate EHP through higher order optical phenomena. This type of testing also allows for spatial mapping of parts that in turn may be used to directly identify part

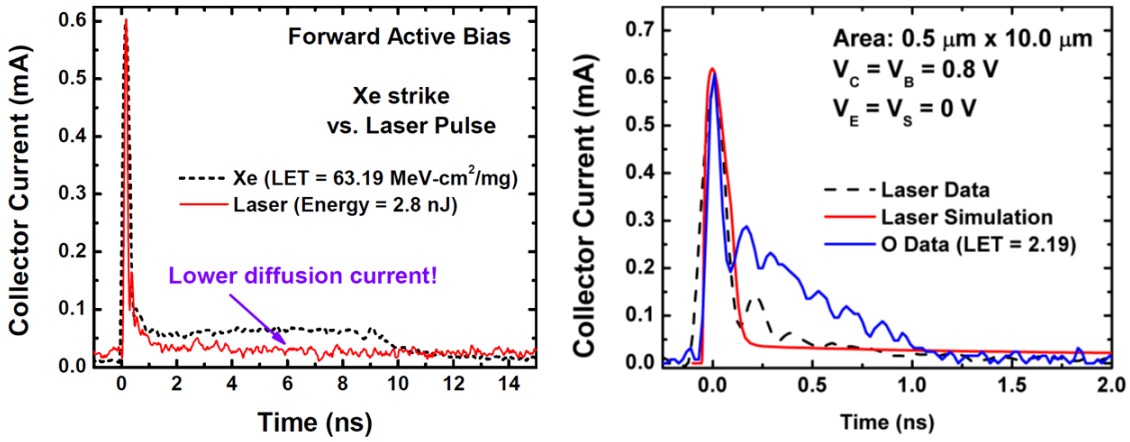

Figure 2.3: Image on the left shows transients for a laser strike condition and a heavy-ion strike. The right image shows a comparison of the laser-induced damage for both an experiment and modeled compared to a Oxygen strike.

sensitivity. However, as seen in the left image of Fig. 2.3, there is a mismatch in the device response between laser and heavy-ion induced transients. Although one can achieve a matched peak transient magnitude between sources, there is a fundamental difference between the device response.

It would be very powerful to equate the laser injection method to an equivalent linear energy transfer (LET) associated with a heavy-ion particle accelerator source. For this study, *npn* SiGe HBT device structures fabricated by GlobalFoundries (formerly IBM) were selected for experimentation at the following geometries, represented in the form of (emitter width $\times$ emitter length) with the emitter width set by the lithographic node of the technology: (0.5 μm $\times$ 10.0 μm), (0.5 μm $\times$ 1.0 μm), (0.12 μm $\times$ 2.5 μm), (0.1 μm $\times$ 4.0 μm), and (0.1 μm $\times$ 6.0 μm). The parts underwent SEE testing at three different facilities. Heavy-ion experiments were conducted at both Lawrence Berkeley National Laboratory (LBNL) in Berkeley, California and at the Grand Accelerateur National d'Ions Lourds (GANIL) in Caen, France. TPA pulsed-laser testing was undertaken at the Naval Research Laboratory (NRL) in Washington, D.C.

These experiments show that at higher energies (greater LET for the heavy-ion

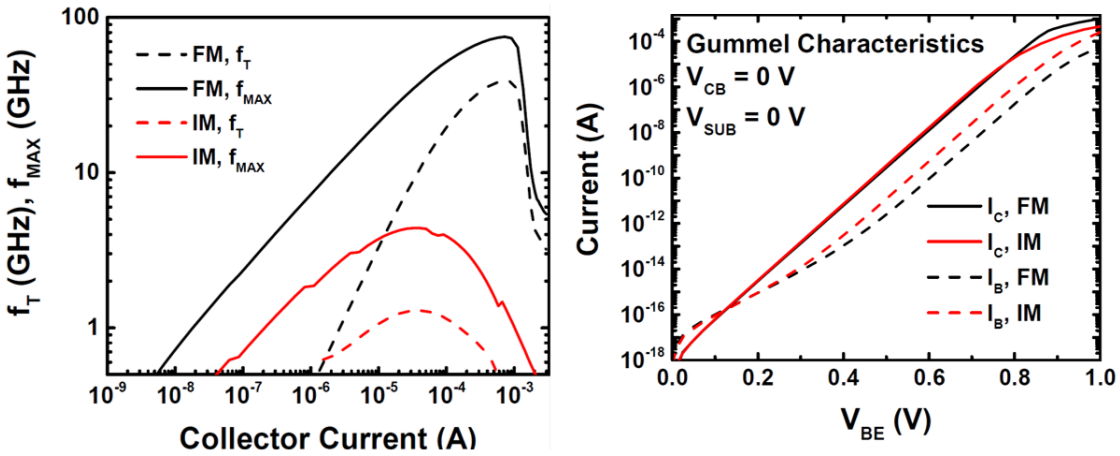

Figure 2.4: Comparison of forward-mode (FM) to inverse-mode (IM) operation. AC performance on left image and DC performance on right image.

case), the resulting SET waveforms for a device that is biased in forward-active for *npn* SiGe HBTs result in more pronounced diffusion tails when compared to the laser results (shown in the right image of Fig. 2.3). Modeling these effects in TCAD have been able to achieve okay matching in terms of amplitude; however, tail matching (i.e. achieving good agreement in collected charge) is still necessary for a proper correlation method. This work identifies a number of future modeling techniques that can be used in future investigations.

2.2.2 Vertical Doping Profile Study

IM operation comes at a severe penalty to the performance of the transistor (DC and AC changes shown in Fig. 2.4). This investigation explores device-level processing changes that lead to an improvement in inverse-mode (IM) operation (IM operation shown in the left image of Fig. 2.5). The idea of this work being to get not only improved IM performance but also leveraging the IM mitigation of single-event transients (SETs). Device profile changes (most substantial of which is shown in the right image of Fig. 2.5) are simulated using technology computer aided design (TCAD) models (designed in [16]), and are based off a first-generation *npn* SiGe HBT technology with a characteristic f_T of 39 GHz and f_{MAX} of 75 GHz (GF 5PAe technology).

Table 2.1: Simulated Device Performance

Parameter	Ctrl #1	#2	#3	#4	#5	Opt #6
Max β	140	385	1975	40	125	540
IM Max β	30	105	855	20	85	695
f_T GHz	39.3	31.2	31.7	49.2	41.4	43.9
IM f_T GHz	1.30	2.69	7.87	1.32	6.28	14.6
f_{MAX} GHz	75.2	66.9	70.9	70.2	68.4	73.9
IM f_{MAX} GHz	4.40	6.79	9.48	7.64	15.8	22.6

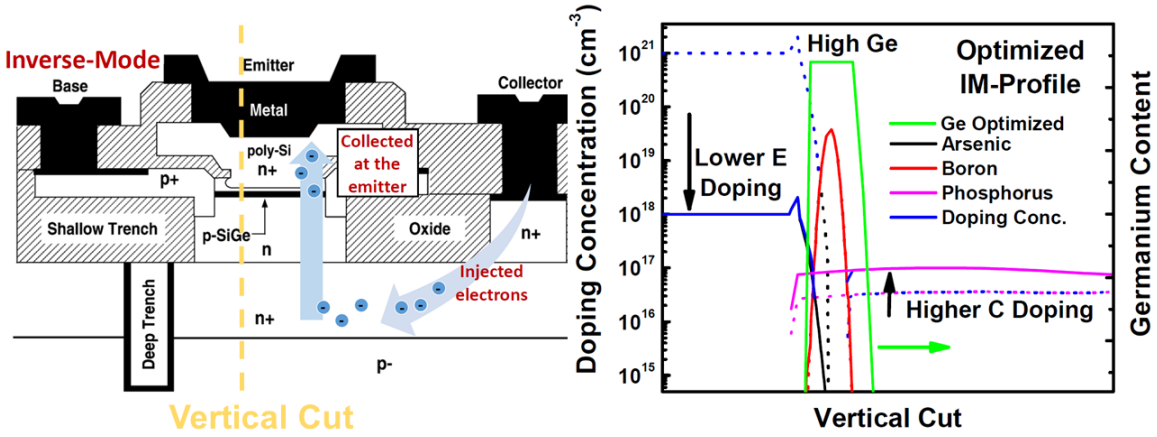

Figure 2.5: Image on the left shows a SiGe HBT operated in inverse-mode with a vertical cut line. The image on the right shows the doping profile across the cut line for a SiGe HBT profile for improved IM performance.

The IM performance, by comparison, has an IM f_T equal to 1.3 GHz and an IM f_{MAX} equal to 4.4 GHz. The model "control" profile designed within TCAD is two-dimensional and has calibrated DC and AC performance, which is matched to device specifications for the technology. Table 2.1 shows six primary profiles that were investigated 1) the control profile, 2) a profile with a Ge box and unchanged doping, 3) a profile with a larger Ge box and unchanged doping, 4) a profile with a triangular profile and altered doping, 5) a profile with a Ge box and altered doping, and 6) an "optimized" profile with a large Ge box and altered doping.

The changes investigated involve increasing the collector doping, decreasing the emitter doping, and shifting from a triangular Ge profile to a box profile. These

changes come without having to modify any lateral dimensions. For the most optimized profile, IM performance improves f_T by a factor of 10, f_{MAX} by a factor of 5, and the DC current gain by over 20 times. The profile modifications show a large hit to standard (normal active) device operation but allow for an emitter up/down designer choice [17]. These profiles have been fabricated and are discussed in further detail (including the TID response) in the chapter on changes to the vertical doping profile of SiGe HBTs. The aim of this investigation is to show a non-invasive method of modifying a silicon-germanium process flow (using existing mask sets) to optimize for IM device operation. Previous work has shown IM SiGe HBTs to be a viable means to mitigate radiation-induced SETs; however, implementing IM in a number of technologies is not possible due to the severe performance degradation. A future goal, not to be investigated as a part of this thesis, would be to implement the doping profile changes along with known radiation hardening strategies to achieve an improved SEE upset cross section – both in terms of threshold and saturated cross section.

2.3 Modeling Heavy-ion/Laser Effects

A key objective of the research conducted for this thesis is to help build more robust SEE modeling techniques for SiGe HBTs. Basic correlation methods have been briefly discussed in this overview section and in prior work [5, 18]. However, these models lack the predictive approach of translating in-lab experiment modifications (such as laser focusing, laser spot size, etc.) to a resulting charge carrier profile in TCAD simulation. This capability now exists using outputs from the non-linear beam propagation method (NLOBPM) software and is written and defined in a file format that is compatible with heavy-ion charge generation profiles. This approach is convenient, because it decouples the source of radiation from the TCAD transistor model. One simply needs to know the depth, radial distribution, and amount of carriers generated

in the device. One challenge in this approach on the optical side is the complex structure of the SiGe HBT. Bandgap narrowing associated with both the introduction of Ge and heavy doping effects can potentially impact the laser-induced charge injection profile and is currently unaccounted for.

Describing a two photon absorption pulsed-laser carrier generation profile in a meaningful, quantitative way with respect to an ionized particle strike would be very impactful to the radiation effects community. Using pulsed-lasers in place of particle accelerator experimentation would save substantial amounts of time and money. This thesis work adds substantially to the knowledge base of correlating heavy-ions to TPA pulsed lasers. One important conclusion of this work is that one must account for every piece of equipment and hardware when developing an accurate model to achieve quantitative agreement. Recommendations are made to enable mixed-mode TCAD solvers to treat everything outside of the meshed transistor model as a simplistic series of two-port networks containing lumped discrete R/L/C components.

CHAPTER 3

SILICON-GERMANIUM TECHNOLOGY

A silicon-germanium heterojunction bipolar transistor (SiGe HBT) is merely a modified vertical silicon bipolar junction transistor (Si BJT). Standard theory and operation of Si BJTs can be found in a number of textbooks on solid state devices (such as [19]). Si BJTs consist of four device terminals: the base, collector, emitter, and substrate. The transistor acts as a current-controlled current source, where a small amount of base current I_B is amplified to a larger collector current I_C with the current gain denoted by I_C/I_B or β. In addition to current gain, there a number of key device operating parameters such as the breakdown voltage (BV), the Early Voltage (Va), the emitter-injection efficiency (γ), the maximum oscillation frequency (f_T), the maximum unity-gain power frequency (f_{MAX}), and more. The addition of germanium in the silicon lattice allows for a bandgap engineering approach to alter, and improve, the Si BJT.

Bandgap engineering enables semiconductor devices to incorporate new materials to physically alter the bandgap of the material(s) in the device. This is extremely challenging to do in semiconductor processing, but if done correctly, will greatly improve device performance. In the case of a SiGe HBT (cross-sectional view of the device shown in Fig. 8.2), the introduction of germanium in the silicon lattice causes an effective shrinking of the "bandgap" in the base of the device. This shrinking, when graded from the emitter-base (EB) junction to the collector-base (CB) junction, causes an effective bending in the conduction band of the Si lattice which is physically realized as an electric-field in the device. This effect is shown in a band diagram in Fig. 3.2) This has a number of benefits for the transistor. First off, the addition

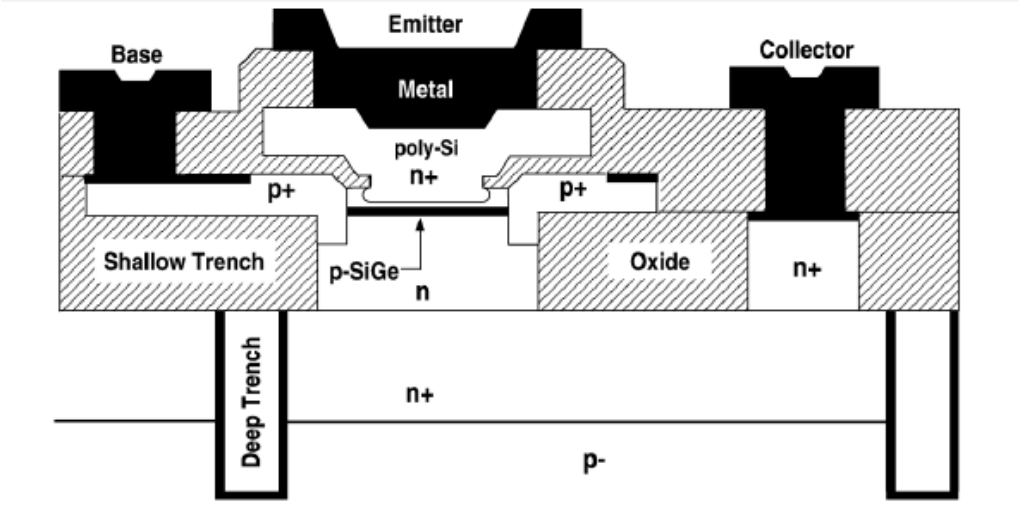

Figure 3.1: Cross-sectional view of an *npn* SiGe HBT. Not shown is a terminal contact for the p^- substrate.

of Ge at the EB junction causes a conduction band lowering which improves the emitter-injection efficiency of the device. This lowering allows for electrons (*npn* case) to more effectively be injected into the base of the device and drastically raises the device current gain. This additional gain allows for the base to be much more heavily doped to maintain a reasonable device current gain ($\beta > 100$). The increase in base doping causes the base resistance to be reduced and consequently improves the maximum unity-gain power frequency of the transistor. In addition, the germanium-induced drift field drastically decreases the minority carrier transit time in the base of the device. Electrons injected from the emitter into the base get caught in the drift field and get accelerated rapidly to the CB junction. This drastically improves both f_T and f_{MAX} and effectively makes the SiGe HBT operate much faster than a Si BJT.

To more closely investigate the impact of germanium on the device operation, it is important quantitatively consider the aforementioned device improvements. The first parameter to consider is the current gain (β) of the device. The impact of germanium on current gain is shown in Equation 3.1.

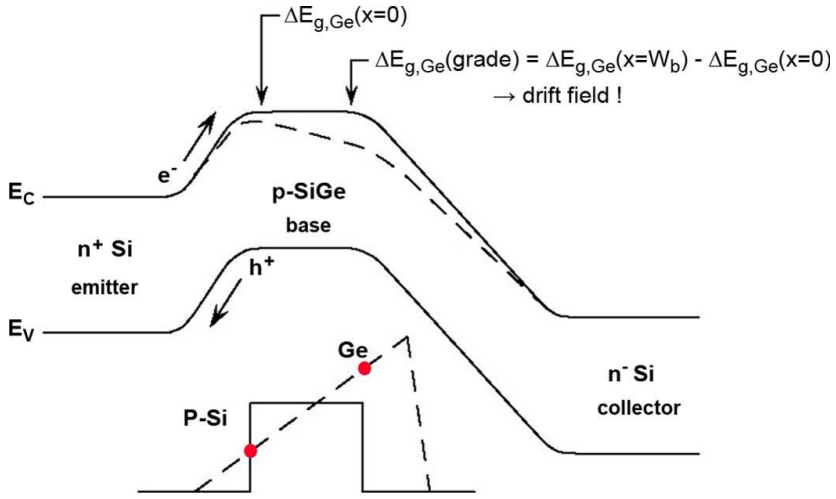

Figure 3.2: Band diagram of SiGe HBT (after [20]). The dashed line in the figure highlights the contribution of the germanium.

$$\beta \propto e^{\Delta \mathrm{Eg}(0)/(\mathrm{kT})} \tag{3.1}$$

Where k is the Boltzmann factor, T is the device temperature, and ΔEg(x) represents the amount of conduction band bending in the base region ($x = 0$ is at the EB junction and $x = \omega b$, the base width parameter, is at the CB junction). For a value of 20% Ge at the EB junction, the DC current gain improves immediately by a factor of 6 at room temperature. An interesting result from germanium of β is the temperature dependence. The germanium-induced conduction band lowering is lowered further as temperature is decreased. Important to consider for extreme environment considerations, such as in deep space where the temperature can get as low as 2.7 K.

Another important relationship is the Ge impact on the maximum oscillation frequency of the device (f_T) and the maximum unity-gain power frequency (f_{MAX}). It is first important to look at the equation for f_T:

$$f_T = \frac{1}{2\pi}\left\{\frac{kT}{qIc}(C_{te} + C_{tc}) + \tau_b + \tau_e + \frac{W_{CB}}{2V_{sat}} + r_c C_{tc}\right\}^{-1} \tag{3.2}$$

The equation is primarily dominated by capacitances and resistances (parasitics) in addition to the base and emitter transit times notated as τ_b and τ_e respectively. Improvements in lithography and scaling have naturally improved much of the impact of parasitics on f_T and device limiting performance is the carrier transit times. As such, the equation may be reduced to the following form [21]:

$$f_T = \frac{1}{2\pi\tau_{ec}} \tag{3.3}$$

In this form, it is clear to see that the limiting factor is τ_{ec} which is a summation of both τ_e and τ_b – the total carrier transit time from the emitter to the collector, which defines the switching speed of the transistor [21]. As mentioned previously, one of the limiting factors is the minority carrier transit time in the base: τ_b. This is where the Ge grading will come into play and the results is shown in Equation 3.4.

$$\tau_b \propto \frac{kT}{\Delta Eg, Ge(grade)} \tag{3.4}$$

Where $\Delta Eg, Ge(grade)$ is equal to the slope in the conduction band (the induced electric field). This value is determined by the difference in conduction band energies from the EB and CB junction where a larger change in energies results in a larger electric field. The electric field reduces the base transit time, τ_b, and allows electrons to travel much more quickly through the base region of the device. This enables a faster device as can be seen in the equation for f_T (equation 3.2).

Improved current gain (β) allows processing engineers to make a further improvement to the device. The improved current gain is essentially traded back to the device engineer to raise the doping of the base region. Device doping profile is shown in Fig. 3.3. Increasing the base doping causes the base resistance r_b to drop. This improves the f_{MAX} of the device through the following relationship:

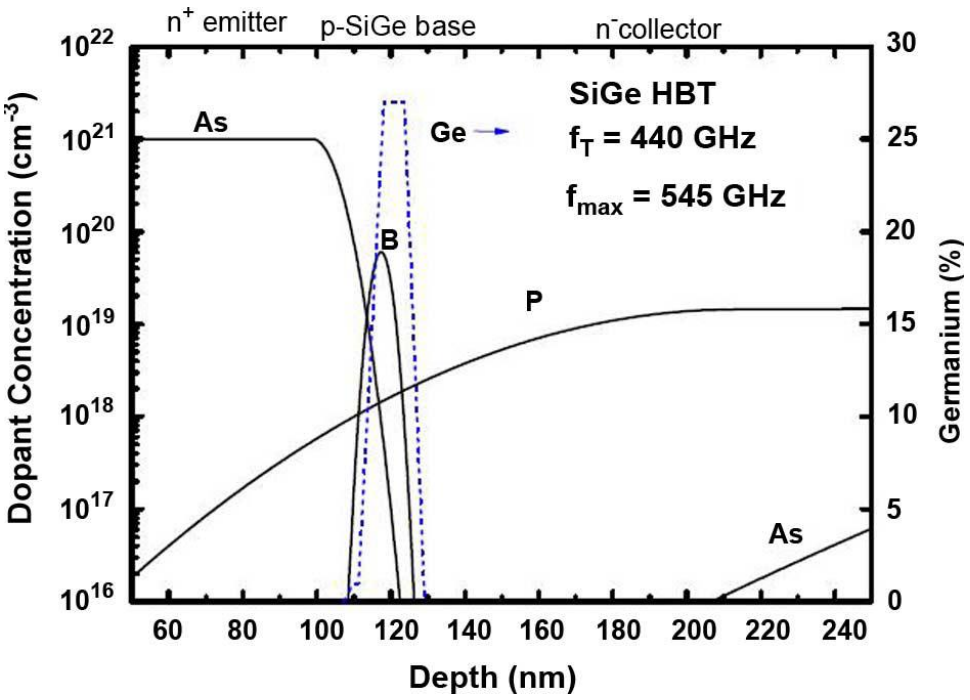

Figure 3.3: Doping profile of a SiGe HBT (after [20]).

$$f_{MAX} \simeq \sqrt{\frac{f_T}{8\pi\ r_b\ C_{CB}}} \tag{3.5}$$

Where C_{CB} is the capacitance between the collector and base terminals. Having high f_{MAX} and f_T is critical to devices designed for high-quality RF and analog circuitry. This makes SiGe HBTs well suited for a number of high-performance space-based mission objectives. A list of major performance metrics for 1^{st}, 2^{nd}, 3^{rd}, and 4^{th}-generation (all major device iterations) for a major semiconductor manufacturer is shown in Table 8.2.

Table 3.1: Parameter Scaling by Generation (GF/IBM)

Parameter	**Units**	**1st**	**2nd**	**3rd**	**4th**
Lith Node	nm	500	180	130	90
WE,eff	μm	0.42	0.18	0.12	0.10
Peak β	-	100	200	400	550
BV_{CEO}	V	3.3	2.5	1.7	1.4
BV_{CBO}	V	10.5	7.5	5.5	5
Peak f_T	GHz	47	120	207	300
Peak f_{MAX}	GHz	65	100	285	350

CHAPTER 4

BASIC RADIATION MECHANISMS

There are three major types of radiation-induced damage: displacement damage (DD), total ionizing dose (TID), and single-event effects (SEE). The two most important types of radiation-induced damage for this dissertation are total ionizing dose effects and single-event effects. Displacement damage effects have been shown in literature to be less consequential due to the heavy doping of the emitter and base region of a SiGe HBT [20].

Total ionizing dose (TID) damage results from charge accumulation at sensitive Si-SiO_2 interfaces in a semiconductor device. Charge accumulation can adversely affect the operation of the device – in the case of a MOSFET, charge accumulation at the sensitive gate oxide (where the channel forms) will result in a shift to the threshold voltage of the device and increase the device leakage current. TID is traditionally defined in the United States with the unit 'rad' which describes the radiation absorbed dose. One rad is equal to 0.01 J/kg within a given material where the accumulated dose is given in rad(material). Another common measurement of dose is the SI unit 'gray (Gy)' where 1 gray is equal to 1 J/kg or 100 rad. When used to describe dose to a person or human tissue, the unit 'rem' is used in place of rad. For reference, it takes only a couple hundred rem for a person to start experiencing symptoms of acute radiation syndrome (ARS).

Although discussed in further detail in the radiation effects in SiGe HBTs section, due to TID, SiGe HBTs experience an increase in base current at the low-injection region of device operation (low forward-biased base-emitter voltage) and this increase consequentially degrades the device current gain. The increase in base current is due

to increased surface recombination within the space charge regions at the emitter-base (EB) spacers oxides and at the shallow trench isolation (STI) oxides. Charge accumulation at the oxides is a result of chemical bonds breaking at the Si-SiO_2 interface. The following process is taking place: 1) a charged particle (with sufficient energy greater than the bandgap of the semiconductor material) passes through a transistor creating large quantities of electron-hole pairs (EHP). Electrons tend to be swept out of oxides quickly (on the order of tens of picoseconds), whereas holes tend to either recombine with electrons quickly (more so if the generated EHPs are very dense) or remain trapped in the lattice as immobile traps. The efficiency at which a radiation source creates oxide traps is known as the charge yield. As the charge yield for gamma rays is normally higher than x-rays or ionized particles, gamma rays are the de facto standard for qualifying electronic components for TID. Regardless of source, there is a clear dependence of the charge yield, or the fraction of unrecombined holes, on the electric-field (E-field) across the oxides in the device. This dependence is shown in Fig. 4.1 where stronger fields more effectively separate generated EHPs. Trapped holes in the oxide are known as polarons and are extremely immobile and slow moving. Over time these polarons, or rather oxide traps, will reach sensitive oxide-Si interfaces. There is an oxygen deficiency at the Si-SiO_2 interface that results in a number of strained Si-Si bonds – instead of normal Si-O-Si bonds [22]. A hole encountering such a bond may break the bond (because it is weakly bound) and then recombine with one of the bonding electrons. This process is known as hole trapping. The resulting positively charged structure relaxes to the E' (E prime) configuration with one of the Si atoms retaining the remaining electron from the broken bond and the positive charge residing on the other "trivalent" Si atom [22]. These defects are not necessarily permanent and may dissipate with time. In addition, annealing processes can result in the removal of these defects. This is achieved by elevating the device temperature for a designated period of time according to military standard

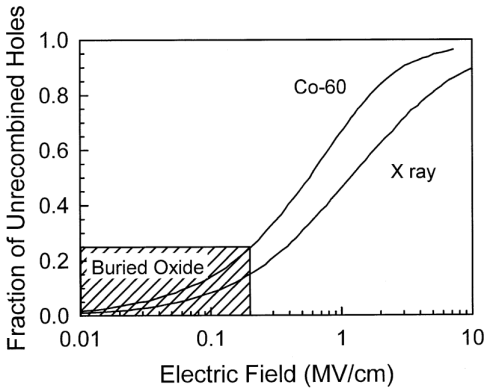

Figure 4.1: Charge yield comparing Cobalt-60 gamma rays to 10 keV x-rays after [23, 24].

specifications (MIL-STD-883E) with the device biased. The use of annealing may also isolate the difference between trapped holes within the oxide (oxide traps) and defects at the Si-SiO_2 interface (interface defect states) where traditionally a 168 hour anneal @ 100^oC is used to reduce the number of oxide traps present and maximize the buildup of interface defect states [12].

The total ionizing dose response of electronics tends to improve along with technology scaling as TID degradation is reciprocally related to oxide thickness (Tox) cubed (degradation $\propto\ 1/Tox^3$). This has allowed some advanced technologies with thin oxides, such as SiGe HBTs, to attain multi-Mrad(SiO_2) levels of TID hardness. As such, SiGe HBT technology is very compelling for high dose environments. It is important to note that most near-Earth based space missions will experience < 1 Mrad(SiO_2) of dose over the entire duration of the mission with very modest shielding. However, higher doses are attainable for missions to Jupiter and its surrounding moons. In addition 'prompt dose' effects associated with the detonation of nuclear weapons and particle accelerators/reactors are capable of reaching multi-Mrad(SiO_2) levels of TID.

In general, TID experiments are preferred to be executed using a gamma source. The reasoning behind this is two-fold: 1) x-ray sources, although very similar to

gamma sources, tend to have "dose enhancement" issues [12] where oxide interfaces may have a higher localized dose than other regions of the device such as in the bulk of the oxide, and 2) proton sources also cause displacement damage (DD) within the structure which may require additional testing to decouple the effect. Interestingly, for most near-Earth space missions, the most prevalent source of TID tends to be protons and electrons as they tend to have the highest fluxes when compared to heavier and more highly energetic particles. As such, most ground-level testing programs require at least proton testing to ensure the total number of particles (known as the fluence, where the fluence = flux * time) that will hit the structure over the duration of its use will not cause any serious effects missed by gamma testing. There is high interest in the radiation effects community to create radiation testing facilities with a 'mixed field', where there exists a slurry of different particles at varying energy which more accurately represents the space environment [25].

Single-event effects (SEE) refers to the the repercussion of an individual particle/photon on electronics and differs greatly from TID which is associated with a large number of events. SEE is a catch-all term used to describe a number of effects such as: single-event latchup (SEL), single-event gate rupture (SEGR), single-event functional interrupt (SEFI), and more. Single-event effects result from a single, incident particle which imparts energy into the device. The energy deposition is realized as electron-hole pair creation where free moving carriers can fundamentally be described as electrical current within the device which may cause damage or have adverse effects on the circuit or system application. In the extreme case an SEE may induce a bit flip and put a digital circuit in an undesirable and possibly irrecoverable state of operation. Such an undesired electronic state can lead to complete electronic hardware failure.

As previously mentioned, there are many different terms which fall under SEE.

All forms of SEE are undesirable; however, not all electronic systems are equally susceptible and susceptibility will vary based on the environment. Literature well covers the distinction between different SEE types [26,27]. At a basic level, though, all types of SEE can initially be thought of as a single-event transient (SET). Where an SET is considered a brief perturbation to the voltage/current of a transistor (or multiple transistors). In this view, SETs can be simply considered as time varying waveforms that describe a particle event. Both the duration and magnitude of the event will depend upon the source of radiation, the strike location, the angle of incidence, the bias of the transistor, the loading of the transistor, and the materials/doping of the transistor. A resulting waveform shows peak current levels and total charge imparted (integration of current as a function of time). This information, with further analysis, will be enough to determine whether or not an error has or will occur in a circuit. Although there are many dependencies that determine the SET waveform, waveform comparisons can be used to isolate the impact of any singular dependency with all others held fixed. As this dissertation work will show, this becomes especially challenging when determining whether or not certain experimental sources can mimic a radiation environment. Of particular interest, is whether or not pulsed-lasers may be used in place of classical ground-level testing with ionized particles. Before further discussion here though, a more in depth discussion of TID and SETs in SiGe HBTs is necessary.

4.1 Radiation Effects in SiGe HBTs

4.1.1 Total Ionizing Dose (TID)

As previously mentioned, total ionizing dose (TID) is exhibited in SiGe HBTs in two primary ways. First, there is an increase in base current when a small forward-bias is applied to the base-emitter (BE) junction (i.e. low injection). And secondly, the increase to base current results in a degradation to the the DC current gain (β) in low

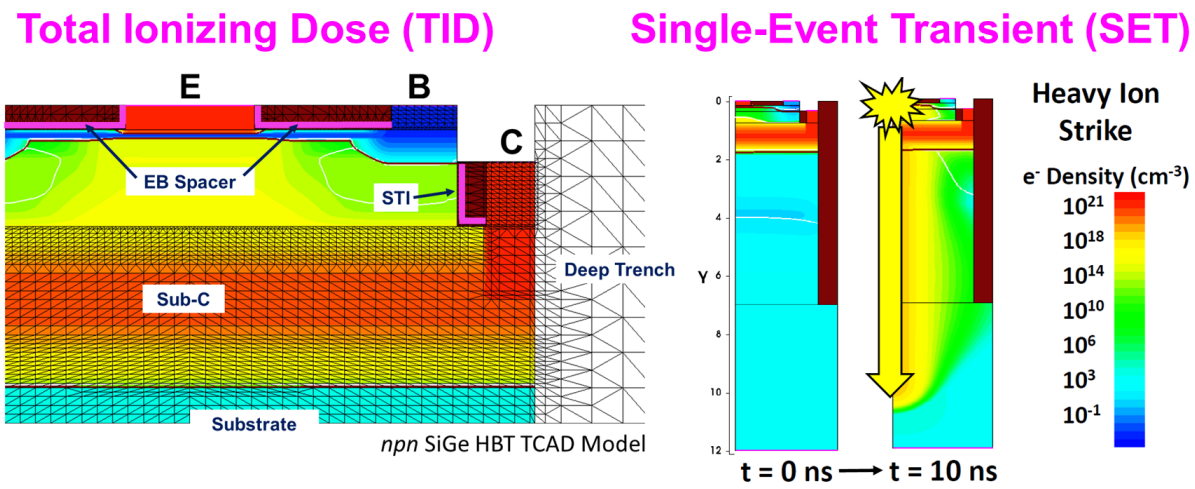

Figure 4.2: Total ionizing dose (TID) shown left and single-event transient (SET) shown right. The deep trench in the left model is marked as a transparent layer as negligible charge trapping occurs in the deep trench oxide.

injection. Low injection is marked by low current densities in the transistor where the current flow and sheer number of carriers does not impact the device operation (as opposed to in high injection where the Kirk Effect adversely affects both the dc and ac operation of the transistor). TID studies in SiGe HBTs were first investigated in the early 1990s after the 1^{st}-generation of SiGe HBTs were fabricated [28, 29]. These first studies used gamma sources and were extended across temperature in [30] and for proton irradiation in [31]. Initial results showed SiGe HBTs to be highly tolerate to TID (much so than MOSFETs at the time) and garnered much interest from the radiation effects community. Since these initial works, many TID investigations have been undertaken as discussed in [20]. These studies show that nearly all SiGe HBTs are very robust (multi-Mrad) to TID effects.

During irradiation, oxides in the SiGe HBT accumulate positive oxide charge. The primary affected regions are the EB spacer and the shallow trench isolation (STI) oxides. These sensitive regions are shown in the left image of Fig. 4.2. It is important to mention that very little charge trapping occurs in the deep trench isolation (DTI) regions as they only contain a thin oxide layer which is filled in with polysilicon.

In addition, the DTI is far removed from the intrinsic device making the impact of any trapped charge negligible on transistor operation. The buildup of positive charge in the EB spacer leads to a generation-recombination center in the emitter-base (EB) space charge region. This leads to increased surface recombination velocity and is effectively an additional source of base current. Similar effects can be seen for a transistor fabricated in a 'dirty' environment where impurities during fabrication lead to impurities which act as generation-recombination centers. Additionally, hot-carriers generated when a SiGe HBT is operated near breakdown can cause similar damage [32–34]. It is important to note that oxide traps and interface defects both occur due to device irradiation. However, for *npn* SiGe HBTs both will result in the formation of positive or neutral traps. Although discussed in many sections of this thesis as a general TID degradation mechanism, ultimately the number, location, and energy level of the traps determine the severity of the TID-induced damage.

4.1.2 Single Event Effects (SEE)

Although well-equipped to handle TID, SiGe HBTs are very sensitive to single-event effects (SEE). Initial investigations on SEE show SiGe HBTs to collect large quantities of charge imparted by individual particles and to have a sensitivity to relatively low-energy particles (LETs of 1 or even smaller), including protons [35, 36]. This sensitivity leads to very high-energy particles having the capability of causing multiple errors in operation as opposed to just a single upset [37]. This sensitivity is mainly attributed to the vertical device structure of the SiGe HBT. Any incident particle that strikes the device along the emitter normal to the surface will traverse through the entire intrinsic region of the device, as shown in the right image of Fig. 4.2. As the incident particle passes through, electrons are immediately stripped off of lattice molecules in an attempt to slow down the incoming ionized particle. These electrons, and the holes they leave behind, are extremely dense about the strike location. This

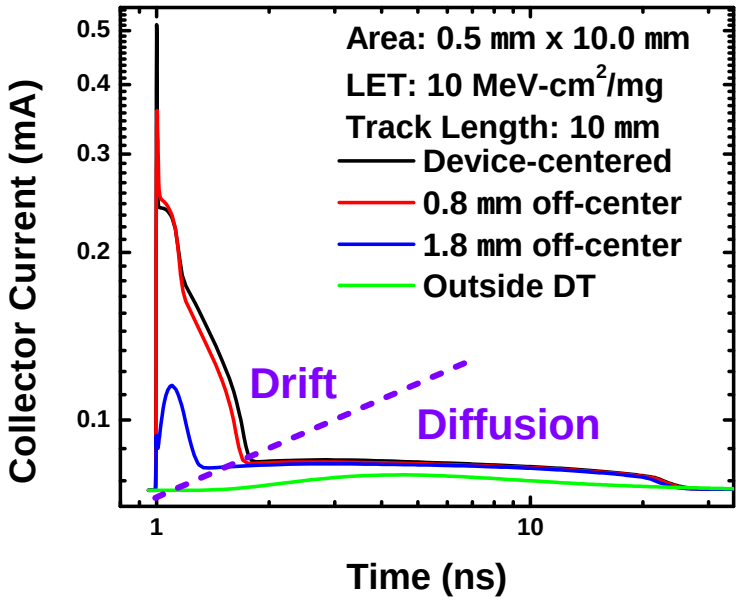

Figure 4.3: Two main features are seen in an SET in SiGe HBTs. First there is a fast (drift) high amplitude component that is associated with the 'ion-shunt' effect and then there is a slow-acting (diffusion) component of charge collection association with the large, reverse-biased collector-substrate junction.

region of electron-hole pairs (EHP) forms a plasma within the lattice which effectively shorts (connects with a low-resistance) the emitter, base, collector, and substrate terminals. This phenomena is known as the "ion-shunt effect." This results in a transient change to the terminal voltage/currents over a brief period of time, known as a single-event transient (SET) as discussed previously. As the junctions re-establish themselves they flush free carriers out of their terminal contacts in response to existing electric fields. The reverse-biased collector-substrate (CS) junction takes the longest time to re-establish as the substrate is very lowly doped and more carriers reach the CS junction due to diffusion in the deep, thick substrate. Previous studies show that a more heavily doped substrate [38] or heavily doped isolation layers [39] may mitigate these effects. Both the fast decay mechanism and the slower 'diffusion tail' may be seen through device simulation of Argon particle strikes in Fig. 8.4.

From a radiation effects testing perspective, it is important to make sure that

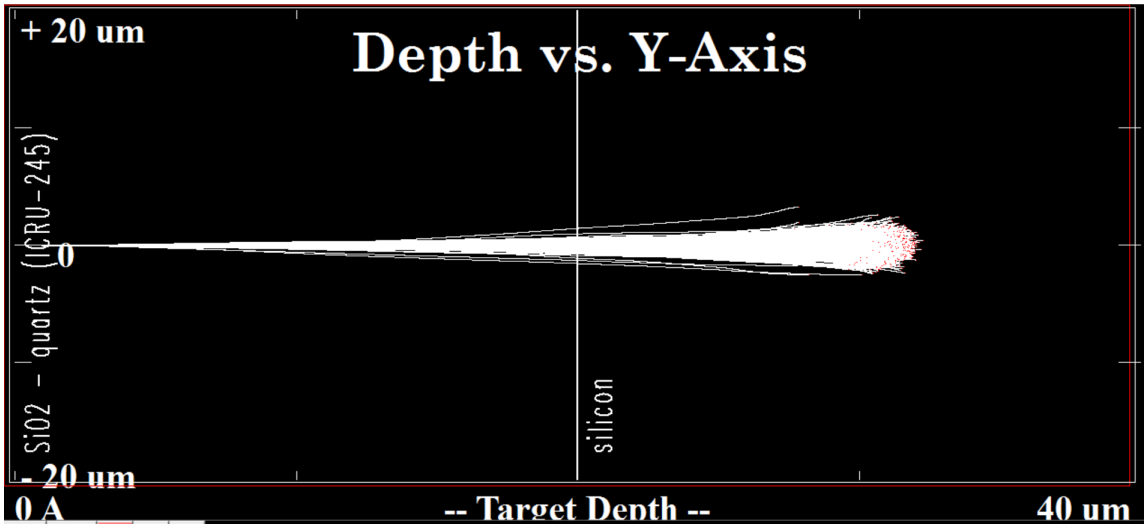

Figure 4.4: 360 MeV Xenons passing through 20 μm of oxide into a block of Si. Sensitive structures in a real structure are present at the Si-SiO_2 interface.

incident particles during experiment have sufficient energy to reach the sensitive device volume to accurately represent particle strikes occurring in space. For various heavy-ion species, simulation software such as SRIM [40], may be used to determine the expected range of the incident particle. In addition, such software may be used to determine the amount of ion energy loss or charge deposition within a given material. When this energy loss is taken per unit length, the linear energy transfer (LET) of the particle is defined with units of [MeV*cm^2/mg] – a primary metric in determining the susceptibility of the device structure. A good way to think about and to derive the LET of a particle is that only two key pieces of information need to be known: the stopping power of the *incident particle* defined as [MeV/cm] and the density of the *target material* given in [mg/cm^3]. Where one simply divides the stopping power by the density. It is important to note that the only reason mg is used in the units instead of g or kg is to provide better intuitive understanding of the LET (i.e. LET normally ranges at facilities from $<$ 1 MeV*cm^2/mg to around 60 MeV*cm^2/mg). An example of a SRIM simulation is shown in Fig. 4.4. The output shows over 2000 incident Xenon particles at an energy of 360 MeV passing through 20 μm of oxide into a block of Si.

4.1.3 Radiation Hardening

A number of radiation SEE hardening measures have been investigated in SiGe HBTs with the goals of: 1) raising the low threshold cross section and 2) lowering the high saturated cross section. The two aims are highlighted by magenta arrows in Fig. 4.5. In simple terms, it is desired to require more energy to flip a bit (or upset a circuit) and for any flips that occur (errors), to have them occur less frequently. Modest improvements have been made by altering the layout configuration (i.e. using low area CBE transistor structures as opposed to CBEBC) or by using different latch configurations (gated feedback cells, GFC and dual-interleaved cells, DI) as shown in [41]. The most significant improvement is achieved by introducing triple modular redundancy (TMR) in the circuit design. This involves triplicating circuitry and designing a voting scheme to avoid errors from occurring. Although, a viable approach for radiation mitigation this approach increases both area and power consumption by over 3X – incurring a severe design penalty.

A less invasive design approach to mitigate radiation-induced upsets is to employ the use of inverse-mode (IM) SiGe HBT transistors. IM, also known as reverse active, involves reversing the current flow of the transistor (effectively flipping the structure upside down). This operation change allows for the new electrical emitter to be set to the same potential as the substrate, which drastically reduces the duration of SETs. Unfortunately, SiGe HBTs are not optimized for reverse operation and suffer from drastic performance penalties (reduced β, f_T, f_{MAX}, breakdown, and Early Voltage). As such, a major aim of this dissertation is to improve IM performance to make the design technique a more viable means of radiation mitigation.

4.2 Harsh Radiation Environments

A significant portion of ionizing particles in our solar system originate from the Sun (see Fig. 4.6). Solar events, such as solar flares, solar prominences, and coronal mass

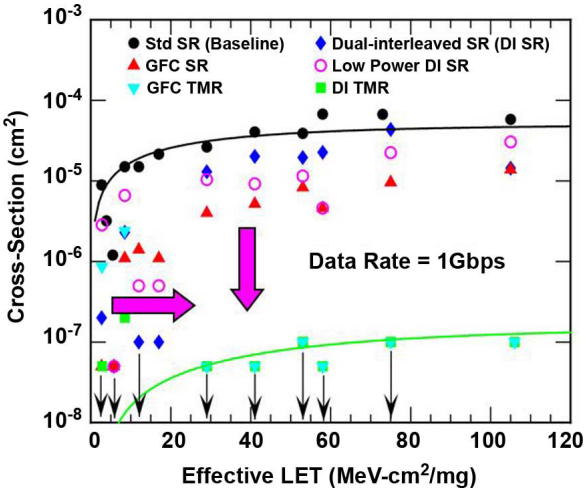

Figure 4.5: SEE cross sections showing that various radiation hardened by design (RHBD) strategies may be used to improve the tolerance of SiGe HBTs to SEE (after [20, 41]).

ejections (CMEs) release protons, electrons, and heavy ions (elements with $Z \geq 2$) that are accelerated towards the Earth near the speed of light [42]. These ionizing particles (primarily protons and electrons) can become trapped in the Earth's magnetosphere and form what is known as the Van Allen Belts. These bands of radiation can pose significant hardness assurance concerns for satellites orbiting the Earth as the flux of electrons and protons in these bands are extremely high. Fortunately for humans, the Earth's magnetosphere provides excellent isolation of solar particles from reaching the surface, as shown in Fig. 4.7. This magnetic field trapping mechanism is not unique to the Earth and is present at any planet or moon with a magnetosphere. The stronger the field the more effective the magnetosphere is at protecting the host body from radiation. However, the stronger field also enhances the energy of the trapped particles making radiation a more serious concern.

Outside of solar events, the most significant contribution to the space radiation environment is galactic cosmic rays (GCRs). GCRs are extraordinarily-high energized particles that exist at low fluxes in space. Particles at extremely high energies cannot easily be stopped by traditional shielding techniques and can cause upsets or dose effects in microelectronics. These particles do not originate from the Sun and are

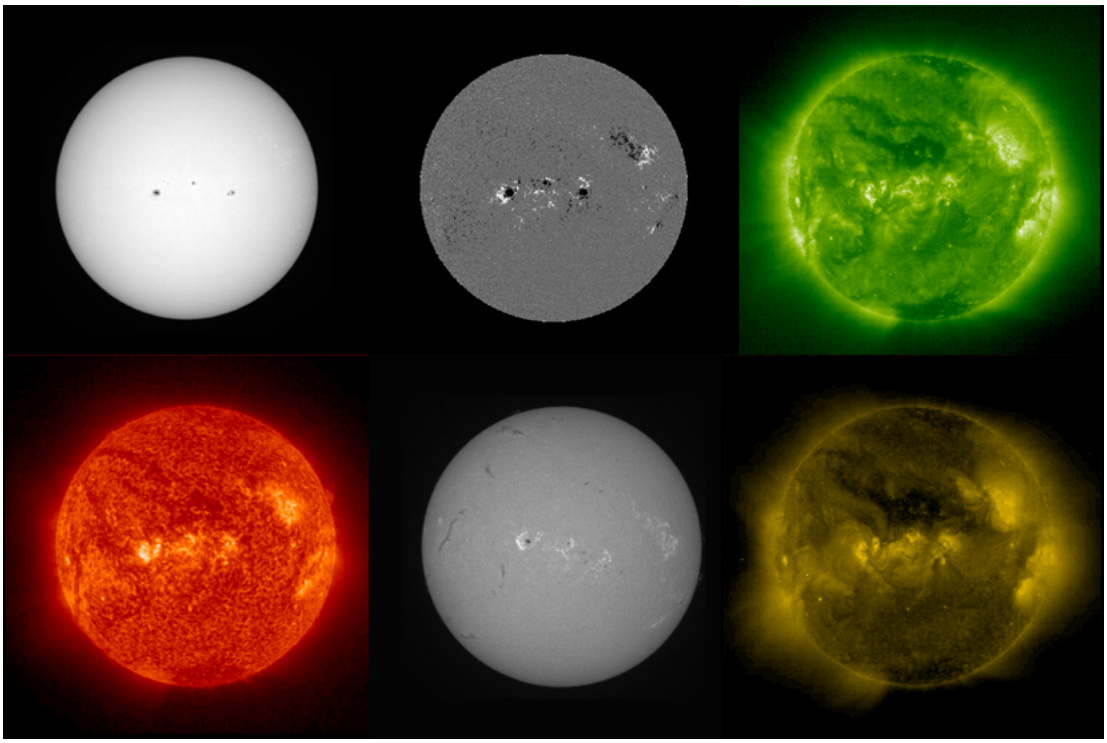

Figure 4.6: Sun with hotspots [43] at various wavelengths. More hotspots tend to correlate to higher solar activity.

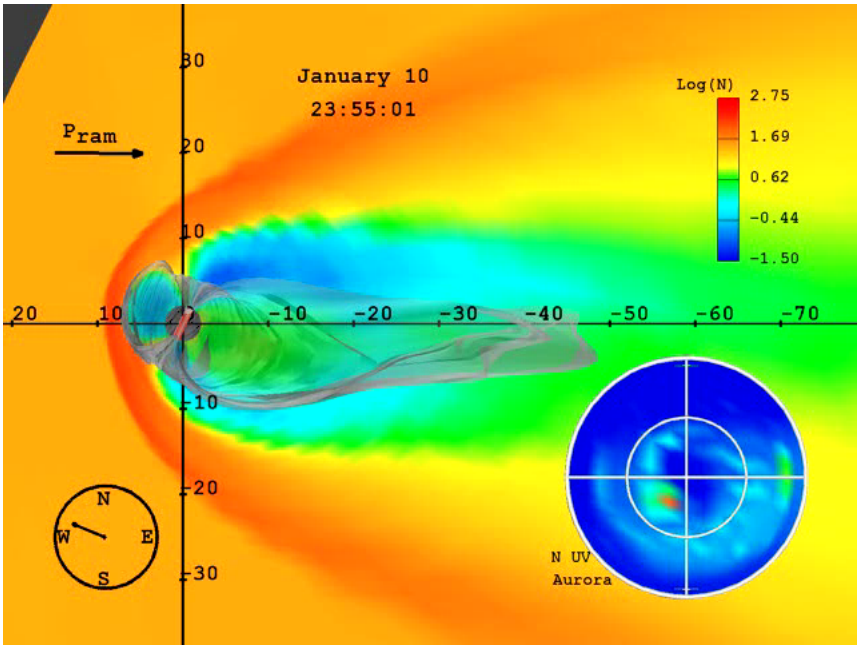

Figure 4.7: Earth's mag field compressing as being blasted by solar particles. [43]

rather believed to originate outside of our galaxy. Theories to explain the existence of these particles vary. However, most people believe these particles are a result of two contributing factors: 1) the death of stars resulting in supernova and 2) the beginning of the universe and the Big Bang. GCRs, although low in number, have a significant impact on electronic design for space radiation. It is interesting to note that these GCRs give rise to the static temperature of deep space (around 2.7 K). GCRs are more prevalent in the near-Earth space environment for satellites maintained at a highly inclined orbit as the magnetosphere less effectively shields radiation at the Earth's poles.

It is very important to mention that radiation environments in the solar system are extremely dynamic and are closely coupled to the solar activity on the Sun. It is impossible to know the exact dose that a given spacecraft or flight system will experience over the duration of its mission. Most radiation simulators (example shown in the next section using SPENVIS [44]) base calculations off of a worst case analysis such as assuming that a given orbital environment will look like a limiting case such as the October 1989 solar event (worst recorded solar storm using modern detection techniques). Even with such assumptions a given design margin of 1.5 to 4X is normally defined to ensure that a rare solar event will not lead to mission failure. Efforts have gone into monitoring solar activity as a way to have a predictive method to prevent radiation-induced damage – however, such approaches are in their infancy and have not proven an effective method to prevent electronic degradation.

Most space missions involve radiation shielding of some sort on board. The simple idea being to use some material (i.e. aluminum) to slow down or completely block an ionized particle. Although shielding will not be able to stop all highly energized GCRs, it is quite effective at preventing a substantial amount of total ionizing dose damage due to low energy protons and electrons. As such, electronics are normally contained within a "warm box" where parts are shielded and kept at an ambient temperature to

ensure proper operation. However, warm boxes are bulky and limit where electronics can be placed on board a spacecraft. Studies have proven that even modest amounts of aluminum shielding can drastically reduce the amount of TID for a given mission lifetime. For example, Bhat in [45], showed that 7 mm of Al results in less than 1 krad of dose over 500 days, whereas the accumulated dose with 2 mm of Al results in about 60 krad over the same time period. This is a substantial difference in dose and shows how the addition of shielding can be used to meet mission specifications for radiation dose at a cost to added size and weight. Electronic component placement is just as important as intentional shielding. Other circuits and systems may be used as additional shielding for components which are more sensitive. The idea being to put as much 'stuff' as possible in between the point of incidence of the radiation and the sensitive volume. It is important to note that shielding is not the only effective method to reduce the overall mission dose. Spacecraft trajectories can be set at highly elliptical orbits for certain science objectives. When done correctly (i.e. having a majority of flight time outside of high radiation flux regions) such a strategy will reduce the exposure time for sensitive instruments.

One of the most interesting applications for SiGe HBTs is space-based missions at Jupiter and its moons (see Fig. 4.8). Due to the extremely large magnetosphere of Jupiter (see Fig. 4.9), the radiation environment at Jupiter and its near vacinity is extremely harsh. The expected radiation dose for such missions, with much of the dose being imparted by high-energy electrons, is much higher than near-Earth missions with multi-Mrad(SiO_2) of dose being easily achieved. According to the Jet Propulsion Laboratory (JPL), the upcoming Europa Clipper mission, scheduled to launch in 2022, will need to tolerate around 3 Mrad(SiO_2) of accumulated dose after 100 mil of Al shielding for non-vault electronic components [46]. Such a high radiation tolerance is rare for microelectronics and primes SiGe HBTs as a highly desirable solution to on-board analog and RF circuit components for such missions.

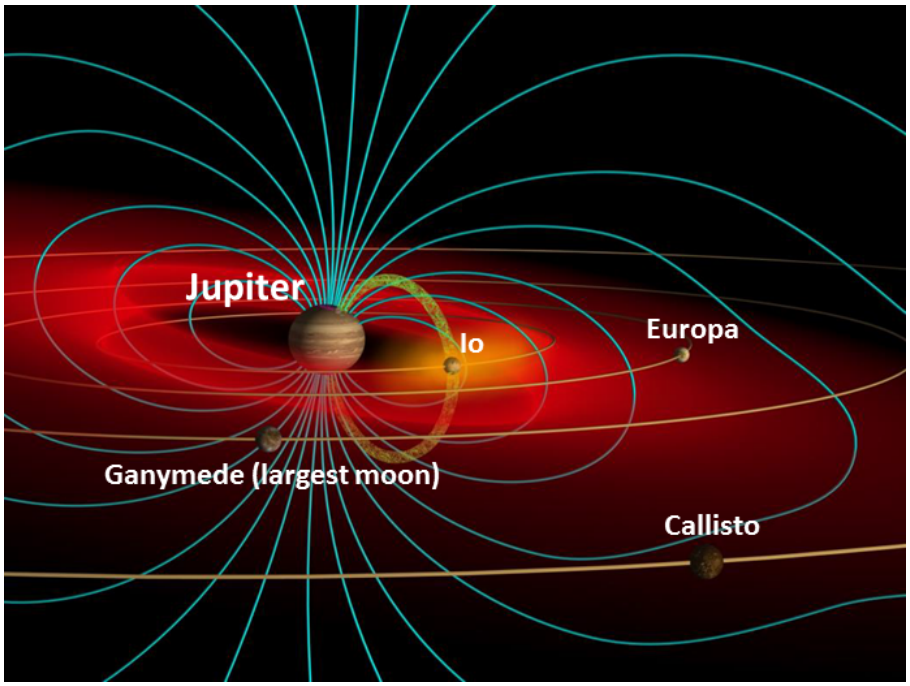

Figure 4.8: Jupiter's magnetic field is enormous and contains a high flux of high energy electrons [46]. Shown in the figure are the four Galilean moons which are key targets for future scientific study.

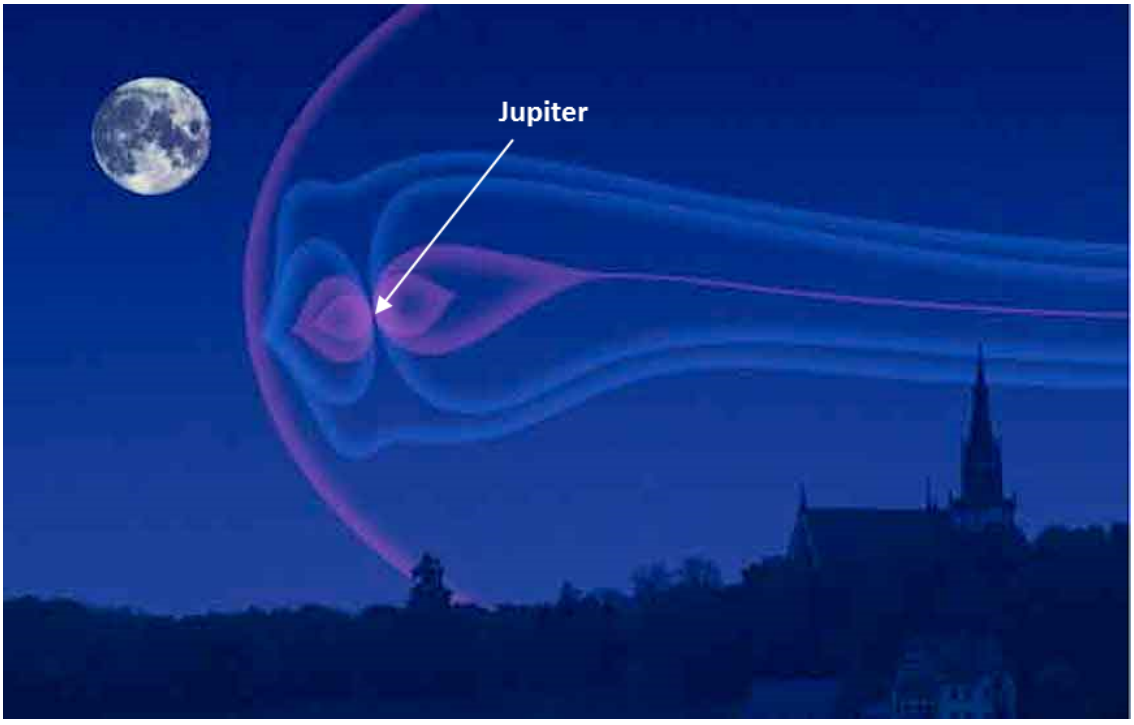

Figure 4.9: Jupiter's magnetic field is enormous and if visible could be easily seen from the Earth [47].

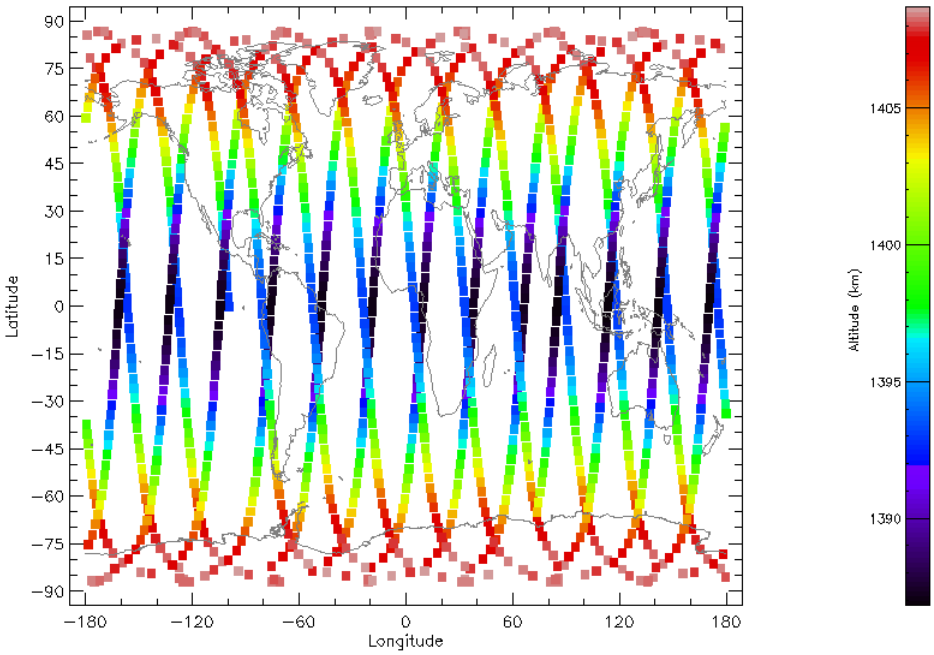

Figure 4.10: SPENVIS generated orbit map for a satellite operated in low-earth orbit at a high inclination (trajectory approaching the poles).

4.3 Modeling Near-Earth Space Environment

Simulation software is often recruited to give an indication of how many particle events are expected over the course of a space mission. The flux, energy, and type of those particles will determine how much dose is imparted into the electronics for a given orbital trajectory (example trajectory of a high inclination orbit shown in Fig. 4.10). In addition the impact of shielding may be accounted for to determine the resulting dose. Dose expectation for a LEO orbit is shown in Fig. 4.11. This simulation accounts for the dose imparted by solar and trapped protons, electrons, and Bremsstrahlung radiation. Bremsstrahlung radiation, also known as braking radiation, is associated with photon emission that occurs as particles are stopped in shielding layers. Such models use information based off of satellite dosimeters from the past, not current readings. Simulation software such as SPENVIS and CREME96 [44, 48] may be used in such a fashion to help provide predictive means to determine

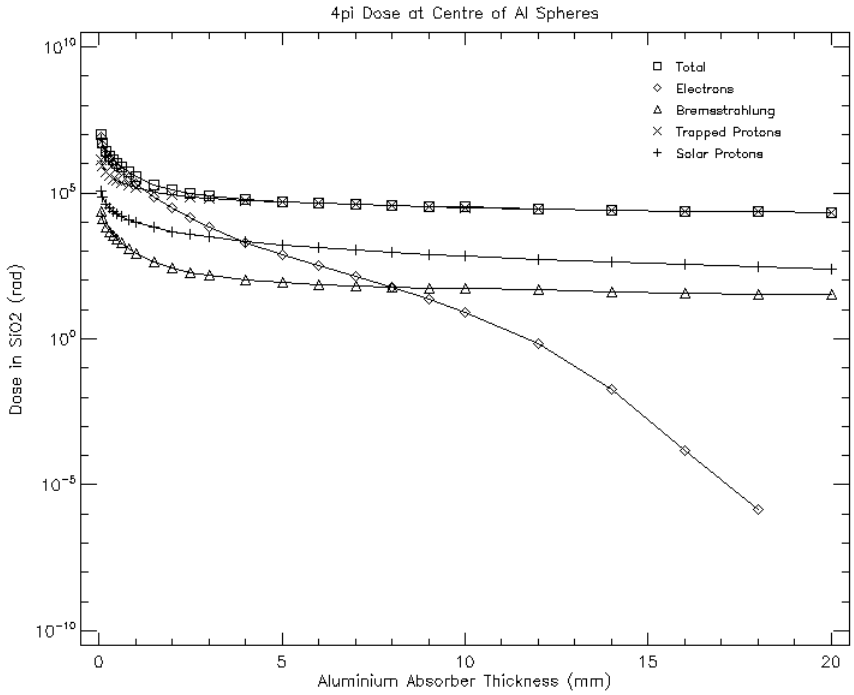

Figure 4.11: Total dose as a function of Aluminum shielding thickness. This figure is generated in SPENVIS and shows the contributions of electrons, protons, and x-rays to the total dose for a satellite mission at low-earth orbit.

how much radiation, and at what doses/fluences, is expected over the course of a space mission.

4.4 Experimental Facilities and Methods

There are a number of terrestrial radiation effects testing facilities in the U.S. and abroad. For this work, testing was conducted at the following facilities: UC Davis (63 MeV proton testing), Lawrence Berkeley National Laboratory (LBNL, 10 MeV/nucleon heavy-ion testing), GANIL (heavy-ion testing), GSI (focused heavy-ion testing), Vanderbilt University (10 keV X-ray testing), Argonne (focused X-ray testing), and the Naval Research Laboratory (NRL for two-photon absorption, 1260 nm pulsed laser testing and Co-60 gamma ray testing). Pictures from the facilities are shown in Fig. 4.12. Each experimental facility has its own unique setup and capability. Experimental setups are defined throughout the course of this thesis and results are presented

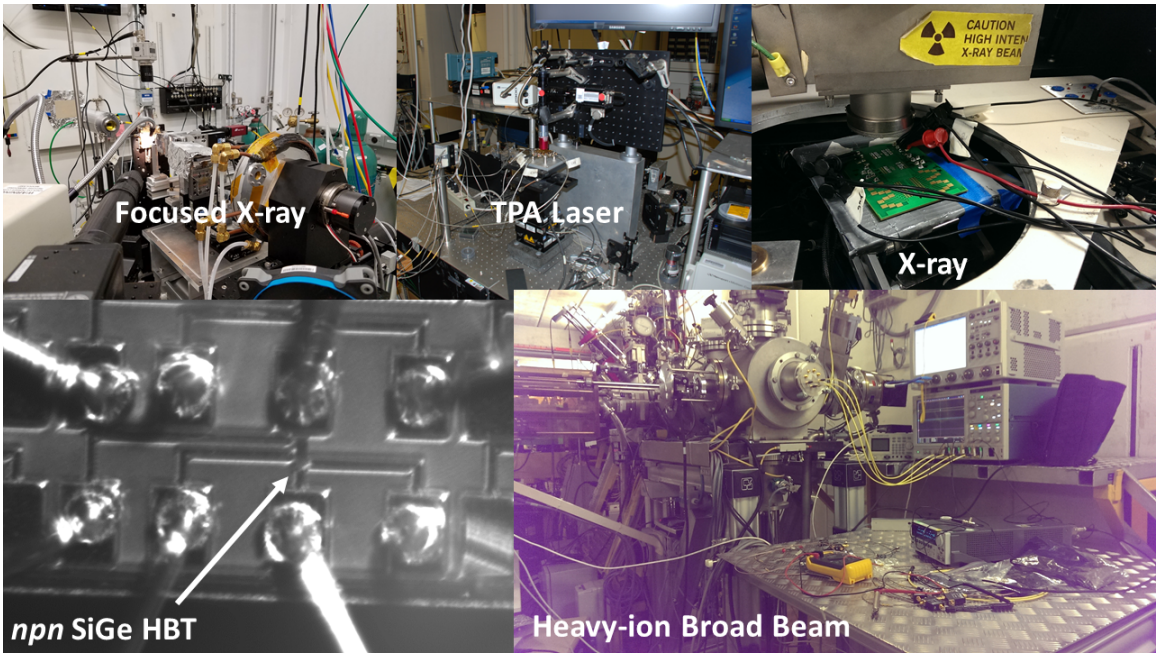

Figure 4.12: Shown are a number of pictures taken at different testing facilities (Argonne National Labs, Naval Research Laboratory, Vanderbilt University, and GANIL).

in the following chapters.

CHAPTER 5

TID IN A BICMOS TECHNOLOGY

5.1 Introduction

In the past decade Silicon-Germanium (SiGe) BiCMOS technology has been investigated as a potential candidate for highly reliable, space-capable electronics [49]. Bandgap-engineered SiGe HBTs exhibit excellent low temperature characteristics and are highly tolerant to total ionizing dose (TID) radiation without modification to the device structure, all while being inexpensively integrated into established CMOS technology nodes, making them ideal for highly-integrated system applications [49]. Total ionizing dose damage is a major reliability concern for electronics used in extreme environments. The radiation-induced damage may increase off-state leakage current in both SiGe HBTs and CMOS devices, and may also cause threshold voltage shifts in CMOS. Depending on the application, such damage may lead to circuit failure. Previous studies on the TID tolerance of IBM SiGe BiCMOS processes have shown multiple generations of SiGe HBTs to be total-dose hard as fabricated to multi-Mrad(SiO_2) levels [50–53]. Additional studies have focused on the CMOS devices fabricated together on-die with these SiGe HBTs (to form the BiCMOS platform), but only evaluating the TID response up to a few hundreds of krad(SiO_2) [7], which is sufficient for most orbital missions. However, some emerging deep space exploration missions, specifically those involving the outer planets and their moons (e.g., Jupiter's moon Europa), will require demonstrated long-term reliability in a multi-Mrad radiation environment for any components operating outside of the shielded electronics vault [11].

The present work evaluates the TID tolerance of Jazz Semiconductor's 180 nm

SiGe BiCMOS (SBC18-HXL, with 150 GHz peak f_T) process technology and its potential suitability for multi-Mrad operation needed to support future space missions and other extreme environments which experience high amounts of total ionizing dose. This technology is a triple-well variant of the standard substrate process presented in [53], which showed a preliminary evaluation of the SiGe HBT proton tolerance. The present work was performed as part of a greater effort to evaluate the feasibility of developing an unshielded focal plane array (FPA) for use in proposed Europa exploration missions [11, 54, 55]. These FPAs can be used for infrared detection without the need for a shielded warm-box, and require a full suite of p-type and n-type MOSFETs in addition to SiGe HBTs. Due to the die area and pitch/density requirements of pixel arrays, the use of annular MOSFETs for TID damage mitigation is unlikely to be feasible due to increased area consumption. We demonstrate that the conventional CMOS devices implemented in this process show better-than-expected total dose tolerance, even up to the 6 Mrad(SiO_2) dose, an objective that is also achieved by the SiGe HBTs. The radiation response of the CMOS devices shows a marked improvement over the previously published response of similar SiGe BiCMOS technology at an identical lithography node [7]. These findings further reinforce the utility of SiGe BiCMOS technology for use in space applications, particularly for deep space exploration where unshielded sensing and detection electronics are required.

5.2 Experimental Details

Minimum length (180 nm) CMOS devices (both nFET and pFET) of varying widths and SiGe HBTs of various emitter geometries were irradiated up to 6 Mrad(SiO_2) using a 10-keV X-ray source at a dose rate of 525 rad(SiO_2)/s. The devices were measured at intermediate dose points immediately following irradiation. A second set of nFETs and SiGe HBTs were also irradiated up to an equivalent 3 Mrad(SiO_2) using the 63-MeV proton source at UC Davis at a dose rate of 1 krad(SiO_2)/s, which has

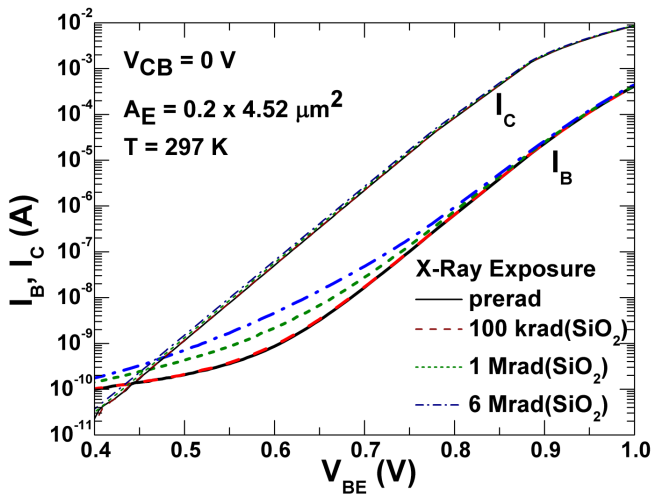

Figure 5.1: Forward Gummel characteristics of the Jazz SiGe HBT, showing radiation-induced degradation. © 2014 IEEE.

been described in [8]. The nFETs were measured at intermediate dose immediately following irradiation. For both experiments, all FETs were biased with the maximum rated gate voltage applied and all other terminals grounded (worst case condition), and all SiGe HBTs were irradiated with all terminals grounded (again, worst case condition).

5.3 SiGe HBT Radiation Response

Fig. 5.1 shows the response of an irradiated SiGe HBT. Past studies have shown that the primary degradation mechanism in the forward characteristics of a SiGe HBT is the generation of traps at the EB spacer oxide/EB space charge region interface [20]. These traps in the EB spacer oxide generated by the ionizing radiation result in excess recombination current with a characteristic $2kT$ slope. This excess non-ideal base current was observed after both the X-ray and proton exposures. The X-ray induced base current is shown in Fig. 5.2.

The magnitude of the excess base current is positively correlated with increasing emitter area. Fig. 5.3 illustrates a logarithmic dependence on the drawn emitter width for the non-ideal base current component, rather than a strong dependence on

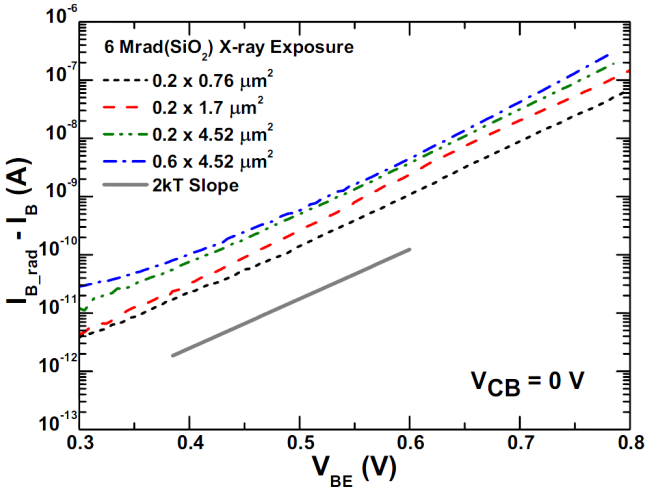

Figure 5.2: Excess base current in SiGe HBTs of various geometries after 6 Mrad(SiO_2) X-ray exposure. © 2014 IEEE.

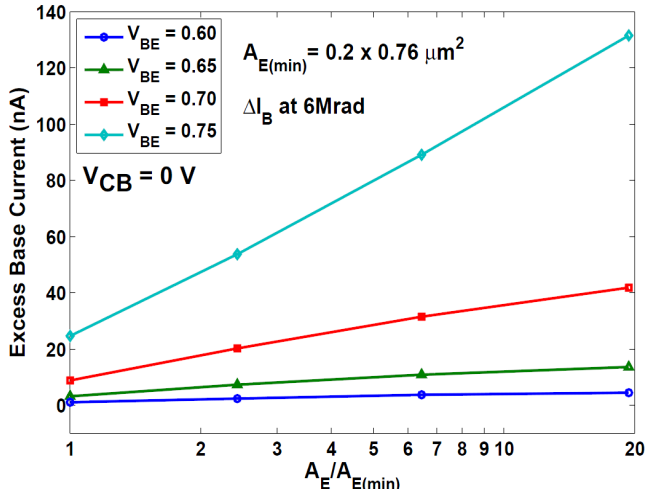

Figure 5.3: Relation of excess base current to drawn emitter area (normalized to the area of minimum geometry device) at 6 Mrad(SiO_2). © 2014 IEEE.

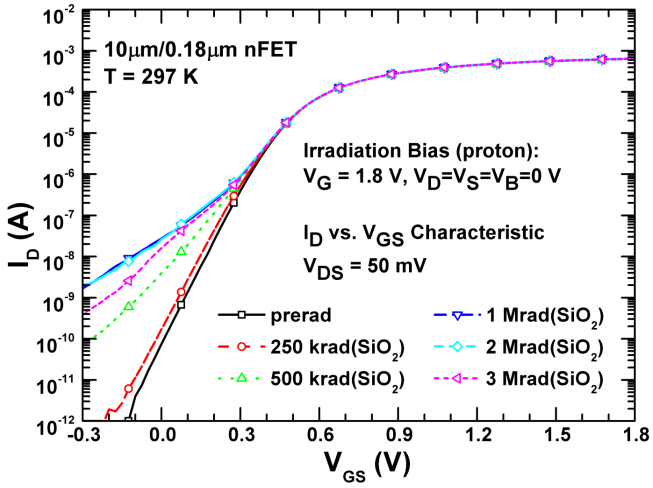

Figure 5.4: Proton-induced degradation of nFET subthreshold characteristics at low V_{DS}. © 2014 IEEE.

perimeter-to-area ratio (P/A) at high dose, as seen in previous work [29], indicating generation of traps throughout the entire emitter area of the device. The data from both X-ray and proton exposures (not pictured) indicate that SiGe HBTs with wider emitter stripes are more resistant to current gain degradation than narrow stripe devices, and that reducing the P/A had some positive effect on the TID tolerance of the devices. In most SiGe technologies, the emitter stripe width is a fixed parameter, so this effect is not observable. However, this platform allows for the use of three distinct emitter widths. Wide emitter devices have slightly higher parasitics, but offer better radiation hardness due to the minimization of the P/A. This allows greater flexibility in designing radiation tolerant circuits, and further increases the utility of this SiGe technology platform for use in unshielded, Mrad-hard electronics.

5.4 CMOS Radiation Response

Fig. 5.4 shows the total dose response of the drain current of a wide (10 μm/0.18 μm) nFET at low V_{DS} as the gate-source voltage is swept. The X-ray and proton responses of all FETs were similar, with the proton exposure resulting in slightly greater degradation. The lack of threshold voltage shift (see Fig. 5.5) for large

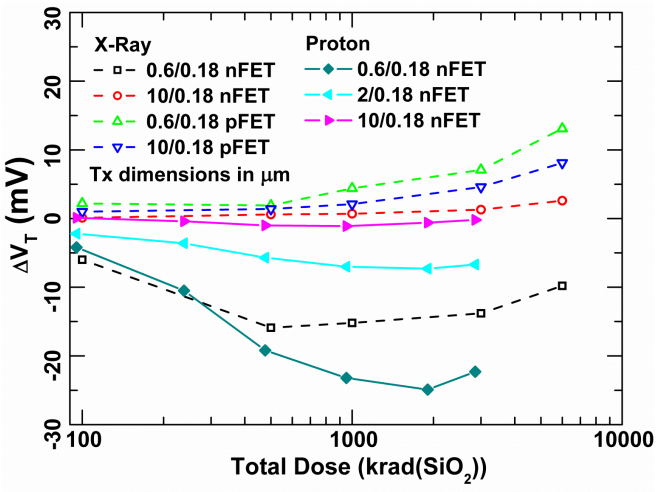

Figure 5.5: Radiation-induced threshold voltage shifts in CMOS transistors. © 2014 IEEE.

devices, even at these very high doses, indicates that there is very little net charge trapping in the gate oxide. The observed degradation is therefore caused primarily by charge in the shallow trench isolation (STI) oxide and its interface with the channel region. For comparison, the response of an identically-sized nFET from a comparable 180 nm SiGe BiCMOS platform (published in [7]) is shown in Fig. 5.6. The change in off-state leakage current for the given technology can also be seen in Fig. 5.7.

The two devices show significantly different degradation characteristics, with the leakage of the nFET from the present technology showing a much stronger V_{GS} dependence. The previously published device response also shows a more classical off-state leakage characteristic independent of V_{GS}, consistent with charge trapping deep along the STI edge, which creates a parasitic inversion channel far removed from the upper STI corner, inducing a shunt leakage path between source and drain. Previous studies have also shown that STI corner leakage causes a sub-threshold "hump" in the I_D-V_{GS} characteristics, while "deep" STI leakage results in a flat, constant leakage current [56, 57]. In [57], a strong dependence of the leakage characteristics on the spatial distribution of the charge in the STI and at the STI/bulk Si interface was reported, potentially offering insight into the differences between the two technologies.

The factors responsible for the different responses of the nFETs from two different SiGe BiCMOS technologies with comparable lithography (180 nm) and performance may include both doping and structural differences. Higher doping concentrations reduce the susceptibility of the well-to-STI edge inversion, and as a triple well process, the present technology will have a uniquely defined doping profile. The p-wells used for the nFET devices are intended to provide device isolation and individual control over body potentials, but the doping control also provides a benefit to the TID response.

The physical structure of the STI dictates the electric field contours and gate-STI interactions and will also dictate the TID response. One known difference between the two BiCMOS platforms is the shape of the STI oxide. In the present BiCMOS technology, the STI exhibits both a slightly recessed top surface (the gate dips down as it crosses the STI channel edge) and a retrograded, or inward-sloped, shallow trench edge. Other STI profiles like those found in [7] feature a nearly vertical profile. This difference in STI structure is likely to influence the mechanical stress on the STI oxide, which may affect charge trapping and TID response [58].

Figs. 5.8-5.9 show the leakage characteristics for a narrow and wide nFET, respectively, at high V_{DS}, and Fig. 5.5 shows the threshold response (extracted by extrapolating to zero from the linear region of the I_D-V_{GS} curve) of all irradiated CMOS devices. Additionally, Fig. 5.10 shows the X-ray response of a narrow nFET, which, contrasted with Fig. 5.8 highlights the two major differences between the proton and X-ray exposures.. The first difference is the increased degradation seen in the proton exposure, and the second is the "turn-around" effect that is seen in both exposures. Unlike X-ray exposure, the proton exposure results in noticeable lattice damage which leads to the slightly increased degradation [12]. This result is not unexpected and as such will not be discussed further and more attention and analysis will instead be put on the other difference.

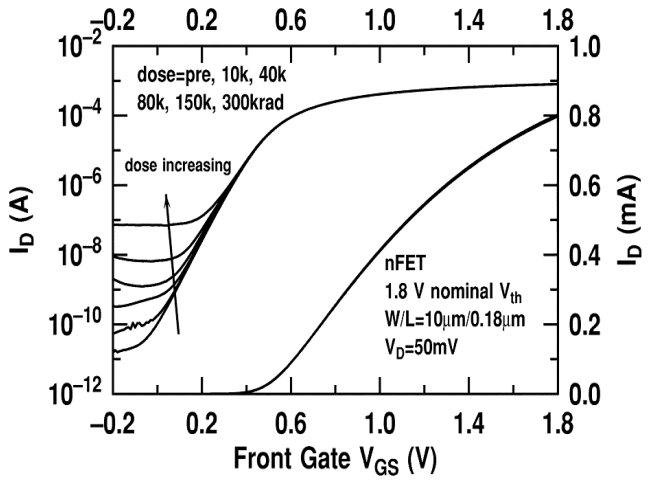

Figure 5.6: Previously-published TID response of nFETs implemented in a different 180 nm SiGe BiCMOS platform (after [7]).

This other difference, a key feature of this device's TID response, is the apparent "turn-around" effect seen in both irradiations (around 2 Mrad in the proton case and 1 Mrad for the X-ray case). This effect is marked by an initial increase in the degradation up to a certain "saturation" point and the subsequent reversal of the degradation past this point. This "turn-around" effect is observed at different levels of total dose due to the sources used. The difference in dose rates and the particles themselves will contribute to a difference in the charge yield in the devices and thus a varying TID response. The device irradiated with the low energy X-rays (10-keV) may also experience some level of "dose enhancement" [12]. This effect is seen in thin oxides irradiated by low-energy X-rays and is marked by an increased oxide dose. This "dose enhancement" along with the source differences causes the apparent acceleration of the "turn-around" effect in the X-ray irradiated device.

The STI leakage effects cause an apparent threshold voltage shift in the small devices, a result of radiation-induced narrow channel effects, as described in [9], since the edge structure and hence magnitude of the leakage current is roughly the same regardless of transistor width. The previously mentioned "saturation" or "turn-around" effect observed in the nFETs at high dose levels results from charge building up at

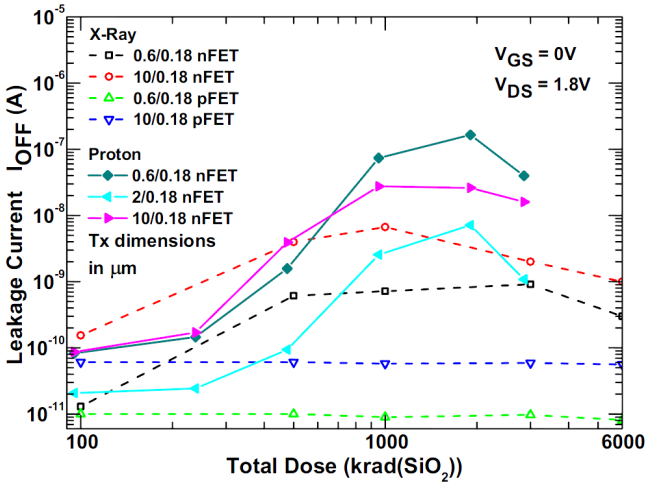

Figure 5.7: Radiation-induced off-state leakage current at high V_{DS}. © 2014 IEEE.

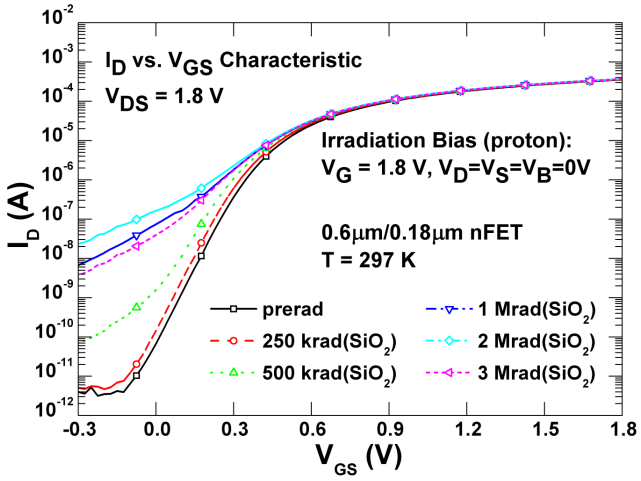

Figure 5.8: Proton induced degradation in narrow nFET at high V_{DS}=1.8 V. © 2014 IEEE.

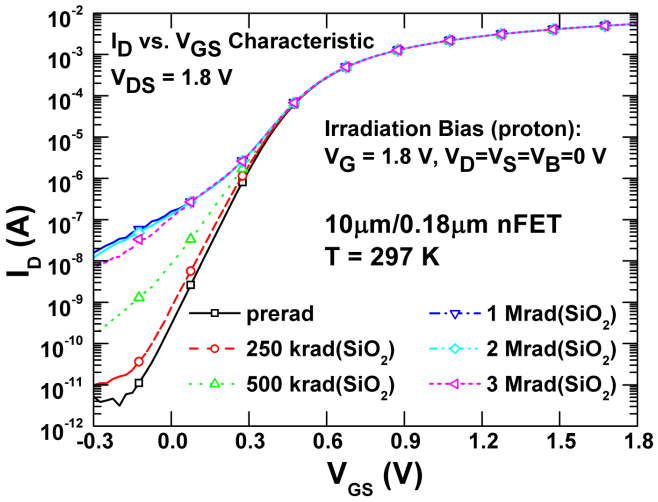

Figure 5.9: Proton induced degradation in wide nFET for V_{GS}=1.8 V. © 2014 IEEE.

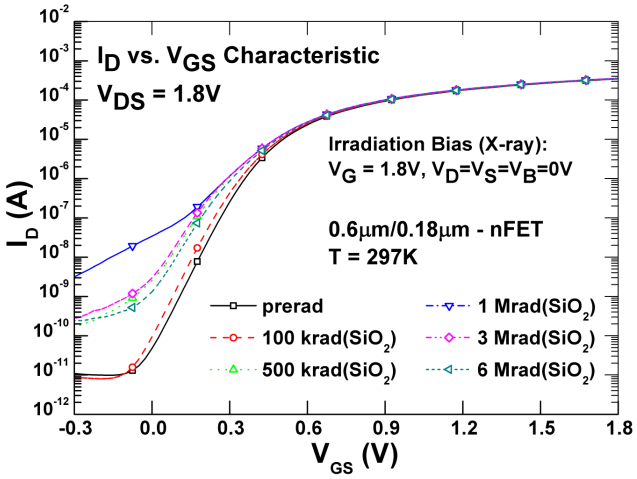

Figure 5.10: X-ray induced degradation in narrow nFET at V_{DS}=1.8 V. © 2014 IEEE.

the oxide/Si interfaces. The radiation-induced interface charges are negative for a p-substrate (nFET) and positive for an n-type substrate or well (pFET) and form at a different rate than bulk STI oxide charges, which are responsible for the degradation at low values of total dose. In the pFETs, the positive interface charge reinforces the effect of the positive bulk STI charge, resulting in a slight increase in threshold voltage, the only observed degradation seen in the pFETs at high total dose. In the nFETs, however, the interface charges are negative and counteract the positive bulk

oxide charges at high total dose values [10], improving the total dose tolerance of the nFETs under these irradiation conditions. An additional buildup of interface traps at lower dose rates would decrease the leakage further [59].

Other circuit-relevant FET parameters, such as transconductance and on-state current, did not show any appreciable degradation or shift above threshold even up to 6 Mrad(SiO_2) dose, and the output characteristics of a wide nFET and pFET (Fig. 5.11) also show very little degradation up to 6 Mrad(SiO_2), again a favorable result.

5.5 Summary

The total ionizing dose response of a Silicon-Germanium BiCMOS platform has been evaluated. The SiGe HBT TID response is shown to be similar to that of previously published technologies, and unique emitter geometry effects are discussed and highlighted. The CMOS devices are shown to have negligible transconductance or on-current degradation, even at multi-Mrad dose levels, and STI leakage levels of the n-type devices demonstrate substantial improvement over previously characterized SiGe BiCMOS compatible nFETs. Together, these results demonstrate that the full SiGe BiCMOS platform is capable of functioning at the extreme dose levels needed

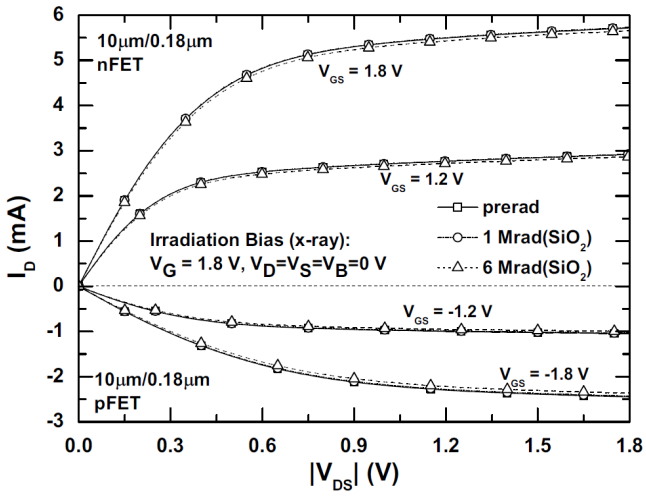

Figure 5.11: Output characteristics of wide nFET and pFET after X-ray exposure. © 2014 IEEE.

for operation in an unshielded space environment.

CHAPTER 6

ELDRS IN SIGE HBTS

6.1 Introduction

Radiation testing facilities permit electronics to be rapidly analyzed for radiation hardness assurance to total ionizing dose (TID) and single event effects (SEE). Most TID studies involve irradiation at dose rates > 50 rad(SiO_2)/s, which is much higher than would be expected in space or many extreme environments [12]. Using higher dose rates for testing saves valuable time and resources. Some integrated circuits (ICs) require low dose rate (LDR) ≤ 10 mrad(SiO_2)/s radiation testing to ensure that latent dose-rate dependent degradation mechanisms are not masked by high dose rate (HDR) irradiation. Most ICs show good agreement between high and low dose rate accumulated TID damage, and as such, radiation effects engineers are justified in their use of high dose rate sources. Unfortunately, some ICs are susceptible to enhanced low dose rate sensitivity (ELDRS). Simply stated, an ELDRS-sensitive device (normally a bipolar transistor) appears to experience significantly more degradation at a LDR than the same device experiences at the HDR, for an equivalent total dose. Numerous studies have been conducted in regards to this occurrence. The community consensus is that the devices are not experiencing increased degradation at the low dose rate but are rather experiencing a suppression of damage in the higher dose rate irradiation [62–64]. This scenario is clearly a major concern for ICs intended for extreme environments such as space, since the radiation tolerance of susceptible devices can be drastically overestimated, potentially resulting in circuit failure much sooner than expected.

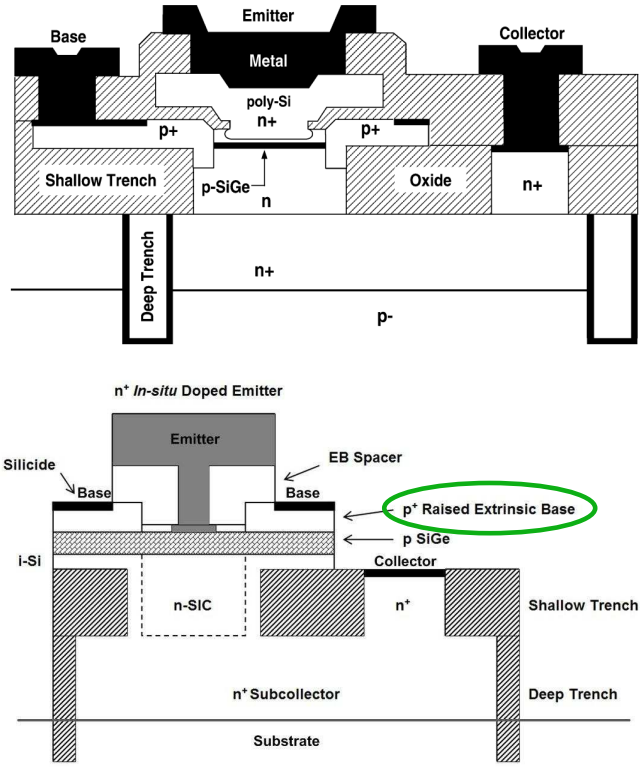

Figure 6.1: Schematic cross-sections of a 1st-generation SiGe HBT (top) [60] and a 4th-generation SiGe HBT (bottom) (after [61]). A key difference (circled on the bottom figure) is the raised extrinsic base in the newer device structure.

Table 6.1: Parameter Scaling by Generation

Parameter	Units	1st	2nd	3rd	4th
Lith Node	nm	500	180	130	90
WE,eff	μm	0.42	0.18	0.12	0.09
Peak β	-	100	200	400	550
BV_{CEO}	V	3.3	2.5	1.7	1.4
BV_{CBO}	V	10.5	7.5	5.5	5
Peak f_T	GHz	47	120	207	300
Peak f_{MAX}	GHz	65	100	285	350

Over the past twenty years, Silicon-Germanium Heterojunction Bipolar Transistors (SiGe HBTs) have emerged as a serious contender for many analog and RF applications. However, very few studies have been conducted to determine whether dose rate has a major impact on degradation mechanisms in this relatively new type of bipolar device [65–67]. It is widely believed that the underlying reasons behind the TID robustness of the SiGe HBT (vertical transport with thin spacer oxides) also lead to a robustness to ELDRS effects [20]; however, no prior study has thoroughly investigated the topic.

No state-of-the-art SiGe HBT (4^{th}-generation with peak $f_T > 300$ GHz) has undergone ELDRS hardness assurance testing. Discernible changes in fabrication have been made for 4^{th}-generation SiGe HBTs in order to improve performance. Those changes include: thinner base and collector profiles, changes to vertical and lateral profiles, and an improved device structure that minimize parasitics associated with the collector-base (CB) junction [68]. In addition, the technology uses rotated wafers, novel emitter contact technology, and reduced thermal cycles [68]. A 2D cross-section of this new structure is compared to a 1^{st}-generation device in Fig. 6.1. Key parameter changes across generations, along with the corresponding lithography node, is also provided in Table. 1. It is uncertain whether changes in fabrication will lead to changes in damage mechanisms at low dose rates. SiGe HBTs are well known for

having an impressive inherent tolerance to TID damage (multi-Mrad) – making them prime candidates for many space applications [20]. Any deviation from this trend of TID robustness would be extremely detrimental to their contention for use in extreme environments.

The aim of the present investigation is to analyze the effects of dose rate on state-of-the-art, 4^{th}-generation, SiGe HBTs at both the device and circuit level, and determine whether or not the newest SiGe BiCMOS (Bipolar and Complementary Metal Oxide Semiconductor) technologies are susceptible to deleterious dose rate effects such as ELDRS. The data presented in this paper, to the authors' knowledge, contains the first circuit study of ELDRS in SiGe HBTs. In addition, this work provides the first investigation of low dose rate effects in 4^{th}-generation SiGe HBTs. Measurements from previous devices generations (1^{st} and 3^{rd}) have also been conducted to expand the analysis across multiple device generations. A discussion is provided that includes past findings on 2^{nd}-generation SiGe HBTs [69] that only not only covers all major technology generations but also provides insight into the future of low dose rate effects for the SiGe HBT.

6.2 ELDRS

Enhanced low dose rate sensitivity (ELDRS) was first identified as a hardware assurance concern for bipolar devices by Enlow *et al.* in 1991 [14]. Since the discovery of the effect, many studies have been conducted to identify ELDRS sensitive parts and to understand the phenomenon. Initial findings by Johnston *et al.* showed that the relative damage of ELDRS parts could be as much as 6 times larger than parts irradiated at higher dose rates of ≥ 50 rad(SiO_2)/s [70]. The ratio of relative damage for ELDRS parts is known as the "enhancement factor" (EF). This term describes how much more sensitive the part is to damage at low dose rates when compared to higher dose rate damage [70, 71]. ELDRS is most commonly a *pnp* device issue; however,

npn devices may also experience ELDRS. A compendium of ELDRS sensitive parts through 2008 may be found in [72].

ELDRS is a "true" dose rate effect (TDRE) and is different from time dependent effects (TDE) traditionally seen in metal oxide semiconductor (MOS) devices irradiated at low dose rates. When comparing circuits irradiated at high and low dose rates, time dependent effects are identified by following a high dose rate irradiation with a room temperature anneal up to the (longer) irradiation time for the low dose rate experiment. In the case of a TDE, the degradation between the low dose rate irradiation and the high dose rate irradiation with the subsequent anneal will be very similar. However, in the case of a TDRE, a disparity in the degradation between the high and low dose rate irradiations will exist even when accounting for annealing [64]. Due to the long time period associated with low dose rate testing, it is not always feasible to increase testing time to account for annealing effects, and because of this, the enhancement factor used in ELDRS testing is based off of measurements taken immediately after irradiation for both the high and low dose rate experiments. The enhancement factor used to compare high and low dose rate degradation will include time dependent effects in addition to possible true dose rate effects such as ELDRS [73]. However, previous studies have shown the calculation of the enhancement factor to be an effective method to determine ELDRS sensitive parts [73].

Enhanced low dose rate sensitivity is a major concern for oxides with high defect densities [59]. These defects can be introduced during oxide growth or may be introduced during passivation in the form of hydrogen as a contaminant [59, 64].The amount of hydrogen introduced to the device and the subsequent interactions of hydrogen can impact the buildup of interface traps at sensitive regions of the device [13, 74]. Additionally, the type of packaging used for a given part may have trace amounts of hydrogen and impact the resulting dose rate response [75].

ELDRS is a potential issue in oxides irradiated at low electric fields [59]. For this

reason, bipolar devices irradiated with terminals grounded may be ELDRS sensitive. MOS devices normally experience maximum degradation from TID when irradiation occurs with rated voltage across the gate. This bias condition creates a much stronger electric field and prevents the presence of ELDRS in the vast majority of MOS devices [73]. However, recent studies have shown that low electric fields within MOS devices, particulary within the shallow trench isolation, may exhibit enhanced degradation at low dose rate irradiation [76–78]. Such studies show that ELDRS is not only a bipolar device concern.

6.3 ELDRS in SiGe HBTs

Total ionizing dose damage in SiGe HBTs is well documented and understood [20]. The radiation-induced damage is marked by an excess leakage base current that results from a build-up of radiation-induced traps in the emitter-base (EB) spacer region. Increased base leakage current degrades current gain at low injection [20]. The result of this damage can be seen in the Gummel characteristics from Lourenco *et. al.* shown in Fig. 6.2 for 4^{th}-generation SiGe HBTs [68]. Due to the vertical profile and the thin EB spacer oxide, SiGe HBTs are, in general, inherently multi-Mrad TID tolerant as built.

Nearly all TID studies on SiGe HBTs are conducted using high dose rates, as dose rate effects are not considered a major hardware assurance concern [20]. In 2009, however, SiGe HBT hardness assurance testing was re-evaluated by Cheng *et al.* in [65] for first-generation SiGe HBTs (IBM 5AM). Some unexpected results were observed in the irradiated hardware. The results in this study suggest that some first-generation *npn* SiGe HBTs could in fact experience shifts in collector current as high as 12% under LDR irradiation. Collector current shifts are an unexpected TID result and could indicate a real effect that is masked by high dose rate irradiation. Changes in collector current can drastically impact operation of both analog and RF circuits

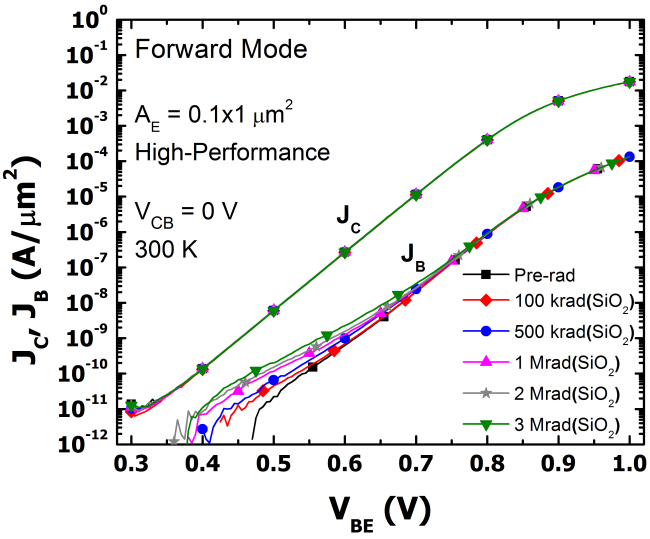

Figure 6.2: Gummel characteristic of 9HP SiGe HBT up to 3 Mrad(SiO_2) [68]. © 2014 IEEE.

and would indicate an overlooked and quite serious hardware assurance concern for SiGe HBTs, thus making it important to investigate further.

6.4 Experimental Details

One of the major challenges in conducting low dose rate experiments is the time involved in accumulating a significant amount of total ionizing dose. An accumulated dose of 100 krad(SiO_2) takes only minutes using a high dose rate X-ray or proton source. However, reaching the same equivalent dose using a low dose rate source $\leq$ 10 mrad(SiO_2)/s takes months. For the present study, both low and high dose rate experiments were conducted at the NASA Goddard Spaceflight Center (GSFC) Radiation Effects Facility (REF). The exposures were made using a gamma source at a dose rate of 50 rad(SiO_2)/s and 10 mrad(SiO_2)/s for the high and low dose rates, respectively.

Individual devices were selected from 1st, 3rd, and 4th-generation Silicon-Germanium HBTs. These devices were all manufactured by IBM and correspond to the 5AM, 8HP, and 9HP BiCMOS technologies, respectively. The devices were irradiated up to

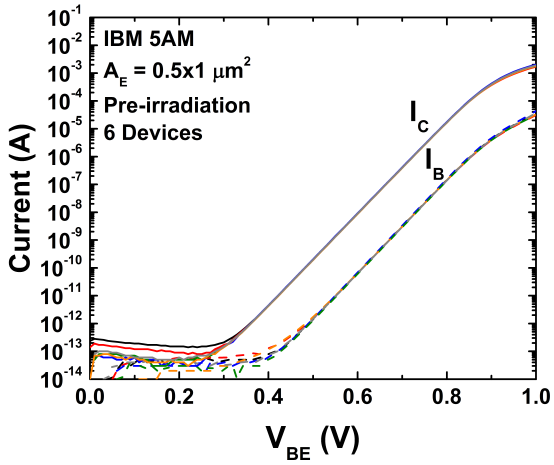

Figure 6.3: Forward Gummel 1st-generation SiGe HBT. © 2014 IEEE.

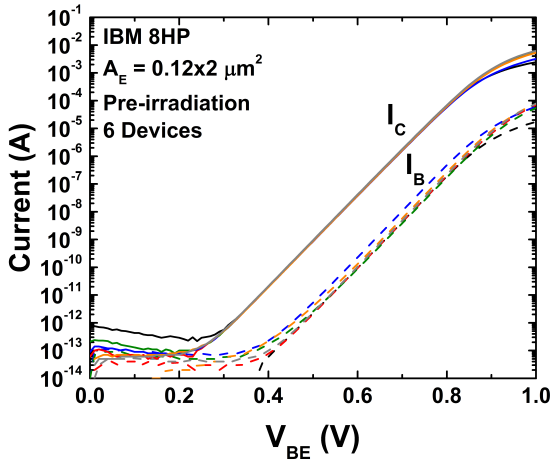

Figure 6.4: Forward Gummel 3rd-generation SiGe HBT. © 2014 IEEE.

a total dose of 80 krad(SiO_2), with all terminals grounded. Pre-irradiation measurements were conducted as well as measurements at 50 krad(SiO_2) and 80 krad(SiO_2). Forward Gummel measurements were taken with $V_{CB} = 0$ V. Irradiation was briefly halted to take the 50 krad(SiO_2) measurements and then quickly resumed. Pre-irradiation forward Gummels ($V_{CB} = 0$ V) for all devices, along with the device geometries used, may be seen in Fig. 6.3, 6.4, and 6.5.

The circuit chosen for the present study is the Brokaw bandgap reference (BGR)

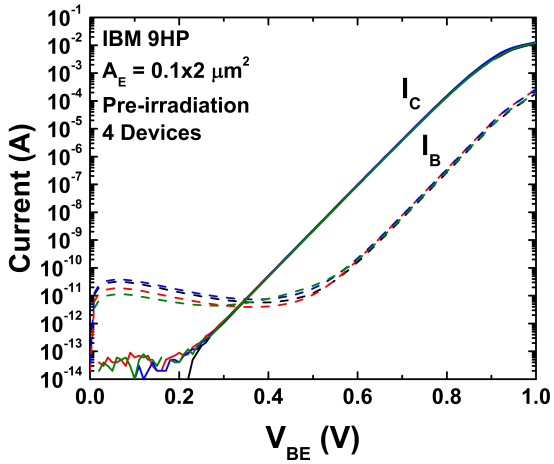

Figure 6.5: Forward Gummel 4th-generation SiGe HBT. © 2014 IEEE.

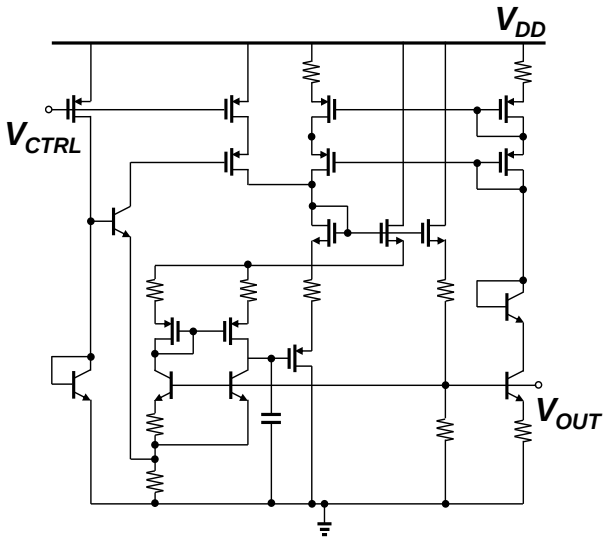

Figure 6.6: Schematic diagram of Brokaw BGR circuit. All devices (SiGe HBTs, nFETs and pFETs) are on die and simultaneously exposed during irradiation. © 2014 IEEE.

[79]. Bandgap references are ubiquitous circuits for setting a bias voltage (or current) to an exact value regardless of temperature, loading effects, and power supply variations. A BGR functions by operating two transistors at different current densities in order to produce a voltage proportional to absolute temperature (PTAT) across a sense resistor [79]. This PTAT voltage is then used to drive the output voltage (V_{OUT}) to a value of V_{BE} and the temperature compensated value that is now constant across temperature [79]. The BGR used in this study (schematic diagram shown in Fig. 6.6) is a unique topology that exhibits an especially good power supply rejection ratio (PSRR). Higher PSRR prevents harmful variations at the voltage rails from effecting the output voltage of the circuit. The circuit includes pFETs, nFETs (both 90 nm) and *npn* SiGe HBTs from IBMs 9HP SiGe BiCMOS platform. The circuit utilizes a 3.0 V supply rail, a 0 V ground, and an input bias (V_{CTRL}) of approximately 1.7 V used to set the output voltage (V_{OUT}) to 1.2 V.

The BGRs underwent ELDRS testing at room temperature at nominal bias conditions, with V_{DD} = 3 V and V_{CTRL} = 1.7 to 1.8 V (V_{CTRL} varied to set V_{OUT} = 1.2 V). Five BGRs (one BGR per die) were exposed up to a total dose of 100 krad(SiO_2) two at the high dose rate and three at the low dose rate. At each accumulated dose point, the samples were briefly removed from the test chamber to be measured using a Keithley 4200 SCS Parameter Analyzer. All significant bias voltages and currents were tracked at each dose point. No measurements across temperature were performed.

6.5 Device Damage Results

A total of 16 SiGe HBTs underwent gamma irradiation up to a total dose of 80 krad(SiO_2). Half of the devices were irradiated at 50 rad(SiO_2)/s, while the other

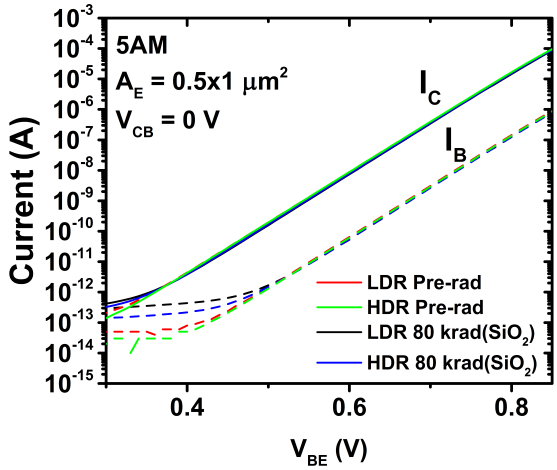

Figure 6.7: Forward Gummel characteristics at LDR and HDR for 1st-generation SiGe HBTs. © 2014 IEEE.

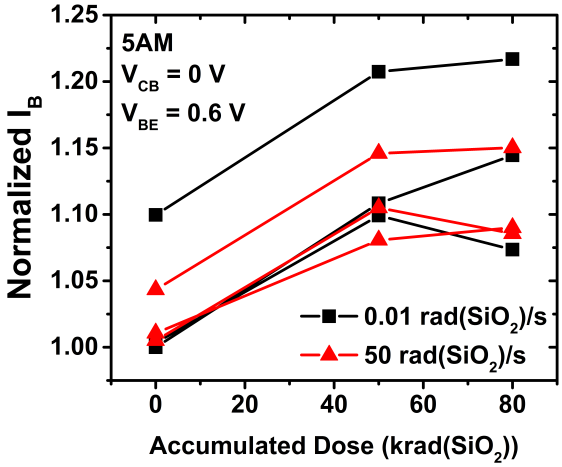

Figure 6.8: Normalized base leakage current of the 1st-generation SiGe HBTs. © 2014 IEEE.

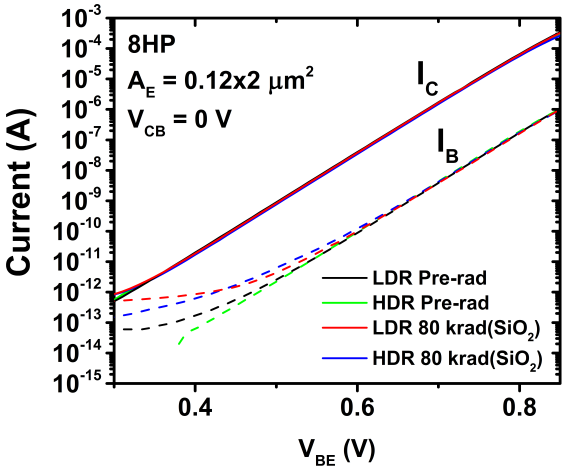

Figure 6.9: Forward Gummel characteristics at LDR and HDR for 3rd-generation SiGe HBTs. © 2014 IEEE.

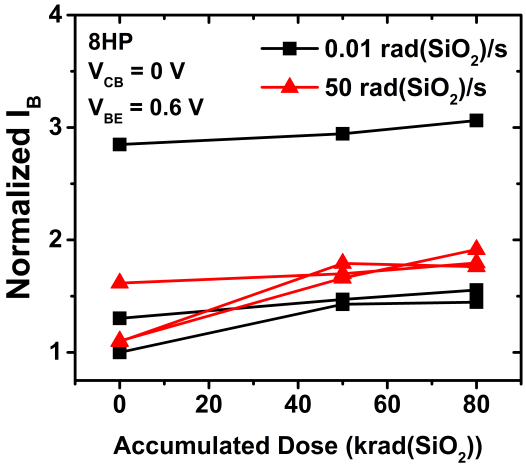

Figure 6.10: Normalized base leakage current of the 3rd-generation SiGe HBTs. © 2014 IEEE.

half underwent low dose rate testing at 0.01 rad(SiO_2)/s. Six of the devices were 1^{st}-generation SiGe HBTs, six were 3^{rd}-generation, and four were 4^{th}-generation. Gummel characteristics are provided for representative devices (one at LDR and one at HDR) from each technology. In addition, normalized base currents are provided for every irradiated device in the generation. The device results are presented in ascending order of generation, followed by a comparison of the device generations.

Of all the generations tested, the 1^{st}-generation SiGe HBTs experienced the smallest overall increase to base leakage current due to TID exposure. This leakage can be seen in Fig. 6.7. The base leakage current appears to be slightly larger in the low dose rate irradiation case. However, it can be shown that any given device has some variability and that the devices follow the same overall trend in TID degradation. By normalizing the base current to the "least leaky" device and selecting a reasonable operating voltage ($V_{BE} = 0.6$ V), we can more clearly see that the devices are degrading in roughly the same fashion regardless of dose rate. The current normalization is based off of the least leaky device's base current pre-irradiation value (subsequent current values are divided by this normalization factor). The voltage $V_{BE} = 0.6$ V is chosen to look at the relative increase in base current for circuit applications. Although the magnitude of the increased leakage is larger at smaller values of V_{BE}, the trends between LDR and HDR are the same. The result of normalizing the base current in 1^{st}-generation SiGe HBTs is shown in Fig. 6.8. Notice that two of the devices, one at LDR and one at HDR, actually improve in terms of leakage from 50 krad(SiO_2) to 80 krad(SiO_2). This occurs because the SiGe HBTs are quite robust to TID damage and minor annealing can occur in between irradiation and measurement. This effect would be much less pronounced at higher levels of accumulated dose; however, reaching higher levels of TID is challenging using a low dose rate irradiation source.

In a similar fashion, base current degradation is also seen for 3^{rd}-generation SiGe

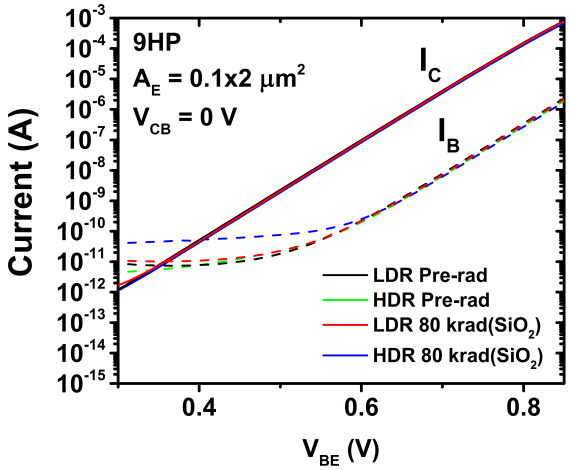

Figure 6.11: Forward Gummel characteristics at LDR and HDR for 4th-generation SiGe HBTs. © 2014 IEEE.

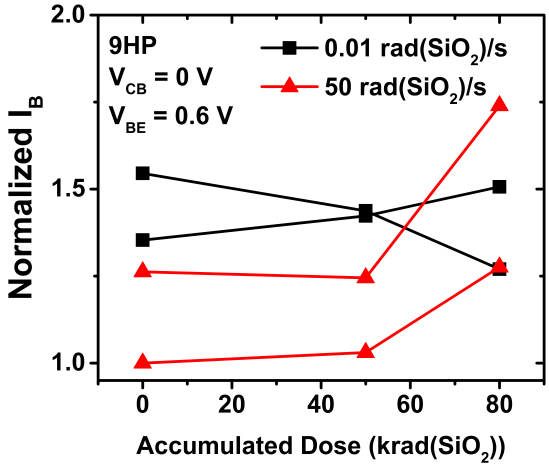

Figure 6.12: Normalized base leakage current of the 4th-generation SiGe HBTs. © 2014 IEEE.

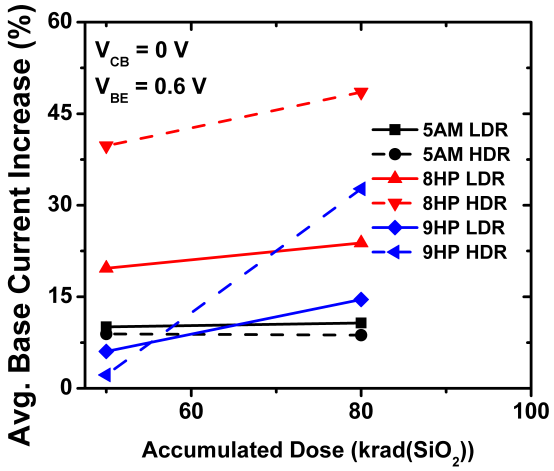

Figure 6.13: Average percent change in base current for all devices investigated. © 2014 IEEE.

HBTs. Fig. 6.9 shows the Gummel characteristics of devices after low and high dose rate irradiation, and Fig.6.10 shows normalized base leakage current for all devices in this technology generation. As in the previous case, degradation appears to be similar for both the HDR and LDR devices. Some of the devices have more base leakage current before any irradiation occurs. The best device starts at a base current roughly three times smaller than the leakiest device, but subsequent increases in base current due to irradiation are consistent.

Finally, the 4^{th}-generation SiGe HBT device results may be seen in Fig. 6.11 and Fig. 6.12. As shown in Fig. 6.11, the devices in this new technology generation have the most overall base leakage current. However, they, too, do not suffer from ELDRS. If anything, it appears in Fig. 6.12 that the HDR devices actually experience worse degradation than the LDR devices. This disparity is likely due to time dependent effects and the test setup rather than a true dose rate effect. Given a larger sample size with irradiations to a larger total dose, it is expected that these curves will better match.

None of the devices under low or high dose rate irradiation experienced any collector current degradation. This result is a good indication that circuits designed

with SiGe HBTs will not behave any differently in a low dose rate environment than a high dose rate environment. The TID response between the three generations is quite consistent. However, 3rd and 4th-generation devices are much more sensitive to experimentation in general and tend to have more leakage after device packaging (before irradiation) than 1st-generation devices. In general, looking at the change in base current for all the devices, at V_{BE} = 0.6 V, the majority of devices experience less than a 15% change to base current up to 80 krad(SiO_2).

For SiGe HBTs to be ELDRS sensitive there should be a discernible increase to base current leakage at a low dose rate when compared to high dose rate irradiation. However, this increase is not seen. By averaging the change in base current for the devices by generation and dose rate, it can be shown that the LDR devices do not experience a marked increase to base current leakage when compared to the HDR devices. This is shown in Fig. 6.13. SiGe HBTs remain multi-Mrad TID hardened by process regardless of dose rate, clearly an important benchmark for use in space environments.

6.6 Circuit Damage Results

The bandgap reference (BGR) used in this investigation is an excellent test vehicle to monitor for changes in collector current due to low dose rate irradiation. Any potential collector current shifts due to irradiation would be clearly detectable by monitoring the bias of the BGR. This circuit topology also may help identify large changes in leakage current between LDR and HDR irradiations by monitoring shifts in the supply current. However, results from the single device data show that the leakage difference between high and low dose rate irradiation is very small, and as such, it would be difficult to separate the increased base current leakage from the nFET leakage current using this circuit.

Fig. 6.14 shows the normalized output voltage for the BGR versus total dose, for

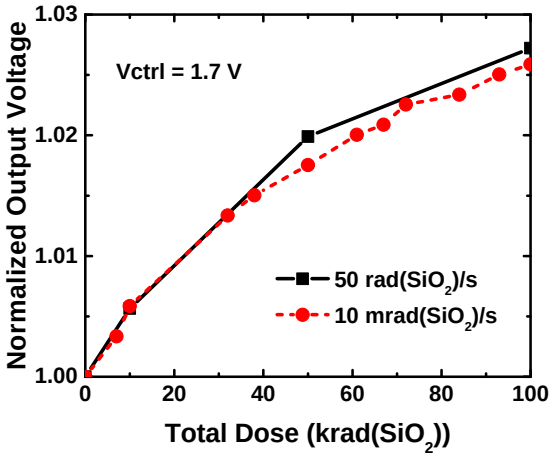

Figure 6.14: Normalized V_{OUT} versus accumulated dose. Normalized values are given for representative circuits and are calculated by dividing the value of V_{OUT} for a given dose by its pre-irradiation output voltage value. © 2014 IEEE.

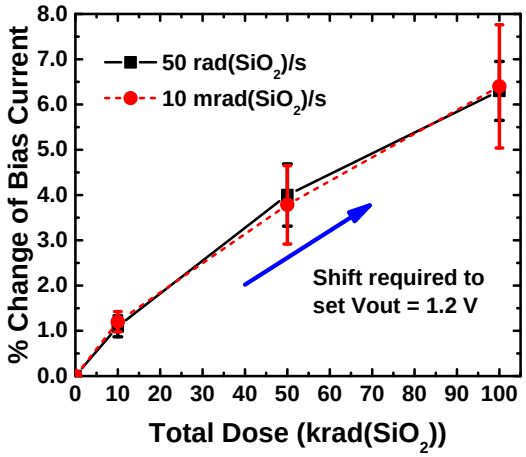

Figure 6.15: Change in input bias versus accumulated dose. Error bars represent one standard deviation of the measured data. © 2014 IEEE.

dose rates of 50 and 0.01 rad(SiO_2)/s. Both dose rates exhibit an increase in V_{OUT} at increasing TID; however, this increase is reasonably consistent between both dose rates. The slight degradation is driven predominately by two factors: 1) the charge accumulation at the EB spacer in the SiGe HBTs and 2) the charge accumulation at the gate oxide and shallow trench isolation (STI) in the nFETs (field effect transistor). The pFETs in the BGR will not contribute to the TID response, as they do not suffer from TID-induced leakage [20]. For the BGR, the nFET radiation response will likely dominate the circuit response. The SiGe HBT damage results in very minor base leakage current and current gain degradation. The increase to base leakage current will not contribute substantially to the increase in V_{OUT}. When compared to the high dose rate, the low dose rate irradiation does not result in a pronounced increase to base or collector leakage current, and as such, this circuit is not sensitive to ELDRS effects, clearly an encouraging result.

To further address this point, V_{CTRL} was tuned at each accumulation point to see what change in supply current was necessary to return the V_{OUT} to 1.2 V. In this case, both dose rates again give results that are nearly identical. The changes in the supply current, shown in Fig. 6.15, vary by less than 80 μA (7%) at the highest dose of 100 krad(SiO_2). This change is attributed to the increased leakage current and the resulting shift in the bias operation of the nFET devices. The radiation response for the nFETS is more sensitive to total ionizing dose in this technology. The resulting radiation induced damage will be marked by threshold voltage shifts which cause V_{OUT} and operating points to drift at higher values of TID; the impact of which is much more pronounced than the SiGe HBT response.

6.7 Discussion

SiGe HBTs are not sensitive to ELDRS, a result due primarily to the device structure. The strict processing requirements needed to incorporate a strained SiGe alloy in an

epitaxially grown base yield multiple benefits to the total ionizing dose response, and consequently, the dose rate response. The emitter-base (EB) spacer oxide is thin and contained within the heavily doped base region – effectively suppressing much of the leakage that results from interface traps at the Si/SiO_2 interface as a result of TID exposure [20]. In ELDRS, many effected devices are lateral or substrate *pnp* devices [73]. These devices differ from the vertical structure of the SiGe HBT, where carrier transport is removed from many sensitive structures (e.g., shallow trench isolation). This is true of all SiGe HBTs, not just the technology examined in the present investigation.

SiGe HBTs, like many Si BJTs, do experience worst case degradation with all device terminals grounded. This could be conceived as an indicator for an ELDRS sensitive device. However, SiGe HBTs are strictly controlled during processing to ensure that hydrogen contaminants are eliminated. Epitaxial Si growth generally involves hydrogen passivation and special care is taken to remove any remaining hydrogen, which would otherwise severely impact device operation. Part of this process involves creating oxides and oxide interfaces that are as defect free as possible. The special processing considerations needed to create a robust, well-functioning SiGe HBT also brings about an immunity to ELDRS effects.

6.8 Summary

The three SiGe BiCMOS technology generations (1^{st}, 3^{rd}, 4^{th}) evaluated in this paper, combined with previous work in [69] on 2^{nd}-generation SiGe HBTs, provide a broad evaluation of ELDRS in SiGe HBTs, up through state-of-the-art devices. Based on both device and circuit results, there is no evidence of ELDRS in any generation for this foundry provider. Although this study is limited to only one manufacturer, the same conclusion can be readily inferred for other advanced BiCMOS platforms as well. The strict processing control required to make SiGe HBTs (high quality oxides,

low defect densities and epitaxially grown Si), combined with the lack of traditional characteristics of ELDRS-sensitive devices, make this statement likely to remain valid for future generations of the SiGe HBT.

CHAPTER 7

VERTICAL SIGE HBT PROFILE CHANGES

7.1 Introduction

Inverse-mode (IM) operated silicon-germanium heterojunction bipolar transistors (SiGe HBTs) have been presented as a viable means to aid in the mitigation of radiation-induced single-event transients (SETs) [20, 80–83]. Operating a SiGe HBT in IM simply requires a flip in standard device operation, forcing the emitter and collector of the device to be electrically swapped (shown in Fig. 7.1). The switch in device operation allows for the new electrical collector to be isolated from the substrate of the device where much of the charge collection occurs during a radiation strike. This radiation-hardening-by-design (RHBD) strategy, has been shown to reduce both the duration and magnitude of SETs (where an SET is marked by a brief change to the current/voltage of the device) [80, 83]. When combined with the relatively high tolerance of SiGe HBTs to total ionizing dose (TID), IM allows for a straight-forward method of mitigating radiation effects in *npn* SiGe HBTs.

However, a number of issues exist with the implementation of IM operated SiGe

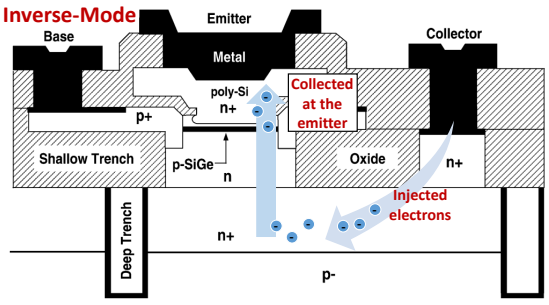

Figure 7.1: Inverse-mode operation for an *npn* SiGe HBT. The base-collector junction is forward-biased and the base-emitter junction is reverse-biased (after [3]).

HBTs. First and foremost, the transistor is not optimized for inverse mode and performance is severely degraded (*ac* degradation shown in Fig. 7.2). The device is specifically designed and fabricated to favor forward-active mode (FM) operation. For example, the introduction of germanium within the device causes the bandgap of the base to progressively narrow. This narrowing of the bandgap introduces an electric field within the base which greatly decreases the minority carrier transit time – leading to a faster operating transistor. This induced drift field opposes carrier flow during IM operation and consequently slows down device operation. Furthermore, the doping of the device is specifically designed to provide adequate *dc* gain during normal operation. The addition of germanium at the base-emitter (BE) junction lowers the conduction band energy, which allows for a greater number of electrons to be injected from the emitter to the base. This raises the *dc* current gain (β) of the device and allows process engineers to trade increased gain to support higher doping of the base region (improving the device f_{MAX} by lowering base resistance). The presence of germanium at the collector-base (CB) junction has the same gain boosting effect when the device is operated in inverse mode. However, the collector region is traditionally doped lower than the emitter (normally by at least three orders of magnitude). Because of this, the IM gain of the device is going to be low with respect to FM operation. Although some modern SiGe HBTs have enough germanium present at the CB junction to offset this large disparity in doping, most SiGe HBTs do not have sufficient gain or performance in this configuration for reasonable circuit designs. This makes IM-operated SiGe HBTs a non-applicable option in all but state-of-the-art platforms unless modifications are made to the device during fabrication.

One possible approach to improve IM performance would be to fabricate the device upside down. For example, the low doped collector can hurt IM performance, so raise the collector doping. The amount of germanium at the CB junction may be too small to adequately boost current gain, so raise that as well and flip the germanium profile

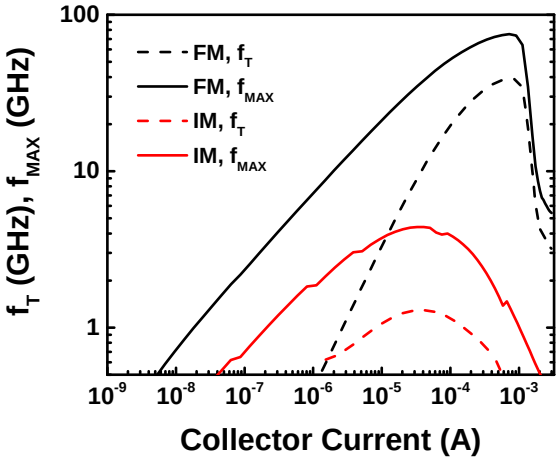

Figure 7.2: Simulated curves for f_T and f_{MAX} in the SiGe HBT technology of interest (GF 5PAe). Max operating speeds drop by over an order of magnitude. © 2018 IEEE.

grading. The high doped emitter hurts IM breakdown, so lower the emitter doping. The goal should be to get the intrinsic device to look exactly the same as a standard profile, simply flipped. However up until now, this has not been investigated. If an entire process flow is completely opened up, it is possible to make a SiGe HBT with an emitter up/down (FM/IM) configuration [17]. However, a cleaner approach would be to add IM optimization as a module within a process that can be seamlessly integrated into an existing design flow – creating a radiation-hardening-by-process (RHBP) strategy for improving radiation tolerance.

In the present investigation, new IM SiGe HBT profiles have been designed through simulation (additional details in [3]), fabricated on a dedicated set of IC wafers, measured for *dc* and *ac* performance, and tested for radiation tolerance. The SiGe HBT profiles used in this work are developed in a 1st-generation SiGe HBT process. Transistors from this technology are not traditionally operated in inverse-mode due to severe performance degradation. The goal of this work is to explore the bounds of how much IM performance can be added to the transistors without completely destroying FM device operation. Special emphasis is given to how each design change can subsequently impact the radiation hardness of the resultant profile. There is a

big question as to how much flexibility exists in a standard SiGe HBT technology and how much performance can be added to IM operation without breaking the existing process flow. A control profile along with two major doping profile splits, which optimize for IM performance, are investigated in this work. An additional SiGe profile [84], focusing on enhancing forward-mode breakdown (at a cost to *ac* performance), is included in this study to show how other profile modifications may impact radiation hardness assurance.

7.2 Profile Descriptions

Four modified *npn* SiGe HBT profiles are investigated in this study. These profiles are designed in an existing 1^{st}-generation SiGe BiCMOS platform (GlobalFoundries 5PAe) with a custom-designed control profile (labeled Ctrl). This profile is designed to closely match the existing technology using our own internal, 2D parameterized process simulation deck. The Ctrl profile was simulated in technology computer aided design software (Synopsys TCAD [16]) and was calibrated to closely match *dc* performance, *ac* performance, and breakdown of the technology. IC wafers were fabricated through GlobalFoundries without the use of through-silicon-vias (TSV) and a metal backside alloy (as is traditionally seen in the technology). These omissions allow for backside optical testing. Subsequent profiles (IM1, IM2, and SJ) are all variants based off modifications to the specified Ctrl profile, not the commercially available technology platform.

IM1 is a modified Ctrl profile that shifts the standard triangular germanium profile into a box shape (shown in Fig. 7.3). This modification creates a more symmetric germanium doping profile such that the introduced drift field does not overly favor either FM or IM operation. This modification effectively trades off FM speed and Early Voltage (V_A) for IM speed and *dc* current gain.

IM2 is a modified Ctrl profile that shifts the Ge content to a box shape (same as

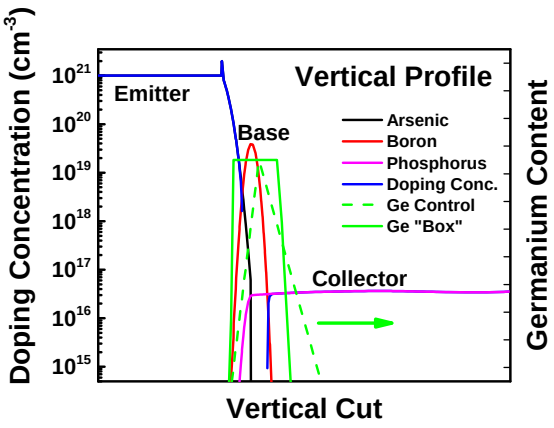

Figure 7.3: Vertical doping profile of the Ctrl profile (triangle) and the first optimized IM profile (box) (after [3]).

IM1), lowers the emitter doping, and raises the collector doping for further optimization. These additional modifications further enhance the IM current gain, boost the IM speed and trade-off FM performance (gain, speed, and breakdown).

Basic performance metrics for both simulations and measurements are shown in Table I. Simulation results shown in the table are extracted from the TCAD profiles. Measured results are acquired using an Agilent 4155C Semiconductor Parameter Analyzer and an Agilent E8361C PNA Network Analyzer. AC performance metrics are shown for a V_{CB} of 0 V. Known discrepancies between simulations and measurements are the following: 1) simulations in IM2 for n-doped polysilicon have the doping set at $1x10^{18}$ cm^{-3} but $1x10^{20}$ cm^{-3} was the minimum doping achievable in fabrication, 2) a perfect Ge box was not achievable in fabrication and a few % Ge content change is seen from the BE junction (high-side Ge content) to the CB junction, and 3) exact placement of the Ge box with respect to the base region is off by a few nm leading to slight mismatches in gain, as verified through secondary ion mass spectroscopy (SIMS) in post processing.

The IC wafers were patterned using an existing test site for the technology. As such, no common collector *ac* structures were available to reliably measure and extract the IM f_T and f_{MAX}.

TABLE I
COMPARISON OF PROFILE PERFORMANCE

Parameter	Ctrl	IM1	IM2	Ctrl	IM1	IM2
Max β	140	385	140	110	180	130
IM Max β	30	105	98	10	30	60
f_T (GHz)	39.3	31.2	37.8	31.4	26.3	25.7
IM f_T (GHz)	1.30	2.69	5.83	–	–	–
f_{MAX} (GHz)	75.2	66.9	66.3	42.7	20.4	17.2
IM f_{MAX} (GHz)	4.40	6.79	9.42	–	–	–
		Simulated			Measured	

It is important to note that these modified profiles were specifically designed to enhance IM operation while sacrificing as little FM performance as possible to allow for known trade-offs to standard device operation. Measured Inverse Gummel Characteristics for the Ctrl, IM1, and IM2 are shown in Fig. 7.4 and marked improvements over the Ctrl are seen in the altered IM profiles. Further information of the design and simulation of the Ctrl profile and both IM profiles are discussed in [3].

The additional non-IM specific profile, designed to improve forward-mode breakdown voltage, known as a 'superjunction' (SJ) profile, has new n/p doping layers within the space charge region of the intrinsic collector which pushes the peak electric field deeper within the device to delay the onset of Kirk Effect. The concept of using a superjunction is prevalent in power MOSFETs to improve ON-resistance and breakdown performance [85]. However, the implementation of a vertical SJ collector in *npn* SiGe HBTs had only been theorized before the fabrication of these profile designs [86]. The SJ profile shows an improvement in breakdown voltage (BV_{CEO}) of 57% when compared to the Ctrl profile [84].

7.3 Experimental Setup

Three terminal *ac* and four terminal *dc* *npn* SiGe HBT device structures, with a characteristic emitter width of 0.8 μm, were used in this study. Samples underwent gamma exposure at the Naval Research Laboratory (NRL) and 10 keV X-ray exposure at Vanderbilt University. TID experiments with the gamma source were conducted

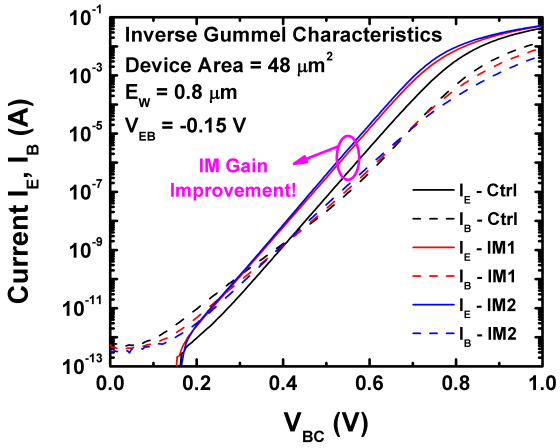

Figure 7.4: Inverse Gummel Characteristics for the Ctrl, IM1, and IM2 profiles. IM1 has improved current gain due to the alterations in the germanium doping profile, and IM2 has further current gain improvements through modified emitter and collector doping changes. © 2018 IEEE.

on *ac* 20 μm emitter length, 6 finger devices at a dose rate of 102.1 rad(Si)/s with an average energy of 1.25 MeV/photon. A thin metal liner was used in the sample container to help prevent device exposure to secondary particles. TID experiments with the X-ray source were conducted on *dc* 20 μm emitter length, 3 finger devices at a dose rate of 525 rad(SiO_2)/s. All samples were irradiated with terminals grounded and were measured at intermediate dose points of 100, 250, 500, and 1000 krad(SiO_2). Irradiation was briefly halted at each dose point to allow for device analysis. Device-level testing was conducted as quickly as possible to minimize annealing effects. A single test consists of five samples that are mounted on a 28-pin dual in-line package (DIP): a 'thin' and 'thick' control (Ctrl) profile, two thinned inverse-mode profiles (IM1 and IM2), and a thick superjunction (SJ) profile. One package was measured using the gamma source, and three packages were measured using the X-ray source. The 'thin' profiles underwent an additional polishing step during fabrication to ensure a smooth backside interface for optical experimentation.

Additonal, two-photon absorption (TPA) pulsed-laser SET testing was conducted at NRL on *ac* 20 μm emitter length, 3 finger device structures. The system provides a 150 fs, 1260 nm optical pulse at a rate of 1 kHz [15]. A spot size of approximately

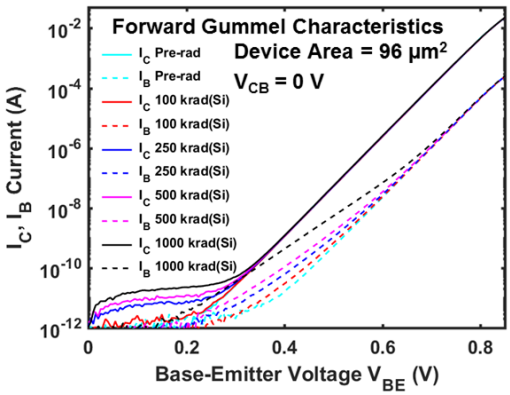

Figure 7.5: TID degradation is primarily marked by an increase in base current at low injection. © 2018 IEEE.

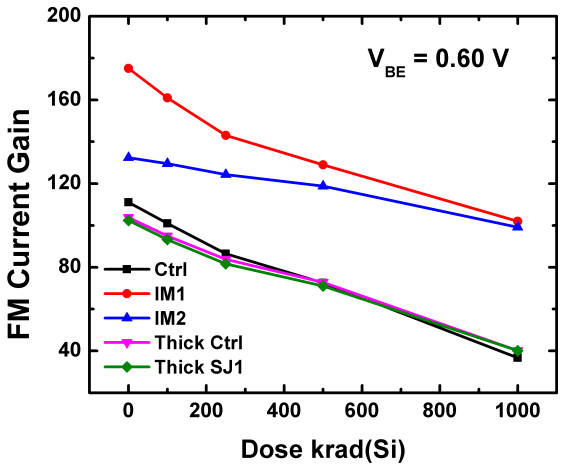

Figure 7.6: FM current gain as a function of TID (gamma) at low injection. A current gain of 100 is desirable for most applications. © 2018 IEEE.

1.19 μm and a laser energy of approximately 320 pJ was used for testing. Charge is deposited using backside TPA carrier-injection, through the Si substrate, and transients are extracted on high-speed circuit boards using a high-bandwidth real-time oscilloscope with a cutoff frequency of 12.5 GHz and a resolution of 20 ps/point (50 GS/s). SET measurement positions were determined by optically focusing (using an IR camera) on device center and performing a Z-position (depth) scan to locate the maximum produced transient response.

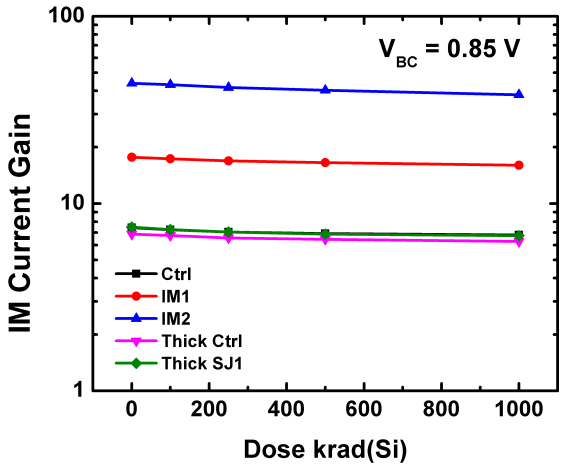

Figure 7.7: IM current gain as a function of TID (gamma) at high injection. The max degradation at 1000 krad(Si) is 13.3% in IM2. © 2018 IEEE.

7.4 Total Ionizing Dose Results

Two separate TID experiments were conducted on the profile structures. The gamma irradiation was first used to probe the TID-induced damage in the *ac* structures, and then the X-ray irradiations were used to both verify the TID response in a 4 terminal structure (uncoupled emitter and substrate) and to provide better statistics for the investigation. Device degradation is primarily marked by increased base current in the low-injection region of operation (small forward bias applied on electrical base-emitter junction), and the increase to base current leads to current gain degradation. The increase to base current, which is present for both FM and IM, is due to increased surface recombination at the EB spacer and shallow trench isolation (STI) oxides respectively [29, 67]. This response is shown for the FM Ctrl case in Fig. 7.5. The TID response is consistent across the Ctrl profiles and the SJ profile (refer to Fig. 7.6). This is due to the intrinsic device remaining unchanged in all regions that are far removed from sensitive Si/SiO_2 interfaces. The SJ profile does modify the collector region of the device; however, the dopant layers are added deep within the collector and will not significantly impact fields or dopants near oxide interfaces. The IM profiles do show a marked difference in their FM TID response. As IM2 has a lower

doped emitter than IM1, there is more hole back-injection into the emitter in IM2. This leads to an increased base current, by design. However, as dose is increased (shown in Fig. 7.6), the gain of IM1 and IM2 begin to converge. This is due to oxide traps at the EB spacer dominating the base current response when the device is heavily dosed and lowly biased. It is important to point out that the design shift to a box profile does provide a higher concentration of Ge at the BE junction. This allows for the IM profiles to maintain a higher usable current gain while operated in FM at low injection with respect to the Ctrl or SJ profile. Fig. 7.7 shows the IM response of all profiles at high injection where the devices are nearly unaffected.

Operated in inverse mode at lower applied bias, IM1 and IM2 show increased base current when compared to the Ctrl and SJ profiles. This is shown for an applied $V_{BC} = 0.6$ V in Fig. 7.8 and compared to an equivalent bias for FM. These data show that IM1 and IM2 have a worse TID response, on average, when compared to the Ctrl profile. Upon further investigation, only select samples from IM1 and IM2 show a substantial increase in base current in response to TID making this a local device-device reliability concern. Due to the presence of this substantial base current increase in only inverse Gummel characteristics, this effect is believed to be associated with defects at or near the STI rather than a global issue associated with the vertical profile doping changes. Fig. 7.9 illustrates this point in two pristine devices for IM2 where one device, pre-irradiation, pulls much more base current at low injection than the other. It is unclear what changes during processing could have led to local defects across the wafer. As only the Ge profile is shifted from the Ctrl profile to IM1, it is possible that the extreme change to the germanium profile (triangular ramp in the Ctrl to a nearly vertical ramp in IM1) caused an issue in the SiGe epitaxial film.

It is worth noting that all transistors in this technology exhibit increased collector current (I_C) in both FM and IM at low applied bias $V_{BE} < 0.4$ V. This is believed to be due to a buildup of shallow traps at the STI interface with silicon. This effect

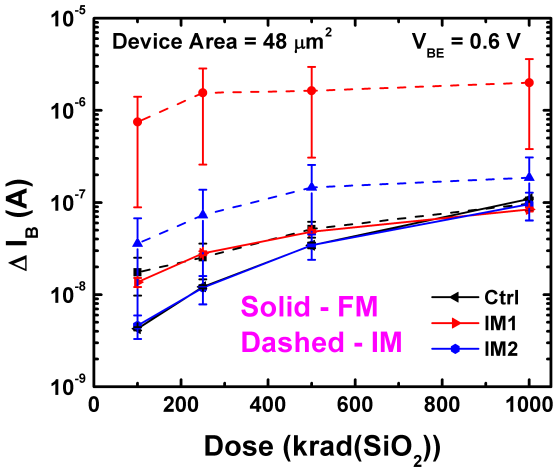

Figure 7.8: X-ray induced increase in base current for the the Ctrl, IM1, and IM2 profiles. STI defects lead to increased TID degradation for the IM profiles. © 2018 IEEE.

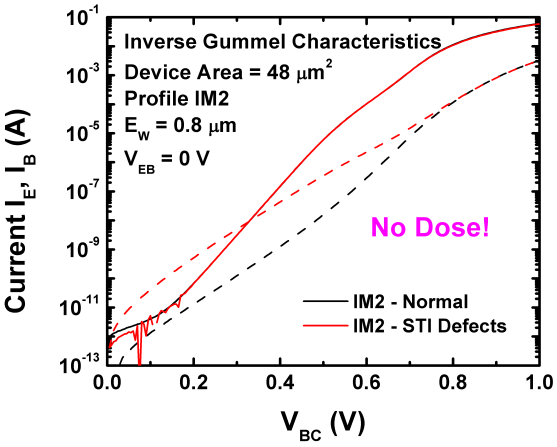

Figure 7.9: Inverse Gummel Characteristics for two separate IM2 devices. The red curve with increased base current is damaged by STI defects before irradiation. © 2018 IEEE.

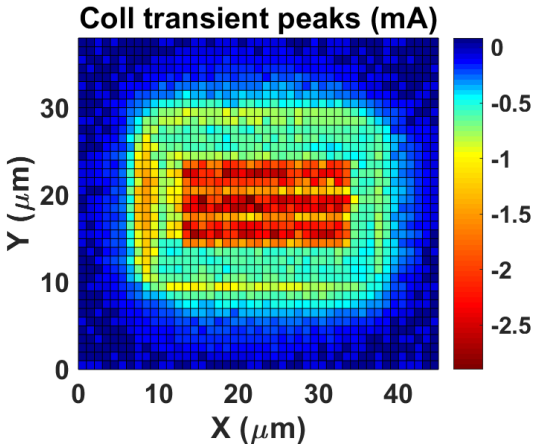

Figure 7.10: Peak collector transients for FM operation of the Ctrl profile. Device size is 48 μm^2, V_{BE} = 0.85 V, and V_{CB} = 0 V. © 2018 IEEE.

appears particularly pronounced in the device structures of interest due to the sheer size of the transistors tested (active areas of 48 and 96 μm^2), and could be masked in smaller devices due to the I_C being on the same range of the measurement equipment. Similar effects have been noted in [29]. At higher biases $V_{BE} > 0.6$ V the collector current shifts seen are within 15% of the pre-irradiated device measurements.

7.5 Single-Event Transient Results

Two-photon absorption (TPA) pulsed-laser experiments were conducted on the *ac* 3 terminal *npn* SiGe HBTs. The goal of these experiments were to benchmark the SET response of the Ctrl profile to that of IM1 and IM2, and to investigate whether or not the presence of a vertical superjunction changes the SET response of the device. Experiments were conducted using an identical laser setup across two days of testing. The first to compare the Ctrl to the IM profiles, and the second to compare the Ctrl to the superjunction profile. Fig. 7.10 is a 2D raster scan, which provides the positional dependence of charge deposition on the DUT. The resulting 2D map shows the sensitive device area and peak collector transients of the Ctrl profile while under FM operation. The worst case SETs occur while the pulsed laser is focused on the emitter stripe(s) of the device. As expected for this structure, three

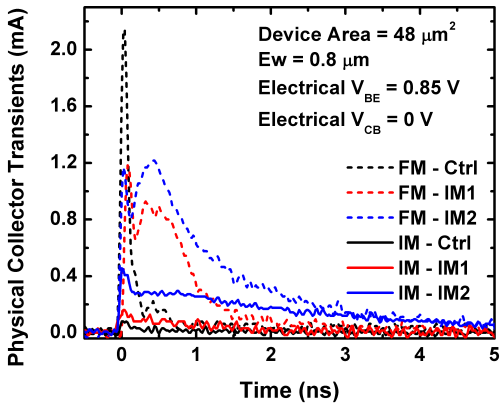

Figure 7.11: Absolute value of physical collector current over time. As measured from the scope, FM transients are negative in sign and IM transients are positive. © 2018 IEEE.

emitter stripes/fingers are clearly visible; however, as is clearly shown in the map, the sensitive area of the structure extends out beyond the intrinsic emitter area (as the subcollector-substrate junction extends out to deep trench isolation). Fig. 7.11 shows a comparison of extracted collector transients from the Ctrl and IM profiles for both FM and IM operation. During FM operation, the Ctrl profile is the worst strike condition in terms of peak transient by roughly a factor of 2X. However, this peak response is marked by an extremely sharp decay period of less than 1 ns. By contrast, the IM profile modifications have clearly impacted the FM transient response. The IM1 and IM2 transients have a peak component that is followed by a slow decay response which shunts away the remaining charge. This response is worse for IM2 than for IM1. The shift from a triangular Ge profile in the Ctrl to a box profile in the IM profiles causes the change in peak SET response. There is no longer a strong drift field present from the BE junction to the CB junction. This field, in the case of the Ctrl profile, allows for quick charge separation of injected electron-hole pairs in the Ctrl; however, in the case of the IM profiles, the induced fields no longer preferentially separate charge along the entire length of the base.

The inverse-mode SET response of the profiles show an interesting trend. As IM device performance improves from emitter and collector doping changes – the SET

response worsens. This is shown in Fig. 7.12 where the resulting collected charge for these waveforms is compared to that of the FM case (equivalent voltage bias). The charge collection points are acquired by averaging approximately 50 waveforms from the most sensitive region of the device, as determined by performing depth scans before data acquisition. These data show, from a collected charge standpoint, that IM2 SETs are worse when compared to the FM Ctrl profile which has far superior *ac* performance – an unforeseen result. TCAD simulations are able to confirm an increase in the expected magnitude of the peak SET of IM2 (shown in Fig. 7.13); however, the long tail component is unexpected. This effect could be associated with defects present at the Si-STI interface as identified through the TID experiments. The presence of shallow traps at this interface could be responding to the 1260 nm photons with a single photon absorption (SPA) signature – unintentionally leading to enhanced charge deposition within the device under test.

For the SJ profile, the thick Ctrl profile is used for laser SET comparison (as opposed to using a thinned sample). However, SET results were consistent in the Ctrl profile for both the thinned and un-thinned samples. The SJ profile shows decreased peak transient magnitude when compared to the control profile (shown in Fig. 7.14). This is due to the peak electric field in the collector region being suppressed and forced deeper within the intrinsic collector. Although not intended for radiation mitigation, experimental data show that the presence of a vertical superjunction will slightly reduce the peak transient amplitude of SETs in SiGe HBTs.

7.6 Simulation Results

The profile modifications shown in this work have been supported with an entire suite of simulations performed in Synopsys TCAD [16]. The Ctrl profile model is fully calibrated in 2D to *dc* performance, *ac* performance, and breakdown (BV_{CEO}) with respect to the commercially available transistor technology. The Ctrl, IM1, and

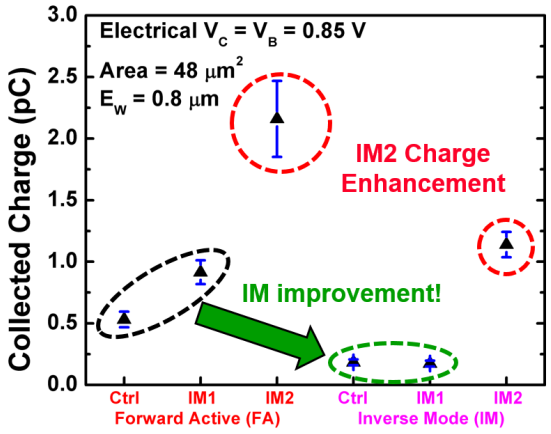

Figure 7.12: Charge collection results for the Ctrl, IM1, and IM2 profiles. Results are extracted from the electrical collector. © 2018 IEEE.

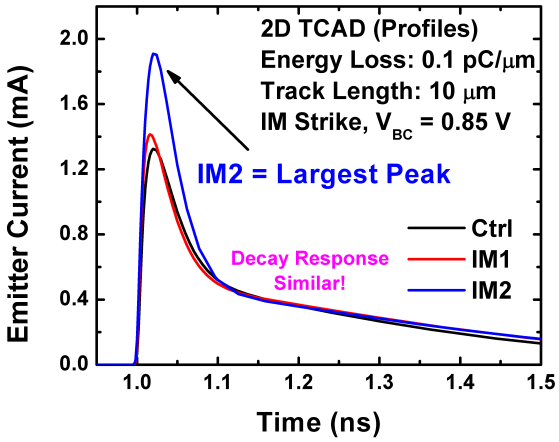

Figure 7.13: Heavy-ion strike simulations in 2D TCAD profile models. The peak of IM2 in simulation is greater than that of IM1 and the Ctrl, as expected. However, the presence of a long tail response is not exhibited in the simulated SETs. © 2018 IEEE.

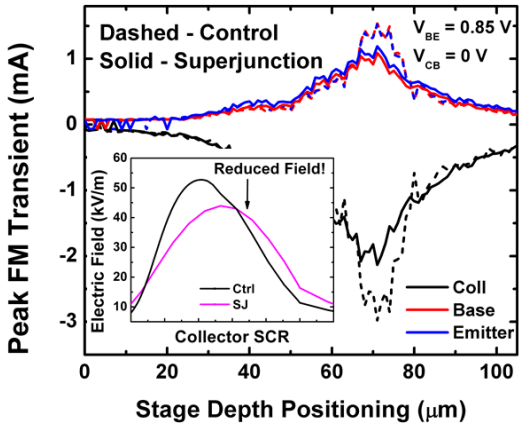

Figure 7.14: Peak transients as a function of stage depth positioning for the Ctrl profile (dashed) and the SJ profile (solid). The SJ profile shows reduced peak transients due to a lower electric field in the intrinsic collector region (shown from simulation in the inset). © 2018 IEEE.

IM2 profiles utilize the same model decks which were supplied to GlobalFoundries for fabrication. 3D TCAD simulations, although able to more accurately model the radial dependence of an ion strike, were avoided for the sake of consistency with the process simulations and to save time on overheard associated with larger device simulations. TCAD is recruited in this work for qualitative understanding purposes only. The simulations utilize hydrodynamic transport models, electric-field dependent mobility, and "mixed-mode" TCAD to model parasitic loading from the bias tees and oscilloscope used during experiment. Gaussian heavy-ion strike simulations are used to represent TPA carrier injection, and strike parameters are set to deposit 0.1 pC/μm for a charge track length of 10 μm in a device with a virtual length of 1 μm. A characteristic strike radius of 100 nm is defined for the heavy-ion simulations with the time of strike occurring at t = 1 ns. A similar experimental and simulation setup is described in [5] along with a discussion of how laser energy deposition compares to heavy-ion energy deposition in SiGe HBTs.

As mentioned in the previous section, SET simulations were performed in the Ctrl, IM1, and IM2 profiles for an IM strike case (V_{BC} = 0.85 V) for comparison to measured data. This plot is shown in Fig. 7.13. These data show that the

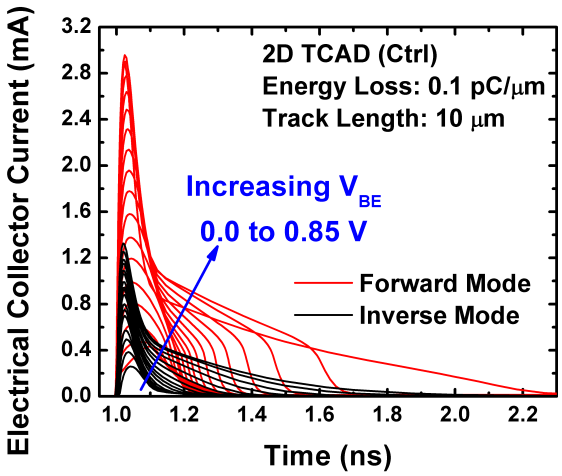

Figure 7.15: Simulated single-event transient waveforms as a function of applied (electrical) base-emitter voltage for both FM and IM. In each case, both the magnitude and duration is increased due to a higher applied bias. © 2018 IEEE.

increased peak response shown in IM1 and IM2 is expected from profile modifications – with the resulting peak increase from IM2 being more pronounced than IM1. These simulations, and other equivalent simulations run for an FM strike condition, are unable to recreate the large decay response exhibited in Fig. 7.11.

In addition to these simulations, the bias (electrical V_{BE}) was swept across the profiles (shown for the Ctrl case in Fig. 7.15). These simulations show, as expected, that increased base-emitter voltage leads to an increase in peak response for the resulting SETs. The increase in bias creates stronger drift fields within the device which leads to decreased recombination of electron-hole pairs during charge deposition.

7.7 Discussion

The doping profile modifications shown in this work represent the first time that a radiation-hardening-by-process (RHBP) approach has been fully investigated in a silicon-germanium semiconductor technology. The methods performed for this research describe an approach to improving IM performance while being able to use existing mask sets. Such an approach can allow designers to feasibly use IM SiGe

HBTs in technologies with performance previously deemed unacceptable for given applications. Specifically, the IM current gain (β) of the SiGe HBT in this study was raised from 10 to 60 (refer to Table I), significantly improving the viability of IM circuit design within this 1^{st}-generation SiGe process. Results of this work show that boosting IM device performance could possibly lead to a degradation in the IM base current of the structure through defect-creation at the STI interface. This effect was not globally exhibited over the wafers investigated and could be due to changes in the Ge profile. It is possible that this could be avoided by using a fully reversed triangular Ge profile. Caution is advised when shifting from a 'box' Ge profile to a reversed Ge triangle as the Ge gradient, although able to greatly improve device performance (better speed and improved Early Voltage), will lead to worsened SETs due to the similarly reversed drift field incorporated within the base. In addition to Ge doping changes, collector and emitter doping changes will lead to a change in the transient response as well. TCAD simulations show the strongest dependence on the collector doping, where a raised collector doping will result in larger peak SETs.

The profile modifications described within this work can be combined with IM layout optimization techniques as described in previous work by Appaswamy, *et. al.* in [87]. Such an implementation in a custom mask set, with doping adjusted profiles will lead to the largest improvement in IM SiGe HBT performance. These improvements will come at a cost to the transient radiation response, but overall, should show less susceptibility to radiation-induced SETs from a sensitive area perspective when compared to an FM only design.

This work postulates that unintentional device defects lead to increased charge enhancement during TPA experimentation through single photon interactions. This theory can be tested in future work using a variable wavelength laser source to identify the energy level associated with the presumed defect states and may give insight into the trap concentration.

7.8 Summary

This work describes semiconductor processing changes which may be used to enhance the IM performance of *npn* SiGe HBTs. These profile modifications can feasibly trade-off FM performance to enable IM circuit designs in technologies where current gain and speed would otherwise be insufficient. The approach taken in this work is to retain as much FM performance as possible to allow for an emitter up/down approach where FM SiGe HBTs are able to be used for performance and IM SiGe HBTs are able to be used for radiation mitigation. Results show that improving IM performance can come at a cost to radiation tolerance – as improved device performance naturally couples to more pronounced single-event transients. This work speculates that drastic changes to the Ge profile can result in an increased number of defects during SiGe epitaxial growth, which is exhibited in these structures as damage at the Si-SiO_2 interface at the STI. Lastly, a vertical superjunction SiGe HBT profile is investigated in this study which exhibits a decreased peak SET response due to a deepened, suppressed electric field within the intrinsic collector of the device. This final profile presents an unintentional method to mitigate transient radiation.

CHAPTER 8

TWO PHOTON ABSORPTION TO HEAVY-ION CORRELATION

8.1 Introduction

Pulsed-laser experimentation has become a widely used tool for analyzing the radiation hardness of semiconductor technologies. Although not accepted as a replacement to heavy-ion experimentation, a number of research institutions and universities have invested in developing pulsed-laser systems to aid in the analysis of single-event effect (SEE) phenomena. Both single-photon absorption (SPA) and two-photon absorption (TPA) pulsed-laser systems allow for rapid-feedback of radiation studies at a fraction of the cost of conventional heavy-ion broadbeam testing [88].

A pulsed-laser system is able to provide time-resolved charge deposition to a structure of interest using position-dependent photon injection. SPA pulsed-lasers inject carriers directly into the surface of the structure, whereas TPA pulsed-lasers feature sub-bandgap photons which are used to create electron-hole pairs (EHP) through high-order non-linear optical (NLO) phenomenon deep within the device. Although proven to be an extremely powerful experimental tool, it has proven challenging to model TPA phenomena accurately in complex semiconductor devices. Even if parameters are clearly isolated within simulation software, the experimental environment must be close to immaculate in order to systematically recreate the simulation environment, which is an overall goal for researchers using TPA pulsed-laser systems.

Matching laser results to a known heavy-ion linear energy transfer (LET) remains a challenge. Although trends and qualitative understanding can be achieved without a perfect laser to heavy-ion correlation, it would be ideal to tune a laser system to a

known effective LET and immediately use the results to aid heavy-ion experiments and accelerate test schedules by either screening parts for sensitivity or analyzing realistic outputs with true quantitative agreement.

The best path to achieving a correlation between two-photon absorption pulsed-laser SEE studies and heavy-ion studies is not obvious. There are a vast number of semiconductor technologies that exist with unique material interfaces, making a "one-size-fits-all" approach difficult. As such, comprehensive investigations must be undertaken in a variety of structures, materials, and a foundation of work must be established in order to fully grasp the physics involved in the proper modeling of non-linear optical phenomena. A great example of such an investigation can be seen for a 0.35 μm technology in [89].

The goal of the present work is to focus on one particular device type, the silicon-germanium heterojunction bipolar transistor (SiGe HBT). SiGe HBTs are known to be highly sensitive to radiation-induced upsets and have detectable single-event transients (SETs) below an LET of 1.2 MeV-cm^2/mg [20], [90], [36]. This sensitivity is beneficial in this study as it allows for the calibration of laser-induced SETs to that of nearly any heavy-ion-induced transient provided the range of the ion is sufficient enough to penetrate through the topside material layers.

8.2 Experimental Details

For this study, *npn* SiGe HBT device structures fabricated by Global Foundries (formerly IBM) were selected for experimentation at the following geometries, represented in the form of (emitter width $\times$ emitter length) with the emitter width set by the lithographic node of the technology: (0.5 μm $\times$ 10.0 μm), (0.5 μm $\times$ 1.0 μm), (0.12 μm $\times$ 2.5 μm), (0.1 μm $\times$ 4.0 μm), and (0.1 μm $\times$ 6.0 μm). The parts underwent SEE testing at three different facilities. Heavy-ion experiments were conducted at both Lawrence Berkeley National Laboratory (LBNL) in Berkeley, California and at the

Grand Accélérateur National d'Ions Lourds (GANIL) in Caen, France. TPA pulsed-laser testing was undertaken at the Naval Research Laboratory (NRL) in Washington, D.C.

For the TPA pulsed-laser experiments, the system provided 150 fs, 1260 nm optical pulses at a repetition rate of 1 kHz with a 1.03 μm full-width-at-half-maximum (FWHM) irradiance profile. Testing is conducted using backside carrier-injection, through the Si substrate, and transients are extracted using a high-bandwidth real-time oscilloscope with a cutoff frequency of 12.5 GHz, a resolution of 25 ps/point (50 GS/s), and 50 Ω terminations. The bias tees, cabling, and high-speed boards used for the experiments to isolate SETs feature cutoff frequencies beyond that of the oscilloscope.

GANIL heavy-ion experiments were conducted using Mo and Xe at LETs of 45.04 and 63.19 MeV-cm^2/mg, respectively using a 16 GHz oscilloscope to record transients. At LBNL, the 10 MeV/u cocktail was selected for experimentation. LBNL device measurements were made using O, Ne, Ar, and Xe with LETs of 2.19, 3.49, 9.74, and 58.8 MeV-cm^2/mg, respectively using a 12.5 GHz oscilloscope for transient measurement. All heavy-ions had a penetration range of 50 μm or greater, as verified using SRIM [40], and were of sufficient energy to pass through the back-end-of-the-line (BEOL) and into the sensitive structure volumes. Device characteristics were monitored both before and after experimentation to check for displacement/dose effects. Measurements at both heavy-ion facilities were performed under vacuum at normal incidence with irradiation from the topside of the device. Triggering thresholds to extract high-speed transients were nominally set above the noise floor of the scope on the collector terminal of the device. Thresholds are set between -2.4 to -2.6 mV, corresponding to SETs that exceed approximately 50 μA of current.

All boards were mounted and wire-bonded using custom high-frequency printed circuit boards. High-frequency connectors and cables were used in all testing setups.

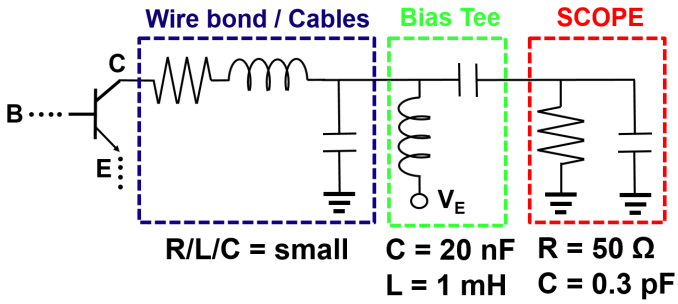

Figure 8.1: Schematic view of a device structure connected to an oscilloscope for SEE testing. Not shown are equivalent connections and parasitics (R/L/C) on the base, collector, and substrate terminals of the device under test. © 2016 IEEE.

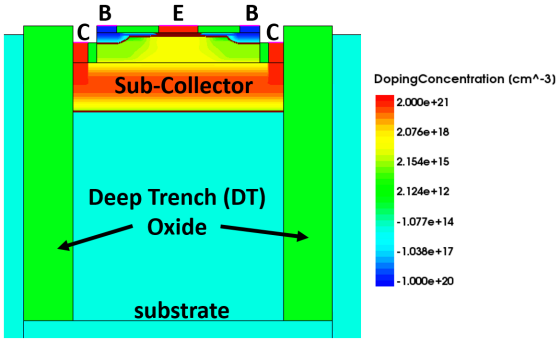

Figure 8.2: 2-D cross section for the calibrated TCAD model. The lateral spacing in between the deep trench isolation (DTI) oxides is approximately 3μm and the DT extends 6 μm into the substrate. © 2016 IEEE.

Bias tees were connected to isolate SETs while allowing device bias. A schematic view of a connected device showing lumped model parasitics may be seen in Fig. 8.1. Fresh devices were used for each set of experiments to mitigate the impact of dose-driven effects. As the flux at GANIL is much higher than that used at LBNL, some total ionizing dose (TID) damaged was incurred. However, this damage was isolated to low-injection (light forward bias of the emitter/base junction) and is comparable to studies involving proton irradiation [51], [68]. It is important to note that the emphasis of the discussion provided within this work is for device operation in the forward-active regime, where $V_{BE} > 0.6$ V and $V_{CB} = 0$ V.

8.3 Simulation Details

The primary device discussed in this study is the largest area *npn* SiGe HBT (0.5 μm $\times$ 10.0 μm), as it yielded the best heavy-ion statistical sample. A fully-calibrated 2-D TCAD model was developed in Synopsys TCAD to describe physical phenomena occurring within this device. Device calibration matched *dc* Gummel characteristics (at $V_{CB} = 0$ and 1 V), *ac* characteristics (f_T and f_{MAX}), and breakdown characteristics (BV_{CEO} and BV_{CBO}). A 2-D cross-section of the model is shown in Fig. 8.2. This model was developed using electric-field dependent mobility, hydrodynamic models, and University of Bologna impact ionization models [91]. Mixed-mode TCAD is enabled within the simulation environment to model parasitics as shown in Fig. 8.1.

Multiple heavy-ion simulations were conducted for this investigation and are based off of the device model using a virtual device length of 10 μm. These simulations included both traditional heavy-ion strikes and a superposition of heavy-ion strikes, which are more closely matched to a TPA pulsed-laser charge-generation profile. The traditional heavy-ion strike simulations that are shown are based off of Ar data and impart 0.1 pC/μm and correlate roughly to an LET of 10 MeV-cm^2/mg . A Gaussian track profile is used with a characteristic radius of 100 nm, strike simulations begin

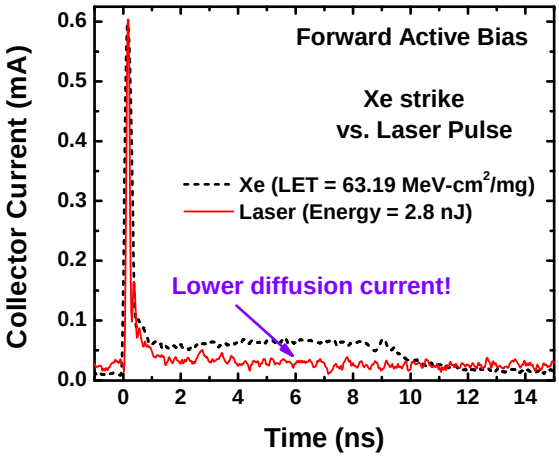

Figure 8.3: Magnitude of collector current for pulsed-laser vs. heavy-ion strike with V_{BE} = 0.8 V and V_{CB} = 0 V. © 2016 IEEE.

at a time t = 1 ns, and feature a track length of 10 μm that assumes constant carrier deposition. The TPA-like charge-generation profile consists of four separate heavy-ion strikes that are superimposed about a given strike location, similar modeling approaches may be seen in [92, 93]. The strikes consist of a normal incidence strike with a 1 μm track length with identical strikes occurring at 45, -45, and 90 degrees offset with the respect to it. Each individual strike is Gaussian and imparts 0.01 pC/μm with the same characteristic radius used in the traditional heavy-ion strike. The initial track length was selected to match the irradiance profile ($\sim$1 μm) and was used to probe the most sensitive regions of the device before being adjusted to match a more realistic profile as shown in [15].

It is important to the note that the 2D profile used for this study neglects that pipe-like structure of a realistic charge track profile and that the emphasis of the analysis shown in this work is on qualitative understanding between heavy-ion and TPA-laser charge-generation profiles.

8.4 Heavy-Ion Results

Fig. 8.3 shows characteristic heavy-ion and laser-induced SETs at the collector terminal of the large area *npn* SiGe HBT. These data, as shown in previous work [94],

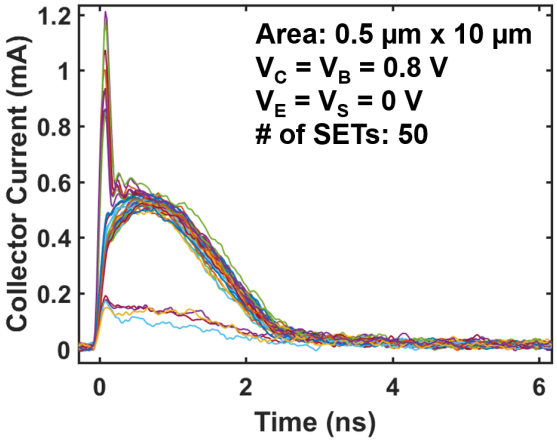

Figure 8.4: Family of curves shown for a series of Ar heavy-ion strikes. Data plotted is the magnitude of the collector current. © 2016 IEEE.

[95], exhibit two distinct regions of interest in the SET. First there is a prompt (on the order of tens of ps) peak transient, due to the ion-shunt effect, followed by a long-lasting diffusion tail [20], [96]. Note that when compared to a heavy-ion transient, the laser transient in Fig. 8.3 has a diffusion tail which rapidly falls to the scope noise floor. Although these two transients have been matched to roughly the same peak amplitude and pulse-width, it would be incorrect to say that the laser response is equivalent to the heavy-ion response. It is clear, at least in terms of stage positioning, where the laser is being focused within the device due to infrared optical imaging at the laser facility; however, there is no direct way to know exactly where the heavy-ion is striking in the broadbeam case. As the overall collected charge from the laser irradiation is much smaller than the heavy-ion case, it is clear that the charge being imparted into the device is different between strike conditions. Comparing only the peak amplitude of single-event transients is not sufficient to fully capture what is occurring, physically, between the two induced transients. This highlights one of the major challenges in trying to directly match laser and heavy-ion transient data. It would be incorrect to say that the laser is equivalent to an LET of 63 MeV-cm^2/mg in this case. Xe strikes that occur closer to the emitter center of the device can easily surpass 2 mA or greater at the collector node.

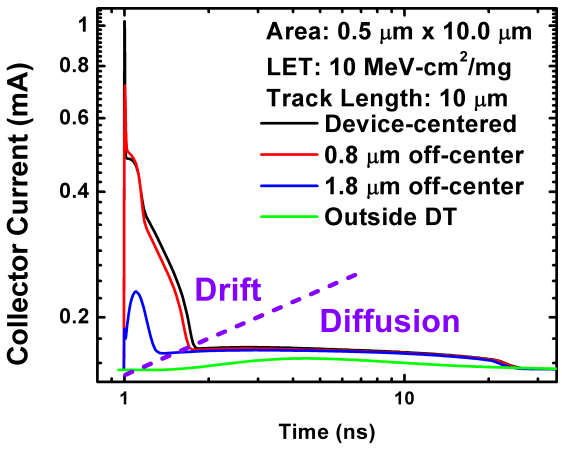

Figure 8.5: Simulated Ar strikes in TCAD at various lateral spacing. © 2016 IEEE.

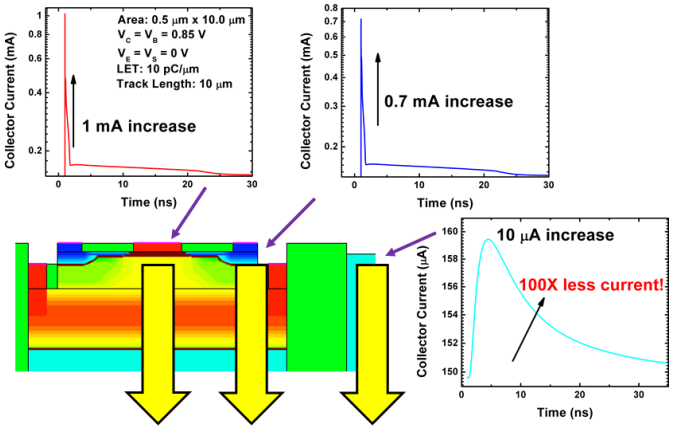

Figure 8.6: Simulated collector transients (magnitude) for various heavy-ion strikes at the emitter center (red), 0.8 μm off-center (blue), and outside the deep trench (teal). Simulated strikes that occur outside of the DTI result in SETs that are smaller in peak amplitude (two orders of magnitude or more) when compared to device-centered strikes. © 2016 IEEE.

As heavy-ion-induced SETs can occur in many different locations, it is difficult to identify where a device is actually struck during an experiment. It is easy to dismiss this limitation as the impetus for requiring a focused ion beam to get at this comparison. However, getting access to such facilities can be more challenging than getting access to a broadbeam facility, and is not entirely necessary. Given a sufficient number of strikes from a broadbeam facility, knowledge of the device geometry, and a proper model – a researcher should be able to say with some confidence where the ion strikes are occurring. Ion strike results for Ar, shown in Fig. 8.4, cluster the data into three separate families of curves. Clearly, based off of knowledge of the device structure, these SETs can be separated into three categories: 1) near emitter-center strike, which shows a strong initial peak transient followed by a longer lasting diffusion tail; 2) an off-center strike fully contained within the deep trench isolation (DTI), like the emitter-centered strike case but without the initial prompt current; and 3) a near device strike that occurs along the device edge or just outside the DTI, that simply contains a low-magnitude diffusive tail component of the transient. To support the clustering of SETs in this fashion, these strike conditions have been re-created in the TCAD environment and are shown in Fig. 8.5 and Fig. 8.6. Fig. 8.5 shows that the same trends emerge in TCAD as from the experimental data. It is important to highlight the strike case for the 1.8 μm off-center strike case (blue curve in Fig. 8.5), where the drift component of the collector transient recovers faster than the more centralized strikes. This is due to the simulated strike occurring close to, but within, the deep trench (DT) sidewall, this confines the charge within the isolating oxides but has a much smaller impact on the intrinsic device. Fig. 8.6 highlights that the amplitude of the diffusive tail current in the outside DT strike case can be orders of magnitude smaller than the device-center strike. During an experiment, many, if not all, particle strikes that occur outside of the DT will not have sufficient current (50 μA) to trigger the scope to register an event. And although this may hold true for

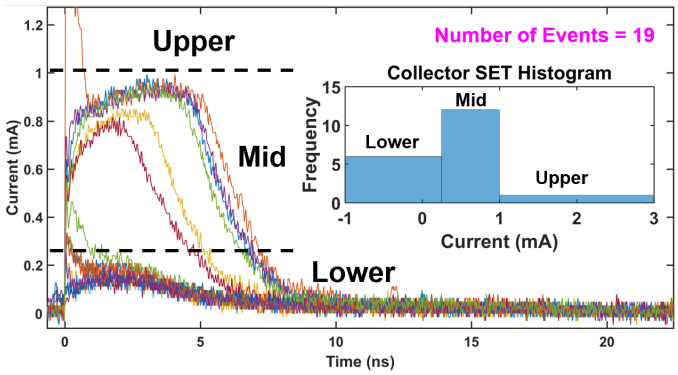

Figure 8.7: Family of curves being partitioned into histogram bins for analysis. Threshold levels are manually added and vary based off of LET and device bias. The case above highlights an LBNL Xe run where 19 hits were registered for a bias of V_{BE} = 0.8 V and V_{CB} = 0 V. © 2016 IEEE.

Table 8.1

Histogram Analysis (0.50 μm × 10 μm)

Species	**O**	**Ne**	**Ar**	**Xe**
LET (MeV-cm^2/mg)	2.19	3.49	9.74	63.19
Number of strikes	54	65	53	450
Upper	9	12	11	66
Middle	45	53	38	108
Lower	–	–	4	276
Percentage (%)	16.67	18.46	20.75	14.67

lower LETs, heavy-ion simulations for Xe in TCAD show that the peak current at the collector for such an event occurring outside of the DT can be sufficient to trigger the scope. This is not to say that an event that occurs below the triggering threshold will have no contribution to the SET response, but rather that these events go unnoticed in our test conditions and are considered minor for the subsequent analysis provided within this work.

The question then becomes: in a broadbeam setting, how many of each strike case can be expected? To arrive at the answer to this question, the SET data were partitioned into separate categories based on the form factor of the transient. An example of this partitioning may be seen in Fig. 8.7 where a number of Xe strikes

are analyzed. These strikes are put into the three corresponding histogram bins for further analysis. This was done for each heavy-ion species where the sample size was great enough to resolve a given number of strikes. For the main *npn* structure the associated results are obtained and shown in Table 8.1. In this table, the percentage category represents transients, which occur either within the emitter window of the device or close enough to impart charge within the emitter-base (EB) junction. In the data the number of worst case strikes is consistently around 15-20% of the strike total. Given enough worst case strikes one can determine when the device is being struck dead center. It is important to note that the Xe data are pulled from the GANIL data set, as it yields a higher number of events when compared to the LBNL data set. From the device structure in this technology, it is known that there is roughly 3 μm in between the DT sidewalls in the lateral dimension in the direction of the emitter width. This spacing, when divided by the emitter width, provides a good approximation of the upper sensitive region. In this case, that quick calculation of 0.5/3.0 is approximately 16.7%, which aligns well with the worst case strike data. It is important to note that there is a suppression effect seen with the data. The three distinct regions become less defined at lower LET. At these energies, strikes that trigger the scope are most probably only those that occur within the deep trench, and thus only two regions may be discerned. Through TCAD investigation (data not shown), heavy-ion strikes that occur outside of the DT for Ar simulations are at a maximum around 26 μA in peak current, whereas Xe simulated strikes can exceed 100 μA, and are of sufficient magnitude to trigger the scope. This is a possible reason why the Xe data skews towards the lower end of the 'upper' strike percentages as there are more strikes occurring outside of the device structure which are being picked up by the scope.

The previous analysis regarding the sensitivity 'worst case' ratio holds well across device geometry. By looking into a smaller device (0.12 μm $\times$ 2.5 μm), it is clear

Table 8.2

Histogram Analysis (0.12 μm × 2.5 μm)

Species	**Mo**	**Xe**
LET (MeV-cm^2/mg)	45.04	63.19
Number of strikes	252	526
Upper	5	13
Middle	52	289
Lower	195	224
Percentage (%)	1.98	2.47

that the ratio of the lateral emitter window distance divided by the distance between the deep trench isolation is a good predictor of worst case strikes being triggered on the oscilloscope. For this 3rd-generation SiGe technology (GF 8HP), the distance in-between DT regions is approximately 4.2 μm which leads to a ratio of 0.12/4.2 which gives a worst case hit chance of approximately 2.86%. The data acquired for this device is hard to discern if the sample size is small (in this case less than 100 or so data points). For this data only the Mo and Xe data from GANIL is taken as the number of events acquired is significantly higher. As seen in Table 8.2, the incidence of worst case events is 1.98% and 2.47% for Mo and Xe, respectively. The small deviation from the expected ratio can be readily explained by statistical variation, slight differences in patterned versus actual structure sizes, and also the regions in the longitudinal direction of the emitter which does not fully extend to the DTI. By accounting for the longitudinal difference, the expectation of worst case strikes is 2.05% for this structure, which is not far off of the measured data displayed in Table 8.2.

To formalize the statistical analysis, the data is represented as a binomial distribution of triggered events where the probability of a worst case strike occurring is denoted by p. As mentioned previously, this probability, in the simplest form, may be represented as the ratio of emitter width (ω_e) to the total lateral separation between

the deep trench sidewalls, or more accurately, as the ratio of the emitter active area (A_E) over the total area confined within the deep trench isolation, shown in Equation 8.1.

$$p = \frac{\text{Emitter Area } (A_E)}{\text{DT Confined Area}} \tag{8.1}$$

Given a number of desired worst case SET events, one may define a cumulative distribution function, mean number of expected events, and confidence intervals consistent with binomial distribution theory. As shown in previous pulsed-laser studies in SiGe HBTs [97], [82], the SET response of a given circuit may be limited by a worst case transient occurring in an amplifying device (i.e., a common-emitter (CE) amplifier in a low-noise amplifier). As such, it is absolutely vital that enough events have been captured during heavy-ion broadbeam testing to guarantee a worst case strike condition for a given LET. Just as important, if the number of events drops significantly at a given lithographic node, it could be an indication that only rare 'p' events are being registered as opposed to other, much more probable, strikes. This, in turn, would drastically reduce the sensitive cross-sectional area of the structure (up to ∼50X for the smaller devices geometries in the present work).

It is important to note that the layout structure of the device in question (CBEBC vs. CBE) will impact the ratio of worst case strike events. This is simply due to the difference in the sensitive area confined by the DT. Viewed from the top of the structure, the contact configuration for CBEBC is: collector-base-emitter-base-collector and CBE is: collector-base-emitter with CBE being the highly preferred structure for RF applications. In the 0.12 μm process for example, the CBEBC device is enclosed by 4.2 μm of DT as opposed to 2.7 μm for the CBE case. This leads to a difference of 36% ([4.2-2.7]/4.2) in expected events. A consequence of this being that the area of the 'active device' will not necessarily describe the total sensitive volume of the circuit/system and that the device layout can significantly

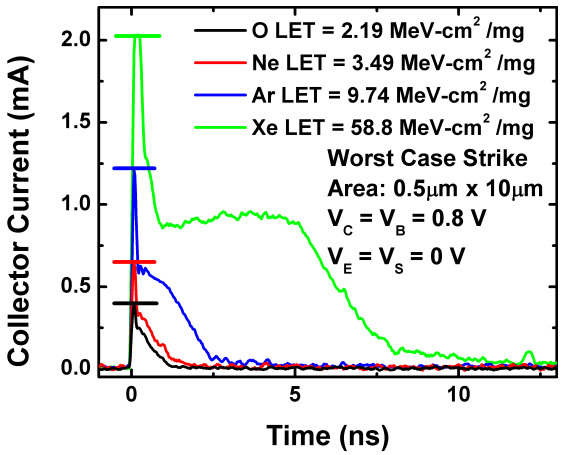

Figure 8.8: Experimental data for emitter-centered strikes. The Xe strike clips at the current limit of 2 mA for the scope settings at the plotted resolution but can exceed 5 mA in peak magnitude. © 2016 IEEE.

increase the number of expected events. It is critical for designers to know whether or not the limitation in their application depends only on worst case strikes in the active area or whether or not any strike occurring within the DT is of significance.

By investigating the signature of SETs as a function of LET, shown in Fig. 8.8, it becomes clear that the duration of the diffusion tail has a large dependence on the energy deposition of an incident particle. As LET increases, there is a monotonic increase to the transient duration, and consequently the collected charge within the device. Although not discussed in detail in this work, charge collection mechanisms for this device structure are discussed in [95]. It is interesting to observe that the transient tail appears to look like an exponential decay until higher levels of LET, while under forward bias. In measurement, ion species with LETs above that of Ne (LET = 3.49 MeV-cm^2/mg) begin to produce very pronounced diffusion tails. This can be recreated in the pulsed-laser experiment by increasing the laser energy while focusing on the sensitive emitter-base-collector stack. As such, during laser testing, it is advisable for radiation effects engineers to use a stand-alone device to achieve a similar SET response as shown in Fig. 8.8 before conducting circuit or system experiments.

By conducting a heavy-ion strike simulation within TCAD, the immediate collapse of the electric field at the collector/substrate junction can be examined, and the field strength does not return until the junction has been re-established and the remaining free carriers are flushed out of the device. It is interesting to note that the emitter/base (EB) junction exhibits the same effect, albeit on a much shorter timescale. The EB field is consistently restored (for any device geometry) within 1 ns after an SET event. This difference in timescale is due to two key device features. First, the emitter and base of the device are more heavily doped than the collector and substrate – requiring a higher carrier density to collapse the field at the junction. Secondly, the addition of germanium within the silicon lattice induces a strong drift field extending from the EB junction to the collector/base (CB) junction due to a progressive narrowing of the bandgap. This field rapidly accelerates free carriers to either the device contacts or the collector/substrate junction and will not collapse due to the excess carriers injected into the device.

8.5 Laser Simulation

As mentioned previously, a laser strike condition was modeled using a superposition of four truncated, low-energy heavy-ion strike profiles (with constant LET) which are overlaid about a central point in the device. The simulated laser pulse exhibits a Gaussian decay in both lateral and depth dimensions about the strike location. A carrier density distribution for a laser pulse at a time 20 ps after the initial carrier injection is shown in Fig. 8.9. This laser profile is symmetric in lateral and depth dimensions and provides a good starting point to modify the spatial profile of the laser simulations used here to better fit the acquired pulsed-laser data.

An example of a modeled laser strike compared to an extracted laser SET is shown in Fig. 8.10. The model laser energy is calibrated to match the peak amplitude of the measured result from a laser-pulse that imparts 2.8 nJ with a characteristic FWHM

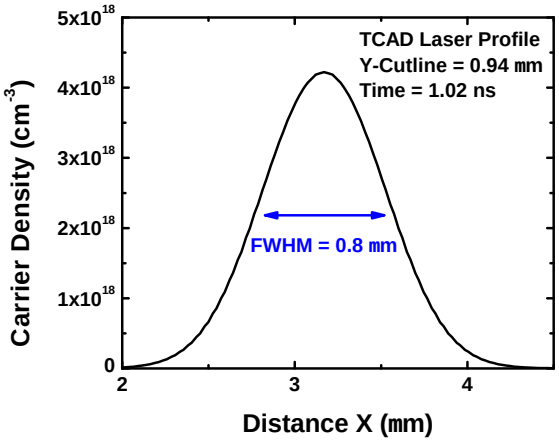

Figure 8.9: Full-width-at-half-maximum based spatially off of the carrier density in the lateral dimension for the custom-defined laser strike simulation in TCAD at a time t = 1.02 ns. © 2016 IEEE.

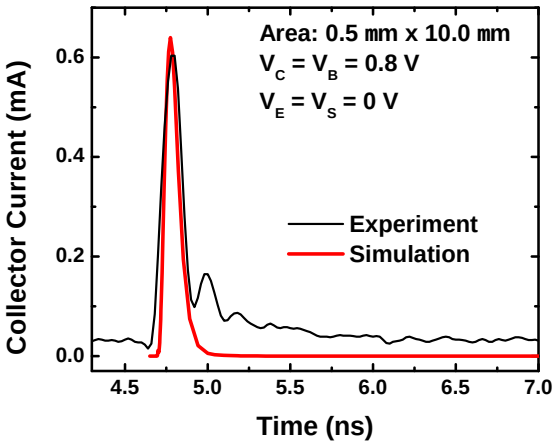

Figure 8.10: Simulated and experimental pulsed-laser SETs. The simulation strike time is delayed to match measured data. With the given (spherical) heavy-ion spatial profile, the recovery time of the model is much quicker than for the acquired experimental data. © 2016 IEEE.

of 1.03 μm. Fig. 8.11 shows this laser strike being stepped across the device in 0.5 μm steps in order to map out the most sensitive region in the device, which occurs at a location just below the emitter contact, as expected. The model closely matches the peak transient amplitude and pulse-width of the SET; however, there is a disparity in the decay characteristics of the two SETs, and consequently the overall charge collection. Such a result is not unexpected, as the TPA spatial profile has been shown in [15] to be much more elongated in form where the depth dimension of the profile is extended from the strike. Since the strike was made in a symmetric fashion, it is easy to tell in the simulation software how the SET response changes as a function of the spatial profile in a given direction (lateral or depth) about the strike location. When increasing the charge deposition in the lateral dimension, there is a clear increase in the peak amplitude of the SET and a slight broadening of the pulse duration as the 'effective' LET of the laser profile is being increased. It is important to note that the by modifying only the standard spatial parameter within the Synopsys heavy-ion model with a single ion profile, this effect is not seen as the LET is normalized to the new spatial profile. When increasing the profile in the longitudinal dimension, one can clearly see the tail magnitude of the SET response increase as the charge profile is extending further into the substrate past the collector/substrate junction. This increase allows more of the charge to be collected over the long duration of the SET response and saturates once the strike profile is pushed a few μm past the collector/substrate junction. Using this methodology, the profile strike used to create Fig. 8.10 was extended out from the 0.8 μm FWHM profile to be slightly broadened in the lateral dimension (out to 2 μm) and greatly in the depth dimension (out to 10 μm) to match a more realistic TPA spatial profiles such as can be seen in [98] and [18]. This improved profile and response can be seen in Fig. 8.12. This profile clearly has better matching to the experimental laser SET. By comparing this improved laser strike simulation to the lower-end LET heavy-ion data, the closest match can be

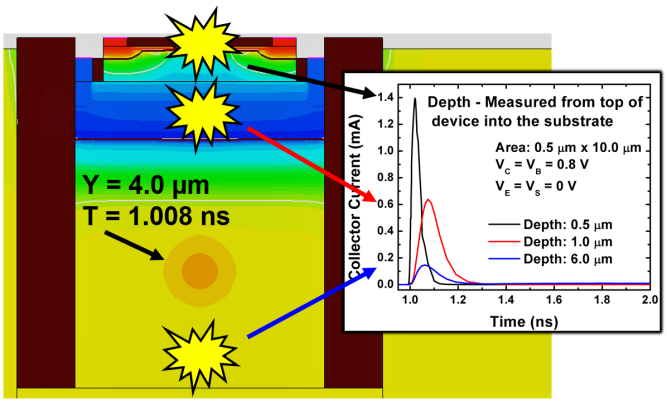

Figure 8.11: Laser strike simulations as a function of depth. There is a strong Y-dependency (depth) on the SETs until the pulse is within the substrate, where the transient amplitude is diminished. © 2016 IEEE.

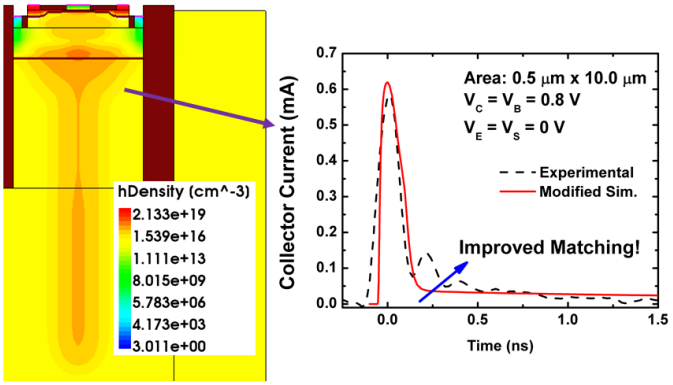

Figure 8.12: Modified laser strike profile with the resulting waveform compared to experimental data. Hole density shown for a time t = 1.05 ns. © 2016 IEEE.

found with O (LET = 2.19 MeV-cm^2/mg) and the SETs are shown in Fig. 8.13. This outlines a basic method in TCAD to get at an O strike with laser data, providing an effective LET. This method of retro-fitting the laser strike profile would work well as the input for mixed-mode SET simulation of circuits within the TCAD environment. However, this method will not necessarily be calibrated in any given strike position in the device profile, a clear limitation.

8.6 Discussion

A more desirable implementation of the method outlined in the laser simulation section would be to take a laser charge-deposition profile directly from equations defining

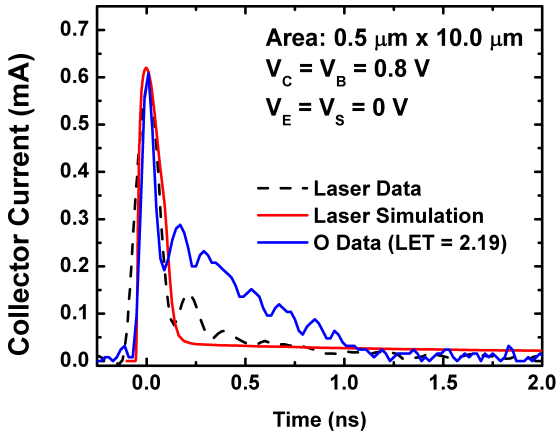

Figure 8.13: Calibrated profile compared to an O strike. Although matching in amplitude, there is still a mismatch in the decay characteristics of the diffusion tail. As a result, both laser curves underestimate the charge collection of a device-centered O strike. © 2016 IEEE.

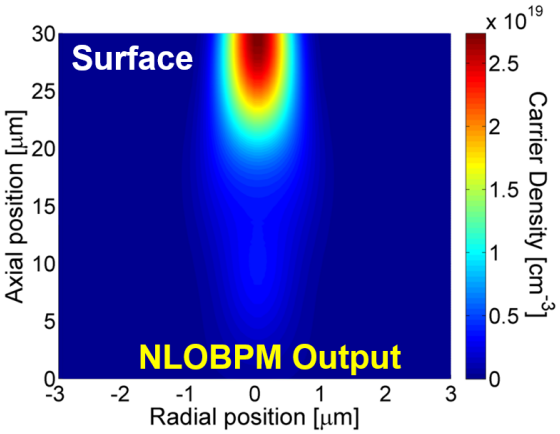

Figure 8.14: NLOBPM simulated carrier density for the large *npn* transistor. Photons are injected from the bottom (backside of the device) and are delivered to the sensitive volume that is near the surface of the die, which is located at the top of the image. © 2016 IEEE.

the optical carrier profile, like that seen in [99]. Fig. 8.14. shows such a profile created through the NLOBPM software package [100], and provides a more realistic spatial profile and holds the key to getting at a more elegant implementation of the carrier profile without having to overlay heavy-ion strike profiles or use a traditional heavy-ion strike. This flexibility will also provide realistic tuning that could be fed into a TPA system. In an improved implementation method, one would be able to say with greater assurance that the optical profile matches an experimental setting. As briefly touched upon in this work, slight modifications to the lateral dimension of the charge density profile will greatly alter the effective LET of the laser profile. Great care must be taken to ensure that generated charge-deposition profiles accurately account for heavily-doped materials and all interfaces that will alter the resulting spatial profile.

8.7 Summary

This work presents a discernible threshold where a heavy-ion strike that is of a modest to high LET ($>$ 3.49 MeV-cm^2/mg in this case) changes the observed decay mechanisms within a SiGe HBT from an exponential decay to a prompt exponential decay with a pronounced diffusion tail. This is a significant step in correlating TPA pulsed-laser data to an equivalent LET in SiGe HBT technologies as researchers may use a stand-alone transistor to calibrate the SET response of the device (i.e., to have a given transient tail) before using the beam to probe a circuit within the same technology. In addition, this work provides a statistical analysis to aid heavy-ion broadbeam testing. Results from this analysis show that there can be a significant disparity in the anticipated sensitive device area if only emitter-centered strikes can corrupt data. TCAD simulations investigate methods of matching pulsed-laser profiles to an effective LET and outlines a strategy for future simulation work. This study contributes a bevy of data which will provide the foundation to build upon a full TPA to heavy-ion correlation method within SiGe HBT technologies.

CHAPTER 9

CORRELATION 3D MODEL DEVELOPMENT AND IMPROVEMENT

The previously covered two photon absorption to heavy-ion correlation study identified a number of logical next steps along the path to using pulsed lasers as a more effective tool for SEE testing. First and foremost, it is necessary to improve the finite-difference time-domain (FDTD) model. Two-dimensional TCAD, although useful in identifying qualitative trends, is severely unequipped to describe an SEE event. Any radial component (think cylindrical coordinates for a charge track) is not extended properly along the virtual length of the device. For example, Sentaurus TCAD defaults a 2D model to have a virtual length of 1 μm. As such, any charge density profile described in 2D will be extended (unrealistically!) along the entire 1 μm segment as opposed to being confined about the strike location. This disparity is shown in Fig. 9.1. This solution will understandably overestimate the charge deposition in the structure for any model that is larger than the characteristic radius of the charge track, which is on the order of 10's of nm. Full three-dimensional TCAD is a must. Calibrating such a model, as will be discussed in this section, is a nontrivial task in itself but hardly all that can be improved upon.

Calibration of the 3D *npn* SiGe HBT in 5AM (the 'Golden Device') was done in Sentaurus TCAD. This calibration was based off of the PDK defined VBIC model which was used in Keysight's Advanced Design Systems (ADS) to simulate Gummel Characteristics for a 0.5 x 10.0 μm^2 transistor. This *dc* calibration is shown in Fig. 9.2. For *ac* calibration, the f_T and f_{MAX} for the model were determined using frequency transient simulations in TCAD. The extracted f_T from the model is 49.3

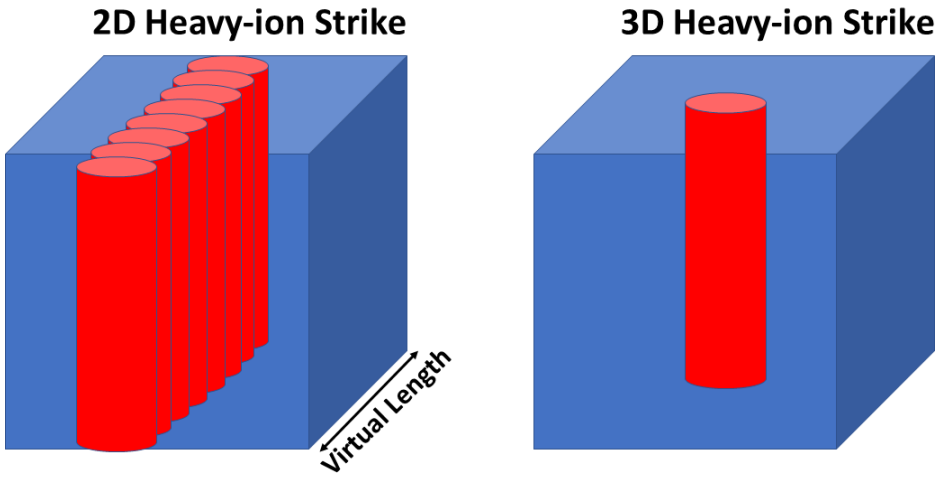

Figure 9.1: This cartoon depicts the difference between 2D and 3D heavy-ion strikes in TCAD. On the left is the 2D view where the charge track is artificially extended along the virtual length of the model. The 2D strike imparts much more charge in the structure than the more realistic 3D case (shown on the right).

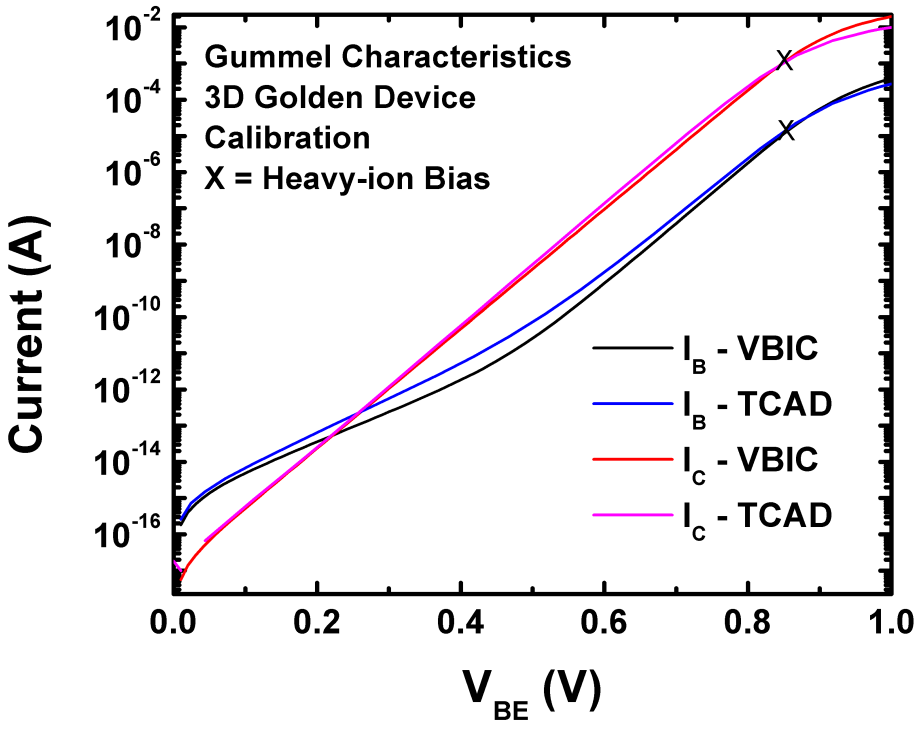

Figure 9.2: Gummel Characteristics for the VBIC model (provided by the PDK) and the calibrated 3D TCAD model. *DC* agreement is excellent, especially at the bias of interest of 0.85 V.

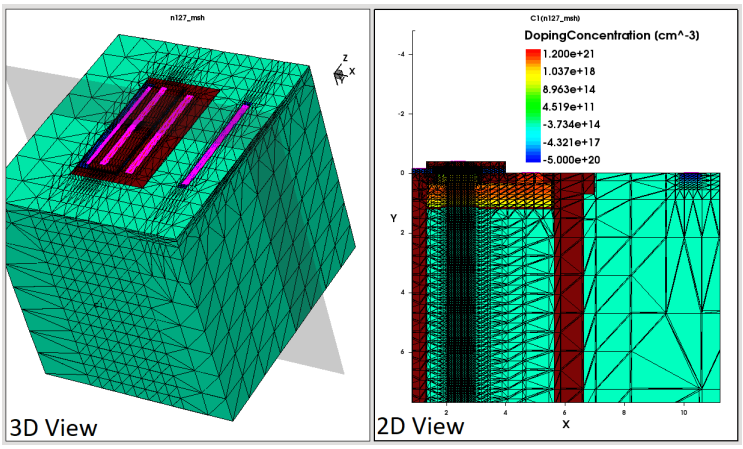

Figure 9.3: The left image depicts the meshed and calibrated 3D model of the Golden Device. The right image depicts a 1D-cut through the model showing how the model is further meshed for a heavy-ion strike.

GHz and the extracted f_{MAX} is 35.6 GHz. By comparison the PDK defined f_T is 47 GHz and the f_{MAX} is 65 GHz. The discrepancy between the f_{MAX} values is likely due to the extrinsic polysilicon base resistance. This is modeled in the TCAD environment simply as polysilicon whereas in reality a silicided polysilicon base is used (to specifically improve base resistance). The mesh of the structure contains roughly 79,000 points that comprise 460,000 individual elements. An example of a meshed 3D model is shown in Fig. 9.3. In terms of Wallclock CPU Time (total time to run a simulation on our network), *dc* simulations take roughly 8 hours and *ac* simulations take roughly 43 hours using fully hydrodynamic code (as opposed to drift-diffusion which solves much faster but is less accurate). The material parameters determining carrier lifetimes and mobility for Silicon, Polysilicon, and Silicon-Germanium is defined in the 'SiGeHBT.par' file provided by Synopsys 2015 version of Sentaurus for the purpose of simulating SiGe HBTs [16]. It is important to note that the mesh of the 3D structure must be altered during a heavy-ion strike about the strike location and depth to accurately solve for carrier deposition (further increasing the simulation time).

To further improve upon the 3D model, we now consider the entire signal path

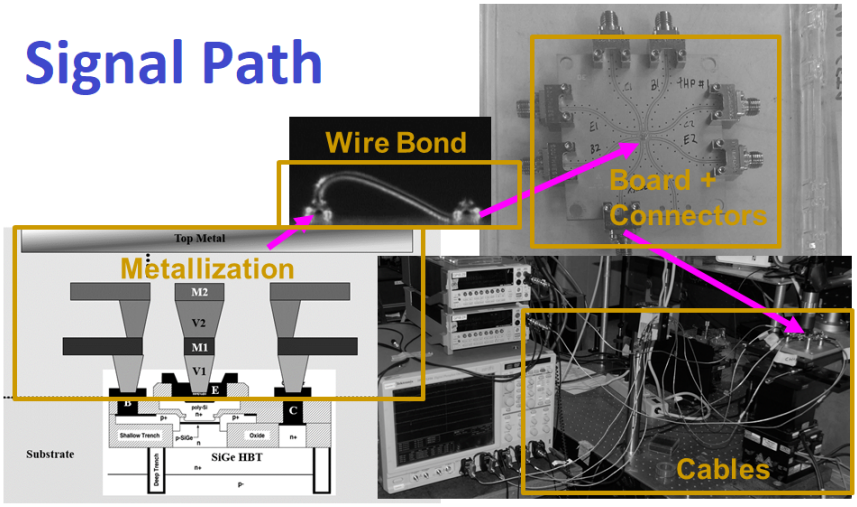

Figure 9.4: The full signal path of an SET starts at the device level but must travel through the top metallization then through the wire bonds, the board, the connector on the board, any cables and coupling, the bias tee, the scope front end, and any internal circuitry of the oscilloscope before it is measured.

from the generation of an SET within the transistor to its point of measurement at an oscilloscope as is seen in experiment. Fig. 9.4 shows this pictorially. The carrier flow is represented as an electrical current which must travel out of the device through contacts and metallization which is ignored in a stand alone FDTD model. Beyond the metal stack, the signal also passes through gold wire bonds, the board signal line, cabling, possibly couplers, bias tees, and the internal electrical circuitry of the oscilloscope where internal analog to digital converters (ADCs) have high noise floors and can only provide so much resolution.

For the extrinsic resistance, there is a finite amount of metal that exists between the device terminal contact and the top metal layer. These metals have a defined thickness, resistivity, and location. All of which should be readily available through a semiconductor process design kit (PDK). For the transistor size used here, the extrinsic collector resistance is 5 Ω, the extrinsic base resistance is 24 Ω, and the extrinsic emitter resistance is 3.4 Ω. It is possible to include these layers as drawn in the TCAD environment; however, these layers primarily contribute a linear resistance term. More involved electromagnetic simulators would be necessary to determine

parasitic capacitance and inductance. As such, one can calculate this extrinsic resistance by hand or pull the information from the PDK. Once acquired this resistor can be represented in simulation in mixed-mode TCAD. A much simpler solution than increasing the complexity of the device model by introducing more materials which in turn must be meshed.

In a similar manner the cable parasitics may be determined and then included in mixed-mode TCAD. This is done by measuring the scattering parameters (S-parameters) of the cable and then using a lumped model of discrete components to represent the S-parameters. A circuit simulator such as ADS may be used to optimize the values of the discrete components to accurately recreate the cable response. The main difference from the determination of the extrinsic resistances being that the cable response will be composed mainly of inductors and capacitors. An interpretation of this is that one can include the extrinsic resistance and cables (and even the board, wire bonds, and bias tees!) in such a fashion that one can consider the SET to be propagating through a series of two-port networks. At each network some portion of the signal will be transfered to the next stage and some portion will be reflected back. A schematic view of these networks is shown in Fig. 9.5. One of the implications of this view point is that electromagnetic and signal processing theory can provide significant contributions to being able to determine how much signal loss occurs from the measurement boards and equipment used during the study of SETs. Knowledge of the impact of any given cable, board, bias tee, etc. to the SET response is necessary to be able to predictively determine how a resulting waveform should appear. This becomes further challenging when one considers that heavy-ion models used here are based off an average occurrence of events, and that a true monte carlo approach is requisite to determine the spectrum of events which could occur. When considering the absolute best match one can achieve with a pulsed laser, one must always consider the average heavy-ion strike condition as a reference point.

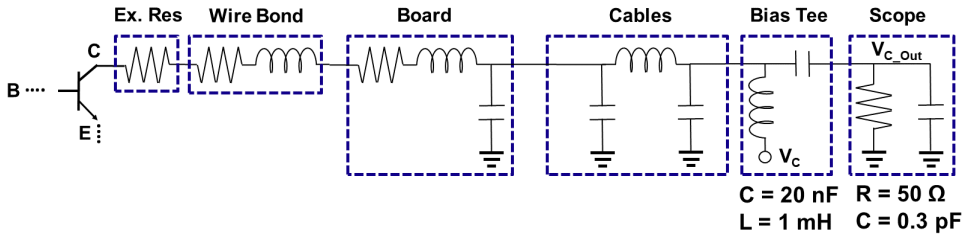

Figure 9.5: Schematic view of mixed-mode TCAD. Each boxed component can be thought of as a two-port network and has an impact on the SET waveform.

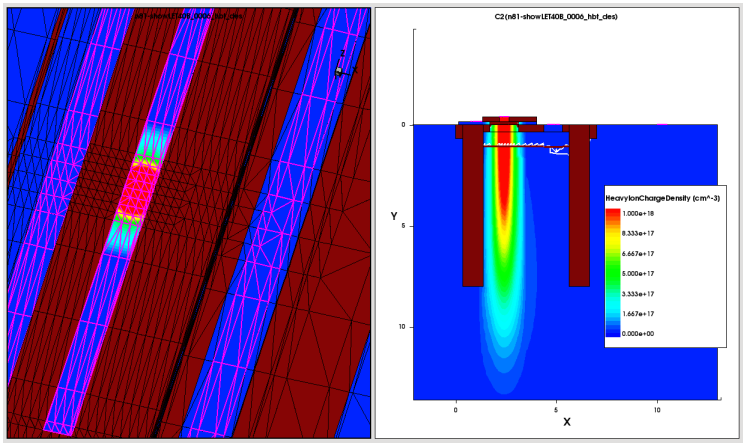

Figure 9.6: The left image shows the 3D view of a TPA pulsed-laser charge density profile in TCAD. The right image shows a cross section of this profile. It is worth noting that the range of the charge density profile is less than typical heavy ion strikes.

Determining the internal circuitry of the oscilloscope is challenging as such information is closely protected by the manufacturer. However the impact of the oscilloscope can be mitigated by using the same equipment at the best resolution settings. For the oscilloscope used in this work (Tektronix DPO71254) this means always setting the channels at a vertical resolution of 10 mV/div and the horizontal resolution at 20 ps/pt. Discretization errors always exist when trying to perfectly represent an analog signal. However, these errors can be mitigated by using identical equipment when comparing signals from different sources of radiation.

Of more importance is the description of the charge density profile be it by heavy-ion or TPA pulsed laser. An example of a TPA pulsed-laser strike in 3D TCAD is shown in Fig. 9.6. Two descriptions may used within Sentaurus's Heavy Ion Model

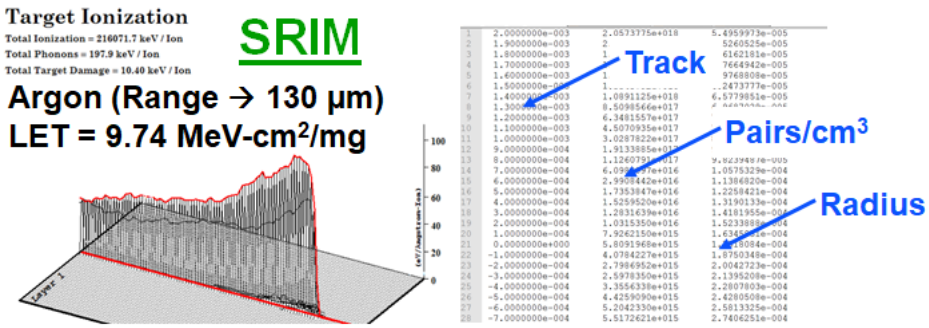

Figure 9.7: The left image shows an output of SRIM where the stopping power is plotting as a function of depth in a silicon substrate. The right image shows the custom generated file from SRIM that can be imported seamlessly in TCAD. The exact same file format is used for output files generated by NLOBPM.

[16]. The first is defining a heavy ion strike in terms of pC/μm and the second is in terms of pairs/cm^3. As the NLOBPM software used to create the TPA pulsed-laser profiles uses pairs that is the method used here. An example of this file format is shown in Fig. 9.7. Both pC/μm and pairs/cm^3 are derivable for silicon where 22.5 MeV/pC comes from the average energy required to create an electron hole pair (3.6 eV in Si) divided by the fundamental charge of an ion pair (1.6*10^{-7} pC). For the case of representing a realistic heavy ion, SRIM may be recruited to determine the most pertinent parameters. Through tracking a large number of simulated strikes, one is able to use a vertical target depth of a material, meshed, represented in Angstroms and get the average ionization of the ion in terms of eV/Angstrom, which is equivalent to the stopping power. These terms may be used, setting a characteristic radius for the ion, to give the necessary pairs/cm^3. Alternatively one can take the stopping power provided by SRIM and then divide by 22.5 MeV/pC to describe the charge profile. The assumption used here is that the characteristic radius of the ion is known. To get the most realistic value of the radius, a more advanced simulation software (such as Geant-4) **must** be recruited to determine the strike radius. The main contributing factor here being the delta-ray production (electron shower) that is created by the target material lattice in an attempt to slow down the ionized particle.

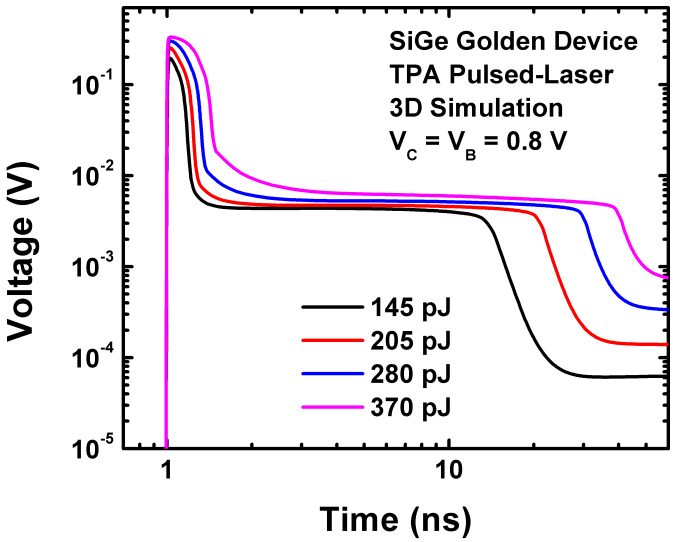

Figure 9.8: Simulated TPA pulsed-laser strikes in TCAD. Results show both the peak and duration of the SET to increase as a function of energy. Focusing spot size is approximately 1 μm using a 100X objective lens.

The NLOBPM profiles used in this work are able to account for the energy of the pulsed-laser, the focusing parameters, and the generation of carriers via two photon absorption. These profiles are generated assuming a pure Si substrate. Refer to [18,98] for more information on the NLOBPM simulations. Example TCAD simulations for varying laser energy in TCAD is shown in Fig. 9.8. These simulations and similar ones varying spot size are able to provide good qualitative understanding of what waveform changes result from altering laser parameters. These simulations provide a proof of concept for importing the charge generation profiles within the TCAD environment. For quantitative comparison purposes, the generated carrier profiles need to account for the contributions of Ge and heavy doping effects. Of particular interest is that these effects can create a more 'single photon' like signature as bandgap narrowing is associated with both the introduction of Ge and with a more heavily doped material (think anything doped greater than $10^{17}/\text{cm}^3$). At 1260 nm, the wavelength used for experiments at the Naval Research Laboratory, the photons are equivalently seen as containing 0.98 eV which is close to the bandgap of silicon, which is 1.12 eV. One possibility is that a lower energy pulsed laser (higher wavelength) could be more

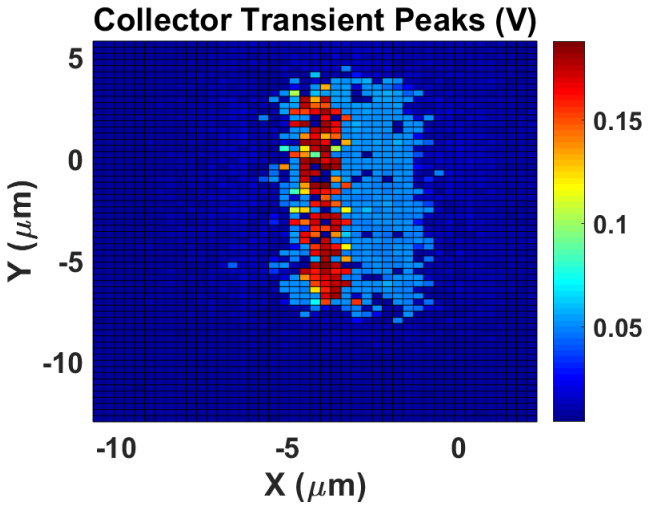

Figure 9.9: 2D strike map for microbeam Calcium heavy ion strikes from GSI.

appropriate for SiGe HBTs. However, such investigations are outside of the scope of this thesis and discussed in further detail in the 'Future Work' section.

One issue that arises when trying to simulate either heavy ions or TPA pulsed lasers in TCAD is the size of the substrate. Ideally one would like to develop the model using the actual substrate size with a reasonable mesh. In 3D such an approach can result in millions of elements and take up too much computer memory to solve or take a very long time to reach a converged solution. One approach taken in previous work is to alter mobility lifetimes in the substrate of the SiGe HBT [101]. One other possible solution is use a wrapper layer around the substrate with greatly reduced carrier lifetimes to mimic carrier out diffusion [102]. Of the two approaches the wrapper layer method is preferred as it is further removed from the intrinsic device operation. Either way though, a non-physical parameter must be tuned for the model – a welcome tradeoff when compared to the extreme computational overhead in substantially increasing the substrate size.

One question that remains, is how close to real heavy-ion data can we get in simulation? And the answer is very close in terms of peak amplitude. Looking at a 2D map of microbeam heavy-ion data from GSI (using a Ca ion with an LET of

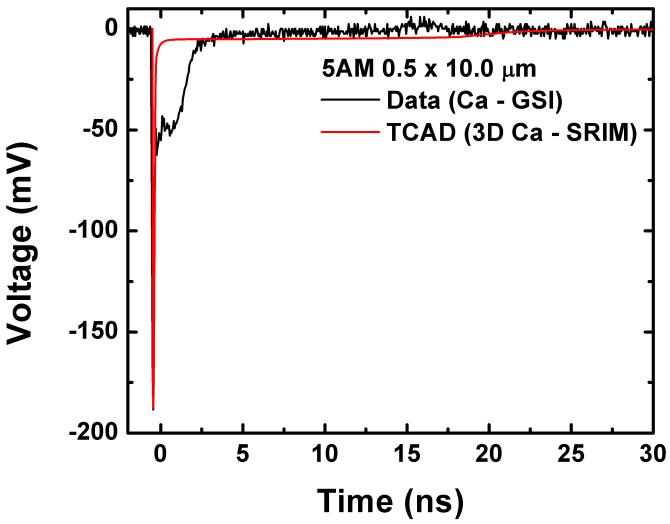

Figure 9.10: Waveform comparison of heavy-ion data to simulation data without parasitics.

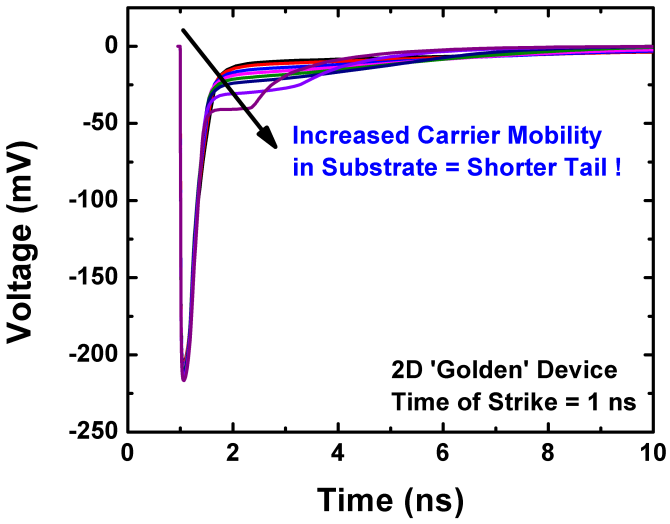

Figure 9.11: Simulation work shows that changing hole mobility in the substrate (increase it) will lead to a tighter, more defined tail without overly effecting the collected charge.

approximately 17) we get peaks at a max amplitude of 188.4 mV. This map is shown in Fig. 9.9. Through TCAD, at an equivalent bias and neglecting parasitics, the max amplitude for a 3D heavy ion strike model is 187.8 mV with a strike perfectly centered on the emitter, so there is nearly a perfect match. This result is shown in Fig. 9.10. In terms of collected charge the TCAD solution provides a collected charge of 2.66 pC whereas the experimental result has 3.10 pC. A percent change increase of 16.5%. As mentioned previously, these simulations results are being run without the impact of the board and the cables. With these L/C components one is able to achieve better tail matching, alternatively one may also increase the effective mobility of holes in substrate, shown for a 2D model in Fig. 9.11, to increase the tail duration as well without affecting intrinsic device operation.

CHAPTER 10

CONCLUSION

This thesis investigates a number of radiation hardness concerns for SiGe HBTs being operated in harsh radiation environments. The first chapter (Introduction) discusses the goals of the work and the layout of the document. The second chapter (Overview) provides a high level view of the research covered. Topics included in this section cover the 4 major studies presented in this work along with their importance to the radiation effects community. The third chapter (Silicon-Germanium Technology) covers the basic operating principals of SiGe HBTs. As Silicon bipolar junction transistors are a basic transistor technology covered in introductory device physics textbooks, emphasis is instead put on how SiGe HBTs differ and improve upon Si BJTs. The fourth chapter (Basic Radiation Mechanisms) covers the three major types of radiation-induced damage, how these effects are exhibited in SiGe HBTs, where radiation comes from, and how basic mitigation strategies work. The fifth chapter (TID in a BiCMOS Technology) covers total dose effects in a TowerJazz Semiconductor technology that is being considered for multi-Mrad dose environments (Jupiter's moon Europa). Results show that both the SiGe HBTs and CMOS are highly tolerant to TID due to the triple-well process of the technology. Large CMOS structures are recommended in such a technology as they experience smaller threshold voltage shifts when compared to small devices. The sixth chapter (ELDRS in SiGe HBTs) covers dose rate effects in *npn* SiGe HBTs. This study includes devices from 1^{st}, 3^{rd}, and 4^{th}-generation GlobalFoundries' processes. The findings of this work show enhanced low dose rate sensitivity (ELDRS) effects to not be present in these technologies. The seventh chapter (Vertical SiGe HBT Profile Changes) covers modifications to

the doping profile of SiGe HBTs to improve inverse-mode (IM) device operation. The results of this work show that improved device performance is naturally coupled to a worsened SET response. In addition, this work identifies higher degradation to the IM response than the forward active mode response. The eighth chapter (Two Photon Absorption to Heavy-ion Correlation) explores the considerations that are needed from both experiments and simulation to correlate pulsed-laser results to heavy-ion results. The work outlines certain waveform characteristics that are only present for certain radiation strike conditions of a sufficient energy. Chapter nine (Correlation 3D Model Development and Improvement) then builds upon the correlation work using 3D models and advanced TCAD techniques. Of particular interest is using real TPA profiles generated through NLOBPM and a unified file format that is compatible with both heavy-ion and pulsed-laser simulations.

This dissertation investigates both total ionizing dose and single-event effect damage mechanisms in SiGe HBTs. In order to qualify SiGe HBTs for space or other intense radiation environments both these topics must be considered. This work adds to the knowledge base of radiation effects in SiGe HBTs in the following ways:

- There exists SiGe HBT technologies (i.e. TowerJazz) that have highly TID tolerant CMOS to pair with the SiGe HBTs.
- True dose rate effects are not a concern in state-of-the-art SiGe HBT platforms.
- Inverse-mode SiGe HBT performance can be improved but it comes at a cost to SEE performance.
- A path has been identified to more accurately simulate and correlate TPA pulsed-laser and heavy-ion carrier density profiles.

CHAPTER 11

FUTURE WORK

The research investigations covered in this dissertation have highlighted a number of future investigations. These ideas are listed below and expanded upon:

1. **Wavelength Dependent Pulsed Laser Studies**

   Wavelength dependent pulsed-laser experiments are a logical next step in understanding and simulating TPA pulsed lasers. Advanced semiconductor materials are rarely one solid block of material. EHP generation due to photon excitation depends on the bandgap of the material and the doping of the material as well. There is concern that single photon excitation can start to play a role in carrier generation when the energy of the photons approach the energy of the bandgap. It is necessary in SiGe HBTs to investigate whether or not this effect is occurring. One way to account for this is to generate optical carrier profiles including the affect of single photon absorption due to Ge films. This modified carrier density profile would give an indication of how pronounced this effect can be for varying wavelengths. Recent SiGe technologies tend to have higher concentrations of Ge than older technologies – indicating that this effect could be more pronounced due to the device structure as opposed to the source of radiation.

2. **Correlation in CMOS and other Structures**

   Although SiGe HBTs are the technology of interest in this work, correlation of heavy-ion and TPA pulsed-laser effects are important for all electronics. As diodes are the simplest semiconductor structure (a single junction) one approach could be to focus on correlating SETs in large, lowly doped diodes. In this way,

one could focus on the effects of say Ge films or heavy doping effects before accounting for both at the same time. It is possible to design custom diode structures without topside metallization as well. This could allow researchers to optically probe from backside or from topside to provide comparison to single photon absorption (SPA) pulsed lasers which generally have a limited range in silicon.

3. **Fully Optimized IM Profiles**

   Previous literature [87] has identified the lateral transistor layout to be an important driver in inverse-mode SiGe HBT performance. An obvious next step would be to combine the vertical doping profile changes discussed in this work along with those lateral transistor modifications to create a further optimized inverse-mode SiGe HBT. It would be interesting to see if near forward active speeds are achievable.

4. **Focused, Pulsed X-ray SEE Study**

   A number of recent investigations from the Aerospace Corporation have identified the Advanced Photon Source (APS) at Argonne National Laboratory as being capable of inducing SETs much in the same way as a TPA pulsed laser [103, 104]. The main difference between the two sources being that the more highly energetic photons (keV x-rays) from the APS source is able to penetrate through topside metal – making backside testing unnecessary. These studies have shown that the source can be focused down to spot sizes similar to those achievable with a standard pulsed laser setup (few microns). The facility has a tunable energy range for high energy x-rays which will result in varying attenuation ranges within silicon. It would be interesting to determine if there is an optimal energy and focusing setup at this facility such that this source could also be used in place of heavy ion testing.

REFERENCES

[1] **Z. E. Fleetwood**, E. W. Kenyon, N. E. Lourenco, S. Jain, E. X. Zhang, T. D. England, J. D. Cressler, R. D. Schrimpf, and D. M. Fleetwood, "Advanced SiGe BiCMOS Technology for Multi-Mrad Electronic Systems," *IEEE Transactions on Device and Materials Reliability*, vol. 14, pp. 844–848, Sept 2014.

[2] **Z. E. Fleetwood**, A. S. Cardoso, I. Song, E. Wilcox, N. E. Lourenco, S. D. Phillips, R. Arora, P. Paki-Amouzou, and J. D. Cressler, "Evaluation of Enhanced Low Dose Rate Sensitivity in Fourth-Generation SiGe HBTs," *IEEE Trans. Nucl. Sci.*, vol. 61, pp. 2915–2922, Dec 2014.

[3] **Z. E. Fleetwood**, B. R. Wier, U. S. Raghunathan, N. E. Lourenco, M. A. Oakley, A. J. Joseph, and J. D. Cressler, "Optimizing the vertical profile of SiGe HBTs to mitigate radiation-induced upsets," in *2015 IEEE Bipolar/BiCMOS Circuits and Technology Meeting - BCTM*, pp. 72–75, Oct 2015.

[4] **Z. E. Fleetwood**, A. Ildefonso, G. N. Tzintzarov, B. Wier, U. Raghunathan, M. K. Cho, I. Song, M. T. Wachter, D. Nergui, A. Khachatrian, J. H. Warner, P. McMarr, H. Hughes, E. Zhang, D. McMorrow, P. Paki, A. Joseph, V. Jain, and J. D. Cressler, "SiGe HBT Profiles with Enhanced Inverse-Mode Operation and their Impact on Single-Event Transients," *IEEE Trans. Nucl. Sci.*, vol. PP, pp. 1–1, Jan 2018.

[5] **Z. E. Fleetwood**, N. E. Lourenco, A. Ildefonso, J. H. Warner, M. T. Wachter, J. M. Hales, G. N. Tzintzarov, N. J. H. Roche, A. Khachatrian, S. P. Buchner, D. McMorrow, P. Paki, and J. D. Cressler, "Using TCAD Modeling to Compare

Heavy-Ion and Laser-Induced Single Event Transients in SiGe HBTs," *IEEE Trans. Nucl. Sci.*, vol. 64, pp. 398–405, Jan 2017.

[6] **Z. E. Fleetwood**, "On the Effects of Total Ionizing Dose in Silicon-Germanium BiCMOS Platforms," *Georgia Tech Theses and Dissertations*, pp. 1–71, Dec 2014.

[7] Y. Li, J. Cressler, Y. Lu, J. Pan, G. Niu, R. Reed, P. Marshall, C. Polar, M. Palmer, and A. Joseph, "Proton tolerance of multiple-threshold voltage and multiple-breakdown voltage CMOS device design points in a 0.18 μm system-on-a-chip CMOS technology," *IEEE Trans. Nucl. Sci.*, vol. 50, pp. 1834–1838, Dec. 2003.

[8] C. Castaneda, "Crocker nuclear laboratory (CNL) radiation effects measurement and test facility," in *Proc. 2001 IEEE Radiations Effects Data Workshop*, pp. 77–81, 2001.

[9] F. Faccio and G. Cervelli, "Radiation-induced edge effects in deep submicron CMOS transistors," *IEEE Trans. Nucl. Sci.*, vol. 52, pp. 2413–2420, Dec. 2005.

[10] M. Gaillardin, V. Goiffon, S. Girard, M. Martinez, P. Magnan, and P. Paillet, "Enhanced radiation-induced narrow channel effects in commercial 0.18 μm bulk technology," *IEEE Trans. Nucl. Sci.*, vol. 58, pp. 2807–2815, Dec. 2011.

[11] K. Clark, G. Tan-Wang, J. Boldt, R. Greeley, I. Jun, R. Lock, J. Ludwinski, R. Pappalardo, T. Van Houten, and T. Yan, "Return to Europa: Overview of the Jupiter Europa Orbiter mission," in *Proc. 2009 IEEE Aerospace Conf.*, pp. 1–20, Mar. 2009.

[12] J. R. Schwank, M. R. Shaneyfelt, and P. E. Dodd, "Radiation hardness assurance testing of microelectronic devices and integrated circuits: Radiation

environments, physical mechanisms, and foundations for hardness assurance," *IEEE Trans. Nucl. Sci.*, vol. 60, pp. 2074–2100, June 2013.

[13] N. L. Rowsey, M. E. Law, R. D. Schrimpf, D. M. Fleetwood, B. R. Tuttle, and S. T. Pantelides, "Mechanisms separating time-dependent and true dose-rate effects in irradiated bipolar oxides," *IEEE Trans. Nucl. Sci.*, vol. 59, pp. 3069–3076, Dec 2012.

[14] E. W. Enlow, R. L. Pease, W. Combs, R. D. Schrimpf, and R. N. Nowlin, "Response of advanced bipolar processes to ionizing radiation," *IEEE Trans. Nucl. Sci.*, vol. 38, pp. 1342–1351, Dec 1991.

[15] D. McMorrow, W. T. Lotshaw, J. S. Melinger, S. Buchner, and R. L. Pease, "Subbandgap laser-induced single event effects: carrier generation via two-photon absorption," *IEEE Trans. Nucl. Sci.*, vol. 49, pp. 3002–3008, Dec 2002.

[16] "Synopsys, [ONLINE] http://www.synopsys.com/home.aspx," 2014.

[17] J. Burghartz, K. Jenkins, D. Grutzmacher, T. Sedgwick, and C. Stanis, "High-performance emitter-up/down SiGe HBT's," *Electron Device Letters, IEEE*, vol. 15, pp. 360–362, Sept 1994.

[18] J. M. Hales, N. J.-H. Roche, A. Khachatrian, D. McMorrow, S. Buchner, J. Warner, M. Turowski, K. Lilja, N. C. Hooten, E. X. Zhang, R. A. Reed, and R. D. Schrimpf, "Two-Photon Absorption Induced Single-Event Effects: Correlation Between Experiment and Simulation," *IEEE Trans. Nucl. Sci.*, vol. 62, pp. 2867–2873, Dec 2015.

[19] B. G. Streetman and S. K. Banerjee, "Solid State Electronic Devices," vol. 6th, Pearson Education, Inc., 2006.

[20] J. D. Cressler, "Radiation Effects in SiGe technology," *IEEE Trans. Nucl. Sci.*, vol. 60, pp. 1992–2014, June 2013.

[21] J. D. Cressler and G. Niu, "Silicon-Germanium heterojunction bipolar transistors," vol. 1, Artech House, INC., 2003.

[22] F. B. McLean and T. R. Oldham, "Basic Mechanisms of Radiation Effects in Electronic Materials and Devices," *Harry Diamond Labs ADELPHI MD*, 1987.

[23] M. R. Shaneyfelt, D. M. Fleetwood, J. R. Schwank, and K. L. Hughes, "Charge yield for cobalt-60 and 10-keV X-ray irradiations of MOS devices," *IEEE Trans. Nucl. Sci.*, vol. 38, pp. 1187–1194, Dec 1991.

[24] J. R. Schwank, M. R. Shaneyfelt, P. E. Dodd, V. Ferlet-Cavrois, R. A. Loemker, P. S. Winokur, D. M. Fleetwood, P. Paillet, J. L. Leray, B. L. Draper, S. C. Witczak, and L. C. Riewe, "Correlation between Co-60 and X-ray radiation-induced charge buildup in silicon-on-insulator buried oxides," *IEEE Trans. Nucl. Sci.*, vol. 47, pp. 2175–2182, Dec 2000.

[25] J. Mekki, M. Brugger, R. G. Alia, A. Thornton, N. C. D. S. Mota, and S. Danzeca, "CHARM: A Mixed Field Facility at CERN for Radiation Tests in Ground, Atmospheric, Space and Accelerator Representative Environments," *IEEE Trans. Nucl. Sci.*, vol. 63, pp. 2106–2114, Aug 2016.

[26] R. A. Reed, J. Kinnison, J. C. Pickel, S. Buchner, P. W. Marshall, S. Kniffin, and K. A. LaBel, "Single-event effects ground testing and on-orbit rate prediction methods: the past, present, and future," *IEEE Trans. Nucl. Sci.*, vol. 50, pp. 622–634, June 2003.

[27] E. L. Petersen, R. Koga, M. A. Shoga, J. C. Pickel, and W. E. Price, "The Single Event Revolution," *IEEE Trans. Nucl. Sci.*, vol. 60, pp. 1824–1835, June 2013.

[28] H. Ohyama, J. Vanhellemont, Y. Takami, K. Hayama, H. Sunaga, J. Poortmans, M. Caymax, and P. Clauws, "Germanium content dependence of radiation damage in strained Si/sub 1-x/Ge/sub x/ epitaxial devices," *IEEE Trans. Nucl. Sci.*, vol. 41, pp. 2437–2442, Dec 1994.

[29] J. A. Babcock, J. D. Cressler, L. S. Vempati, S. D. Clark, R. C. Jaeger, and D. L. Harame, "Ionizing radiation tolerance of high-performance SiGe HBT's grown by UHV/CVD," *IEEE Trans. Nucl. Sci.*, vol. 42, pp. 1558–1566, Dec 1995.

[30] J. D. Cressler, R. Krithivasan, A. K. Sutton, J. E. Seiler, J. F. Krieg, S. D. Clark, and A. J. Joseph, "The impact of gamma irradiation on SiGe HBTs operating at cryogenic temperatures," *IEEE Trans. Nucl. Sci.*, vol. 50, pp. 1805–1810, Dec 2003.

[31] J. M. Roldan, G. Niu, W. E. Ansley, J. D. Cressler, S. D. Clark, and D. C. Ahlgren, "An investigation of the spatial location of proton-induced traps in SiGe HBTs," *IEEE Trans. Nucl. Sci.*, vol. 45, pp. 2424–2429, Dec 1998.

[32] K. A. Moen, P. S. Chakraborty, U. S. Raghunathan, J. D. Cressler, and H. Yasuda, "Predictive Physics-Based TCAD Modeling of the Mixed-Mode Degradation Mechanism in SiGe HBTs," *IEEE Transactions on Electron Devices*, vol. 59, pp. 2895–2901, Nov 2012.

[33] U. S. Raghunathan, P. S. Chakraborty, T. G. Bantu, B. R. Wier, H. Yasuda, P. Menz, and J. D. Cressler, "Bias- and Temperature-Dependent Accumulated Stress Modeling of Mixed-Mode Damage in SiGe HBTs," *IEEE Transactions on Electron Devices*, vol. 62, pp. 2084–2091, July 2015.

[34] C. Mukherjee, T. Jacquet, G. G. Fischer, T. Zimmer, and C. Maneux, "Hot-Carrier Degradation in SiGe HBTs: A Physical and Versatile Aging Compact

Model," *IEEE Transactions on Electron Devices*, vol. 64, pp. 4861–4867, Dec 2017.

[35] G. Niu, J. D. Cressler, M. Shoga, K. Jobe, P. Chu, and D. L. Harame, "Simulation of SEE-induced charge collection in UHV/CVD SiGe HBTs," *IEEE Trans. Nucl. Sci.*, vol. 47, pp. 2682–2689, Dec 2000.

[36] P. W. Marshall, M. A. Carts, A. Campbell, D. McMorrow, S. Buchner, R. Stewart, B. Randall, B. Gilbert, and R. A. Reed, "Single event effects in circuit-hardened SiGe HBT logic at gigabit per second data rates," *IEEE Trans. Nucl. Sci.*, vol. 47, pp. 2669–2674, Dec 2000.

[37] P. Marshall, M. Carts, A. Campbell, R. Ladbury, R. Reed, C. Marshall, S. Currie, D. McMorrow, S. Buchner, C. Seidleck, P. Riggs, K. Fritz, B. Randall, and B. Gilbert, "A comparative study of heavy-ion and proton-induced bit-error sensitivity and complex burst-error modes in commercially available high-speed SiGe BiCMOS," *IEEE Trans. Nucl. Sci.*, vol. 51, pp. 3457–3463, Dec 2004.

[38] J. A. Pellish, R. A. Reed, R. D. Schrimpf, M. L. Alles, M. Varadharajaperumal, G. Niu, A. K. Sutton, R. M. Diestelhorst, G. Espinel, R. Krithivasan, J. P. Comeau, J. D. Cressler, G. Vizkelethy, P. W. Marshall, R. A. Weller, M. H. Mendenhall, and E. J. Montes, "Substrate Engineering Concepts to Mitigate Charge Collection in Deep Trench Isolation Technologies," *IEEE Trans. Nucl. Sci.*, vol. 53, pp. 3298–3305, Dec 2006.

[39] S. D. Phillips, K. A. Moen, L. Najafizadeh, R. M. Diestelhorst, A. K. Sutton, J. D. Cressler, G. Vizkelethy, P. E. Dodd, and P. W. Marshall, "A Comprehensive Understanding of the Efficacy of N-Ring SEE Hardening Methodologies in SiGe HBTs," *IEEE Trans. Nucl. Sci.*, vol. 57, pp. 3400–3406, Dec 2010.

[40] J. F. Ziegler, J. P. Biersack, and M. D. Ziegler, "SRIM 2013," *[Online] http://www.srim.org/SRIM/SRIM2011.htm.*

[41] R. Krithivasan, P. W. Marshall, M. Nayeem, A. K. Sutton, W. M. Kuo, B. M. Haugerud, L. Najafizadeh, J. D. Cressler, M. A. Carts, C. J. Marshall, D. L. Hansen, K. C. M. Jobe, A. L. McKay, G. Niu, R. Reed, B. A. Randall, C. A. Burfield, M. D. Lindberg, B. K. Gilbert, and E. S. Daniel, "Application of RHBD Techniques to SEU Hardening of Third-Generation SiGe HBT Logic Circuits," *IEEE Trans. Nucl. Sci.*, vol. 53, pp. 3400–3407, Dec 2006.

[42] K. Avery, "Selection of Integrated Circuits for Space Systems," *Nuclear and Space Radiation Effects Conference Short Course Notebook*, vol. Ch. 2, pp. 1–44, July 2009.

[43] V. Bothmer, "Invited Talk: The Sun and Space Weather in 3D – From Research to Operations," *in RADECS 2016*, Bremen, Germany, 2016.

[44] H. Evans, S. Calders, E. D. Doner, M. Kruglandski, and N. Messios, "SPENVIS 4.6.9," *[Online] https://www.spenvis.oma.be/*, 1997-2016.

[45] B. R. Bhat, N. Upadhyaya, and R. Kulkarni, "Total radiation dose at geostationary orbit," *IEEE Trans. Nucl. Sci.*, vol. 52, pp. 530–534, April 2005.

[46] I. Jun, "Short Couse: Past, Present, and Future NASA Missions to Jupiter," *in RADECS 2016*, Bremen, Germany, 2016.

[47] S. Smith, "Dynamic jupiter," *The Thunderbolts Project, 2015*, [ONLINE] https://www.thunderbolts.info/wp/2015/03/02/dynamic-jupiter-2/.

[48] A. J. Tylka, J. H. Adams, P. R. Boberg, B. Brownstein, W. F. Dietrich, E. O. Flueckiger, E. L. Petersen, M. A. Shea, D. F. Smart, and E. C. Smith,

"CREME96: A Revision of the Cosmic Ray Effects on Micro-Electronics Code," *IEEE Trans. Nucl. Sci.*, vol. 44, pp. 2150–2160, Dec 1997.

[49] J. Cressler, "On the potential of SiGe HBTs for extreme environment electronics," *Proc. IEEE*, vol. 93, pp. 1559–1582, Sept. 2005.

[50] J. Cressler, M. Hamilton, G. Mullinax, Y. Li, G. Niu, C. Marshall, P. Marshall, H. Kim, M. Palmer, A. Joseph, and G. Freeman, "The effects of proton irradiation on the lateral and vertical scaling of UHV/CVD SiGe HBT BiCMOS technology," *IEEE Trans. Nucl. Sci.*, vol. 47, pp. 2515–2520, Dec. 2000.

[51] J. Cressler, R. Krithivasan, G. Zhang, G. Niu, P. Marshall, H. Kim, R. Reed, M. Palmer, and A. Joseph, "An investigation of the origins of the variable proton tolerance in multiple SiGe HBT BiCMOS technology generations," *IEEE Trans. Nucl. Sci.*, vol. 49, pp. 3203–3207, Dec. 2002.

[52] Y. Lu, J. Cressler, R. Krithivasan, Y. Li, R. Reed, P. Marshall, C. Polar, G. Freeman, and D. Ahlgren, "Proton tolerance of third-generation, 0.12 μm 185 GHz SiGe HBTs," *IEEE Trans. Nucl. Sci.*, vol. 50, pp. 1811–1815, Dec. 2003.

[53] J. Comeau, A. Sutton, B. Haugerud, J. Cressler, W.-M. L. Kuo, P. Marshall, R. Reed, A. Karroy, and R. Van Art, "Proton tolerance of advanced SiGe HBTs fabricated on different substrate materials," *IEEE Trans. Nucl. Sci.*, vol. 51, pp. 3743–3747, Dec. 2004.

[54] K. Clark, "Europa explorer—an exceptional mission using existing technology," in *Proc. 2007 IEEE Aerospace Conf.*, pp. 1–20, Mar. 2007.

[55] R. Lock, K. Hibbard, R. Rasmussen, K. Clark, T. Magner, R. Pappalardo, and M. Jones, "Building operability into the Jupiter Europa orbiter design to endure

a high radiation environment," in *Proc. 2010 IEEE Aerospace Conf.*, pp. 1–14, Mar. 2010.

[56] G. Niu, S. Mathew, G. Banerjee, J. Cressler, S. Clark, M. Palmer, and S. Subbanna, "Total dose effects on the shallow-trench isolation leakage current characteristics in a 0.35 μm SiGeBiCMOS technology," *IEEE Trans. Nucl. Sci.*, vol. 46, pp. 1841–1847, Dec. 1999.

[57] M. Turowski, A. Raman, and R. Schrimpf, "Nonuniform total-dose-induced charge distribution in shallow-trench isolation oxides," *IEEE Trans. Nucl. Sci.*, vol. 51, pp. 3166–3171, Dec. 2004.

[58] N. Rezzak, R. Schrimpf, M. Alles, E. X. Zhang, D. Fleetwood, and Y. Li, "Layout-related stress effects on radiation-induced leakage current," *IEEE Trans. Nucl. Sci.*, vol. 57, pp. 3288–3292, Dec. 2010.

[59] D. Fleetwood, "Total ionizing dose effects in MOS and low-dose-rate-sensitive linear-bipolar devices," *IEEE Trans. Nucl. Sci.*, vol. 60, pp. 1706–1730, June 2013.

[60] J. D. Cressler, "On the Potential of SiGe HBTs for Extreme Environment Electronics," *Proc. IEEE*, vol. 93, pp. 1559–1582, Sept 2005.

[61] B. Jagannathan, M. Khater, F. Pagette, J.-S. Rieh, D. Angell, H. Chen, J. Florkey, F. Golan, D. R. Greenberg, R. Groves, S. J. Jeng, J. Johnson, E. Mengistu, K. T. Schonenberg, C. M. Schnabel, P. Smith, A. Stricker, D. Ahlgren, G. Freeman, K. Stein, and S. Subbanna, "Self-aligned sige npn transistors with 285 ghz f/sub max/ and 207 ghz f/sub t/ in a manufacturable technology," *Electron Device Letters, IEEE*, vol. 23, pp. 258–260, May 2002.

[62] D. M. Fleetwood, S. L. Kosier, R. N. Nowlin, R. D. Schrimpf, J. Reber, R. A., M. DeLaus, P. S. Winokur, A. Wei, W. E. Combs, and R. L. Pease, "Physical

mechanisms contributing to enhanced bipolar gain degradation at low dose rates," *IEEE Trans. Nucl. Sci.*, vol. 41, pp. 1871–1883, Dec 1994.

[63] H. P. Hjalmarson, R. L. Pease, S. C. Witczak, M. R. Shaneyfelt, J. R. Schwank, A. H. Edwards, C. E. Hembree, and T. R. Mattsson, "Mechanisms for radiation dose-rate sensitivity of bipolar transistors," *IEEE Trans. Nucl. Sci.*, vol. 50, pp. 1901–1909, Dec 2003.

[64] R. L. Pease, R. D. Schrimpf, and D. M. Fleetwood, "ELDRS in bipolar linear circuits: A review," *IEEE Trans. Nucl. Sci.*, vol. 56, pp. 1894–1908, Aug 2009.

[65] P. Cheng, J. A. Pellish, M. A. Carts, S. Phillips, E. Wilcox, T. Thrivikraman, L. Najafizadeh, J. D. Cressler, and P. W. Marshall, "Re-examining TID hardness assurance test protocols for SiGe HBTs," *IEEE Trans. Nucl. Sci.*, vol. 56, pp. 3318–3325, Dec 2009.

[66] M. Ullan, M. Wilder, H. Spieler, E. Spencer, S. Rescia, F. M. Newcomer, F. Martinez-McKinney, W. Kononenko, A. A. Grillo, and S. Diez, "Enhanced low dose rate sensitivy (ELDRS) tests on advanced SiGe bipolar transistors for very high total dose applications," *Nuclear Instruments and Method in Physics Research*, vol. 724, pp. 41–46, Dec 2012.

[67] A. K. Sutton, A. P. G. Prakash, B. Jun, E. Zhao, M. Bellini, J. Pellish, R. M. Diestelhorst, M. A. Carts, A. Phan, R. Ladbury, J. D. Cressler, P. W. Marshall, C. J. Marshall, R. A. Reed, R. D. Schrimpf, and D. M. Fleetwood, "An Investigation of Dose Rate and Source Dependent Effects in 200 GHz SiGe HBTs," *IEEE Trans. Nucl. Sci.*, vol. 53, pp. 3166–3174, Dec 2006.

[68] N. E. Lourenco, R. L. Schmid, K. A. Moen, S. D. Phillips, T. D. England, J. D. Cressler, J. Pekarik, J. Adkisson, R. Camillo-Castillo, P. Cheng, J. E. Monaghan, P. Gray, D. Harame, M. Khater, Q. Liu, A. Vallett, B. Zetterlund,

V. Jain, and V. Kaushal, "Total dose and transient response of SiGe HBTs from a new 4th-generation, 90 nm SiGe BiCMOS technology," in *Radiation Effects Data Workshop (REDW), 2012 IEEE*, pp. 1–5, July 2012.

[69] D. L. Hansen, S. Pong, P. Rosenthal, and J. Gorelick, "Total ionizing dose testing of SiGe 7HP discrete heterojunction bipolar transistors for ELDRS effects," in *Radiation Effects Data Workshop, 2007 IEEE*, pp. 215–220, July 2007.

[70] A. Johnston, G. Swift, and B. Rax, "Total dose effects in conventional bipolar transistors and linear integrated circuits," *IEEE Trans. Nucl. Sci.*, vol. 41, pp. 2427–2436, Dec 1994.

[71] R. L. Pease, L. M. Cohn, D. M. Fleetwood, M. A. Gehlhausen, T. L. Turflinger, D. B. Brown, and A. H. Johnston, "A proposed hardness assurance test methodology for bipolar linear circuits and devices in a space ionizing radiation environment," *IEEE Trans. Nucl. Sci.*, vol. 44, pp. 1981–1988, Dec 1997.

[72] R. L. Pease, "2008 update to the ELDRS bipolar linear circuit data compendium," in *Radiation and Its Effects on Components and Systems (RADECS), 2008 European Conference on*, pp. 75–78, Sept 2008.

[73] R. Pease, "Total ionizing dose effects in bipolar devices and circuits," *IEEE Trans. Nucl. Sci.*, vol. 50, pp. 539–551, June 2003.

[74] I. S. Esqueda, H. J. Barnaby, and P. C. Adell, "Modeling the Effects of Hydrogen on the Mechanisms of Dose Rate Sensitivity," *IEEE Trans. Nucl. Sci.*, vol. 59, pp. 701–706, Aug 2012.

[75] P. C. Adell, S. McClure, R. L. Pease, B. G. Rax, G. W. Dunham, H. J. Barnaby, and X. J. Chen, "Impact of hydrogen contamination on the total dose response of linear bipolar microcircuits," in *Radiation and Its Effects on Components*

and Systems, 2007. RADECS 2007. 9th European Conference on, pp. 1–8, Sept 2007.

[76] I. S. Esqueda, H. J. Barnaby, P. C. Adell, B. G. Rax, H. P. Hjalmarson, M. L. Mclain, and R. L. Pease, "Modeling Low Dose Rate Effects in Shallow Trench Isolation Oxides," *IEEE Trans. Nucl. Sci.*, vol. 58, pp. 2945–2952, Dec 2011.

[77] S. C. Witczak, R. C. Lacoe, J. V. Osborn, J. M. Hutson, and S. C. Moss, "Dose-rate sensitivity of modern nMOSFETS," *IEEE Trans. Nucl. Sci.*, vol. 52, pp. 2602–2608, Dec 2005.

[78] A. H. Johnston, R. T. Swimm, and T. F. Miyahira, "Low dose rate effects in shallow trench isolation regions," *IEEE Trans. Nucl. Sci.*, vol. 57, pp. 3279–3287, Dec 2010.

[79] A. P. Brokaw, "A simple three-terminal IC bandgap reference," *Solid-State Circuits, IEEE Journal of*, vol. 9, pp. 388–393, Dec 1974.

[80] S. D. Phillips, T. Thrivikraman, A. Appaswamy, A. K. Sutton, J. D. Cressler, G. Vizkelethy, P. Dodd, and R. A. Reed, "A Novel Device Architecture for SEU Mitigation: The Inverse-Mode Cascode SiGe HBT," *IEEE Trans. Nucl. Sci.*, vol. 56, pp. 3393–3401, Dec 2009.

[81] S. D. Phillips, K. A. Moen, N. E. Lourenco, and J. D. Cressler, "Single-Event Response of the SiGe HBT Operating in Inverse-Mode," *IEEE Trans. Nucl. Sci.*, vol. 59, pp. 2682–2690, Dec 2012.

[82] I. Song, S. Jung, N. E. Lourenco, U. S. Raghunathan, Z. E. Fleetwood, S. Zeinolabedinzadeh, T. B. Gebremariam, F. Inanlou, N. J. H. Roche, A. Khachatrian, D. McMorrow, S. P. Buchner, J. S. Melinger, J. H. Warner, P. Paki-Amouzou, and J. D. Cressler, "Design of Radiation-Hardened RF Low-Noise Amplifiers

Using Inverse-Mode SiGe HBTs," *IEEE Trans. Nucl. Sci.*, vol. 61, pp. 3218–3225, Dec 2014.

[83] T. K. Thrivikraman, E. Wilcox, S. D. Phillips, J. D. Cressler, C. Marshall, G. Vizkelethy, P. Dodd, and P. Marshall, "Design of Digital Circuits Using Inverse-Mode Cascode SiGe HBTs for Single Event Upset Mitigation," *IEEE Trans. Nucl. Sci.*, vol. 57, pp. 3582–3587, Dec 2010.

[84] B. R. Wier, U. S. Raghunathan, Z. E. Fleetwood, M. A. Oakley, A. J. Joseph, V. Jain, and J. D. Cressler, "On the use of vertical superjunction collectors for enhanced breakdown performance in SiGe HBTs," in *2016 IEEE Bipolar/BiCMOS Circuits and Technology Meeting (BCTM)*, pp. 21–24, Sept 2016.

[85] T. Fujihira, "Theory of Semiconductor Superjunction Devices," *Japanese Journal of Applied Physics*, vol. 36, pp. 6254–6262, October 1997.

[86] J. Yuan and J. D. Cressler, "Design and Optimization of Superjunction Collectors for Use in High-Speed SiGe HBTs," *IEEE Transactions on Electron Devices*, vol. 58, pp. 1655–1662, June 2011.

[87] A. Appaswamy, S. Phillips, and J. D. Cressler, "Optimizing Inverse-Mode SiGe HBTs for Immunity to Heavy-Ion-Induced Single-Event Upset," *IEEE Electron Device Letters*, vol. 30, pp. 511–513, May 2009.

[88] S. Buchner, K. Kang, W. J. Stapor, A. B. Campbell, A. R. Knudson, P. McDonald, and S. Rivet, "Pulsed laser-induced SEU in integrated circuits: a practical method for hardness assurance testing," *IEEE Trans. Nucl. Sci.*, vol. 37, pp. 1825–1831, Dec 1990.

[89] J. R. Schwank, M. R. Shaneyfelt, D. McMorrow, V. Ferlet-Cavrois, P. Dodd, D. F. Heidel, P. W. Marshall, J. A. Pellish, K. A. LaBel, K. P. Rodbell,

M. Hakey, R. S. Flores, S. E. Swanson, and S. M. Dalton, "Estimation of Heavy-Ion LET Thresholds in Advanced SOI IC Technologies From Two-Photon Absorption Laser Measurements," *IEEE Trans. Nucl. Sci.*, vol. 57, pp. 1827–1834, Aug 2010.

[90] R. A. Read, P. W. Marshall, J. C. Pickel, M. A. Carts, B. Fodness, G. Niu, K. Fritz, G. Vizkelethy, P. E. Dodd, T. Irwin, J. D. Cressler, R. Krithivasan, P. Riggs, J. Prairie, B. Randall, B. Gilbert, and K. A. LaBel, "Heavy-ion broad-beam and microprobe studies of single-event upsets in 0.20- um SiGe heterojunction bipolar transistors and circuits," *IEEE Trans. Nucl. Sci.*, vol. 50, pp. 2184–2190, Dec 2003.

[91] M. C. Vecchi and M. Rudan, "Modeling electron and hole transport with full-band structure effects by means of the Spherical-Harmonics Expansion of the BTE," *Electron Devices, IEEE Transactions on*, vol. 45, pp. 230–238, Jan 1998.

[92] T. Makino, D. Kobayashi, K. Hirose, Y. Yanagawa, H. Saito, H. Ikeda, D. Takahashi, S. Ishii, M. Kusano, S. Onoda, T. Hirao, and T. Ohshima, "LET Dependence of Single Event Transient Pulse-Widths in SOI Logic Cell," *IEEE Trans. Nucl. Sci.*, vol. 56, pp. 202–207, Feb 2009.

[93] M. Raine, M. Gaillardin, J. E. Sauvestre, O. Flament, A. Bournel, and V. Aubry-Fortuna, "Effect of the Ion Mass and Energy on the Response of 70-nm SOI Transistors to the Ion Deposited Charge by Direct Ionization," *IEEE Trans. Nucl. Sci.*, vol. 57, pp. 1892–1899, Aug 2010.

[94] J. A. Pellish, R. A. Reed, D. McMorrow, J. S. Melinger, P. Jenkins, A. K. Sutton, R. M. Diestelhorst, S. D. Phillips, J. D. Cressler, V. Pouget, N. D. Pate, J. A. Kozub, M. H. Mendenhall, R. A. Weller, R. D. Schrimpf, P. W. Marshall, A. D. Tipton, and G. Niu, "Laser-Induced Current Transients in

Silicon-Germanium HBTs," *IEEE Trans. Nucl. Sci.*, vol. 55, pp. 2936–2942, Dec 2008.

[95] J. A. Pellish, R. A. Reed, D. McMorrow, G. Vizkelethy, V. F. Cavrois, J. Baggio, P. Paillet, O. Duhamel, K. A. Moen, S. D. Phillips, R. M. Diestelhorst, J. D. Cressler, A. K. Sutton, A. Raman, M. Turowski, P. E. Dodd, M. L. Alles, R. D. Schrimpf, P. W. Marshall, and K. A. LaBel, "Heavy Ion Microbeam- and Broadbeam-Induced Transients in SiGe HBTs," *IEEE Trans. Nucl. Sci.*, vol. 56, pp. 3078–3084, Dec 2009.

[96] A. R. Knudson, A. B. Campbell, J. R. Hauser, M. Jessee, W. J. Stapor, and P. Shapiro, "Charge Transport by the Ion Shunt Effect," *IEEE Trans. Nucl. Sci.*, vol. 33, pp. 1560–1564, Dec 1986.

[97] N. E. Lourenco, S. Zeinolabedinzadeh, A. Ildefonso, Z. E. Fleetwood, C. T. Coen, I. Song, S. Jung, F. Inanlou, N. J. H. Roche, A. Khachatrian, D. McMorrow, S. P. Buchner, J. H. Warner, P. Paki, and J. D. Cressler, "An Investigation of Single-Event Effect Modeling Techniques for a SiGe RF Low-Noise Amplifier," *IEEE Trans. Nucl. Sci.*, vol. 63, pp. 273–280, Feb 2016.

[98] J. M. Hales, A. Khachatrian, N. J.-H. Roche, J. Warner, S. P. Buchner, and D. McMorrow, "Simulation of Laser-Based Two-Photon Absorption Induced Charge Carrier Generation in Silicon," *IEEE Trans. Nucl. Sci.*, vol. 62, pp. 1550–1557, Aug 2015.

[99] A. L. Sternberg, Y. Boulghassoul, L. W. Massengill, D. McMorrow, W. T. Lotshaw, J. Melinger, S. Buchner, and R. L. Pease, "Three-Dimensional Modeling of the Two Photon Absorption Effect in a Complex Bipolar Transistor," in *Radiation and Its Effects on Components and Systems, 2005. RADECS 2005. 8th European Conference on*, pp. PC22–1–PC22–8, Sept 2005.

[100] D. I. Kovsh, S. Yang, D. J. Hagan, and E. W. Van Stryland, "Nonlinear optical beam propagation for optical limiting," *Applied optics*, vol. 38, no. 24, pp. 5168–5180, 1999.

[101] J. A. Pellish, "Bulk Silicon-Germanium Heterojunction Bipolar Transistor Process Feature Implications for Single-Event Effects Analysis and Charge Collection Mechanisms," *Dissertation*, Sept 2008.

[102] M. Turowski, J. A. Pellish, K. A. Moen, A. Raman, J. D. Cressler, R. A. Reed, and G. Niu, "Reconciling 3-D Mixed-Mode Simulations and Measured Single-Event Transients in SiGe HBTs," *IEEE Trans. Nucl. Sci.*, vol. 57, pp. 3342–3348, Dec 2010.

[103] D. M. Cardoza, S. D. LaLumondiere, M. A. Tockstein, S. C. Witczak, Y. Sin, B. J. Foran, W. T. Lotshaw, and S. C. Moss, "Single Event Transients Induced by Picosecond Pulsed X-Ray Absorption in III-V Heterojunction Transistors," *IEEE Trans. Nucl. Sci.*, vol. 59, pp. 2729–2738, Dec 2012.

[104] D. Cardoza, S. D. LaLumondiere, M. A. Tockstein, D. L. Brewe, N. P. Wells, R. Koga, K. M. Gaab, W. T. Lotshaw, and S. C. Moss, "Comparison of Single Event Transients Generated by Short Pulsed X-Rays, Lasers and Heavy Ions," *IEEE Trans. Nucl. Sci.*, vol. 61, pp. 3154–3162, Dec 2014.

VITA

Zachary E. Fleetwood was born in Albuquerque, New Mexico in 1989. At the age of 9, he and his family relocated to Nashville, TN where he received the rank of Eagle Scout in the Boy Scouts of America at age 17 and then attended college at Vanderbilt University from 2008 – 2012 where he received his Bachelor's of Electrical Engineering with Honors and a minor in Engineering Management. For his senior design work on developing a radiation test bed for a Cube Satellite, Zachary and his team received Vanderbilt University's Walter Criley Prize for the best paper on an advanced senior project in electrical engineering. Upon his graduation, Zachary decided to continue his studies in Graduate School at the Georgia Institute of Technology in Atlanta, GA with Dr. John D. Cressler. While at Georgia Tech, Zachary has authored or co-authored more than 40 publications primarily focused on the study of radiation effects in Silicon-Germanium Heterojunction Bipolar Transistors (SiGe HBTs). His accolades include receiving two Best Paper rewards (one as co-author and one as the primary author), receiving the 2016 Paul Phelps Continuing Education Grant, and receiving the 2016 NPSS (Nuclear and Plasma Sciences Society) Graduate Scholarship Award. Zachary received his Masters Degree in Electrical Engineering from Georgia Tech in 2014 and his PhD (pending) in 2018. Following the completion of his doctorate, Zachary will be joining SpaceX out in Redmond, Washington.